

Nebular Spectra of 111 Type Ia Supernovae Disfavor Single Degenerate Progenitors

M. A. Tucker^{1,★†}, B. J. Shappee¹, P. J. Vallely², K. Z. Stanek^{2,3}, J. L. Prieto^{4,5}, J. Botyanszki⁶, C. S. Kochanek^{2,3}, J. P. Anderson⁷, J. Brown², L. Galbany⁸, T. W.-S. Holoien⁹, E. Y. Hsiao¹⁰, S. Kumar¹⁰, H. Kuncarayakti^{11,12}, N. Morrell¹³, M. M. Phillips¹³, M. D. Stritzinger¹⁴, and Todd A. Thompson^{2,3}

¹ Institute for Astronomy, University of Hawai‘i at Manoa, 2680 Woodlawn Dr., Honolulu, HI 96822

² Department of Astronomy, The Ohio State University, 140 West 18th Avenue, Columbus, OH 43210, USA

³ Center for Cosmology and AstroParticle Physics (CCAPP), The Ohio State University, 191 W. Woodruff Avenue, Columbus, OH 43210, USA

⁴ Núcleo de Astronomía de la Facultad de Ingeniería y Ciencias, Universidad Diego Portales, Av. Ejército 441, Santiago, Chile

⁵ Millennium Institute of Astrophysics, Santiago, Chile

⁶ Physics Department, University of California, Berkeley, CA 94720, USA

⁷ European Southern Observatory, Alonso de Cordova 3107 Casilla 19001, Vitacura, Santiago, Chile

⁸ PITT PACC, Department of Physics and Astronomy, University of Pittsburgh, Pittsburgh, PA 15260, USA

⁹ Carnegie Observatories, 813 Santa Barbara Street, Pasadena, CA 91101, USA

¹⁰ Department of Physics, Florida State University, 77 Chieftan Way, Tallahassee, FL 32306, USA

¹¹ Finnish Centre for Astronomy with ESO (FINCA), FI-20014 University of Turku, Finland

¹² Tuorla Observatory, Department of Physics and Astronomy, FI-20014 University of Turku, Finland

¹³ Las Campanas Observatory, Carnegie Observatories, Casilla 601, La Serena, Chile

¹⁴ Department of Physics and Astronomy, Aarhus University, Ny Munkegade 120, DK-8000 Aarhus C, Denmark

Accepted XXX. Received YYY; in original form ZZZ

ABSTRACT

We place statistical constraints on Type Ia supernova (SN Ia) progenitors using 227 nebular phase spectra of 111 SNe Ia. We find no evidence of stripped companion emission in any of the nebular phase spectra. Upper limits are placed on the amount of mass that could go undetected in each spectrum using recent hydrodynamic simulations. With these null detections, we place an observational 3σ upper limit on the fraction of SNe Ia that are produced through the classical H-rich non-degenerate companion scenario of < 5.5%. Additionally, we set a tentative 3σ upper limit on He star progenitor scenarios of < 6.4%, although further theoretical modelling is required. These limits refer to our most representative sample including normal, 91bg-like, 91T-like, and “Super Chandrasekhar” SNe Ia but excluding SNe Iax and SNe Ia-CSM. As part of our analysis, we also derive a Nebular Phase Phillips Relation, which approximates the brightness of a SN Ia from 150 – 500 days after maximum using the peak magnitude and decline rate parameter $\Delta m_{15}(B)$.

Key words: supernovae – general; galaxies – distances and redshifts

1 INTRODUCTION

Type Ia supernovae (SNe Ia) are utilised across many astronomical disciplines, including the extragalactic distance scale, dark energy studies, and Galactic chemical evolution. Despite their prevalence, the origins of SNe Ia are still unclear even after decades of study. The general consensus

is that they are explosions of carbon/oxygen (C/O) white dwarfs (Hoyle & Fowler 1960) with fairly homogeneous properties. For example, the magnitude of SNe Ia at peak is well constrained ($M_{\max} \sim -19$, e.g.; Folatelli et al. 2010a), and, after correcting for light curve decline and color, they have an intrinsic scatter of ~ 0.1 mag (e.g., Fig. 19, Folatelli et al. 2010a). Many formation mechanisms for SNe Ia have been proposed to reproduce this level of uniformity, which can be grouped into two main categories: the double degenerate (DD) and single degenerate (SD) scenarios (see Maoz et al.

* E-mail: tuckerma@hawaii.edu

† DOE CSGF Fellow

2014; Livio & Mazzali 2018; Jha et al. 2019, for reviews on SNe Ia and their progenitors).

The DD scenario consists of two degenerate stars, usually C/O white dwarfs, which induce a SNe Ia through accretion, collision, or merger. This can occur due to gravitational wave emission (Tutukov & Yungelson 1979; Iben & Tutukov 1984; Webbink 1984), collision/violent merger due to perturbations by external bodies (Thompson 2011; Katz & Dong 2012; Shappee & Thompson 2013; Pejcha et al. 2013; Antonini et al. 2014), accretion from a low-mass white dwarf onto a smaller, higher-mass white dwarf (Taam 1980; Livne 1990; Tutukov & Yungelson 1996; Pakmor et al. 2012), or a "double detonation" where an accreted helium layer detonates and drives the core to detonate (Woosley & Weaver 1994; Fink et al. 2010; Kromer et al. 2010). Due to the intrinsic faintness of both components in these systems, observational confirmation of DD systems is exceptionally difficult (e.g., Rebassa-Mansergas et al. 2018). Some progress has been made on this front, such as bimodal emission in the nebular phase (Dong et al. 2015a; Valley et al. 2019a) and possible hyper-velocity remnants (Shen et al. 2018; Ruffini & Casey 2019). However, most of the evidence for DD systems comes from the exclusion of SD progenitors (e.g., Shappee et al. 2017).

The SD scenario involves a WD with a nearby non-degenerate companion (Whelan & Iben 1973; Nomoto 1982; Yoon & Langer 2003), usually undergoing Roche Lobe overflow (RLOF). The WD accumulates material until reaching critical mass and then explodes. This critical mass is typically considered the Chandrasekhar mass ($M_{ch} \sim 1.4 M_{\odot}$), although sub- M_{ch} explosions, including double detonation scenarios, are also possible (e.g., Livne & Arnett 1995). There are several predicted observational signatures of the SD degenerate scenario due to the interaction of the ejecta/explosion and the donor star (Wheeler et al. 1975), including effects on the rising SN Ia light curve (Kasen 2010), soft X-ray emission in the accretion phase (Lanz et al. 2005; Tutukov & Fedorova 2007; Woods et al. 2018), surviving companions with anomalous characteristics (e.g., Canal et al. 2001; Shappee et al. 2013b), and the amount of ^{56}Ni decay products synthesized in the explosion (e.g., Röpke et al. 2012; Shappee et al. 2017).

One of the most promising signatures of a RLOF companion to an exploding WD are emission lines produced by material stripped/ablated from the non-degenerate companion (e.g., Wheeler et al. 1975; Chugai 1986; Marietta et al. 2000; Mattila et al. 2005; Pan et al. 2012), observable in nebular-phase spectra once the SN Ia has faded considerably and become optically thin. For example, Boehner et al. (2017) simulated stripping from red giant (RG), main sequence (MS), and sub-giant (SG) stars, finding approximately 0.33, 0.25, and $0.17 M_{\odot}$, respectively, of stripped mass. Botyánszki et al. (2018) converted these estimates into expected H α luminosities and found that the emitted H α luminosity does not vary linearly with amount of stripped companion mass, which had been the assumption of previous studies (e.g. Leonard 2007; Shappee et al. 2013a), but instead the relation is closer to logarithmic. Additionally, the H α emission is powered by gamma-ray deposition from the SN Ia ejecta and roughly follows the bolometric luminosity.

In this work we compile a comprehensive sample of SNe Ia nebular spectra spanning 200 – 500 days after explosion

(181 – 481 days after maximum assuming a rise time of ~ 19 days from Firth et al. 2015) to search for the expected emission from stripped/ablated material. We find no such emission in any spectrum in our sample, and place new or updated stripped/ablated mass constraints for each SN Ia. The entirety of similar work in the literature totals 33 SNe Ia (Mattila et al. 2005; Leonard 2007; Shappee et al. 2013a; Lundqvist et al. 2013, 2015; Maguire et al. 2016; Graham et al. 2017; Shappee et al. 2018; Sand et al. 2018a; Holmbo et al. 2018; Dimitriadis et al. 2019a; Tucker et al. 2018; Sand et al. 2019), a fraction of the sample analyzed in this work. All SNe Ia included in this study are listed in Table B2 and photometric parameters (t_{max} , Δm_{15} , μ , $E(B - V)_{host}$) are provided in Table B3.

We outline our data sources and reduction techniques, including absolute flux calibration, in §2. In §3, we discuss our methodology in searching for and placing limits on material stripped from a RLOF companion. Our upper limits on stripped material are provided in §4, and our findings are discussed in the context of SNe Ia formation in §5. Included in §5 are discussions about peculiar SNe Ia and their role in our study including SNe Ia-CSM. Finally, in §6, we summarize our results.

2 DATA SOURCES AND REDUCTION

Our sample of 227 spectra of 111 SNe Ia comes from the 40 instruments on 29 telescopes listed in Table 1. All spectroscopically peculiar SNe Ia are included except for those exhibiting signatures of circumstellar material (SNe Ia-CSM). These SNe Ia exhibit H α emission, but the velocity and magnitude of the emission is inconsistent with material stripped from a nearby companion; instead, these SN Ia appear to have exploded in a dense circumstellar environment (e.g., SN 2002ic, Wang et al. 2004) and exhibit H α emission before the SN enters the nebular phase (e.g., Silverman et al. 2013). A discussion of SNe Ia-CSM and their role in our results is provided in §5.2. For non-CSM SNe Ia we impose the following criteria when selecting nebular spectra:

- Obtained between 200 and 500 days after explosion to maintain consistency with the models of Botyánszki et al. (2018), assuming a typical rise time of $t_{rise} \approx 19$ days (Firth et al. 2015).
- Cover $\pm 1000 \text{ km s}^{-1}$ of at least one H or He line in Table 2.
- Have at least one method of absolute flux calibration, outlined in §2.3.
- Published, posted, or observed by our team before the submission date of this article (15 March 2019).

The complete list of new and archival spectra is provided in Table B4. Additionally, we include new and archival photometry to supplement our spectral data and analysis. Early-phase photometry ($\lesssim 50$ days after maximum light) is used in deriving the photometric properties of each SN Ia using the photometric fitting code **SNooPy** (Burns et al. 2011), including time of maximum (t_{max}), the decline rate parameter Δm_{15} , extinction along line of sight, and the distance modulus. Late- and nebular-phase photometry are used for flux calibrating the nebular spectra and deriving a Nebular Phase Phillips Relation (NPPR). The NPPR approximates

the nebular magnitude of a SN Ia given its peak magnitude and decline rate, calibrated to an extensive sample of new and archival SNe Ia photometry. A complete description of the NPPR, its derivation and usage is provided in Appendix A.

2.1 New Spectra and Photometry

We present 14 new nebular-phase spectra of 13 SNe Ia, of which 10 have no prior published nebular spectra. These spectra were acquired in our ongoing study of SNe Ia progenitors, taken with MagE and IMACS on Baade, MUSE on the VLT, and WFCCD on duPont (see Table 1 for telescope and instrument designations). For the new spectra presented here, each spectrum was reduced using telescope and instrument-specific pipelines, if available, otherwise typical IRAF¹ tasks were used. The spectra acquired with MagE/Baade were reduced with a pipeline provided by the Carnegie Observatories² (Kelson et al. 2000; Kelson 2003), with the exception of standard star calibrations and stitching together each echellette spectrum, which was done with custom Python routines. For newly presented MUSE data acquired as part of the AMUSING survey (Galbany et al. 2016), spectra were extracted in a 1'' circular aperture at the SN Ia location using the PyMUSE package (Pessa et al. 2018), and corrected for host galaxy contributions using a background annulus extending from 2'' to 3''. New IMACS/Baade spectra were reduced with typical IRAF procedures including bias subtraction, flat-field correction, arc lamp exposures for wavelength calibration and standard star observations to correct for instrument and atmospheric response.

For absolute flux calibrations, we also include nebular photometry for any SNe Ia in our sample. This includes new observations and reprocessed archival images for which we could not find a published magnitude. New photometry includes *V*-band images taken with FORS2, *r*-band images from MODS1, and *BVRI* images from WFCCD. Archival imaging includes *UBVRI* imaging from FORS1/2 and *BVRgi* imaging from EFOSC2 (Table B6). All images are bias subtracted and flat-field corrected before performing aperture photometry with the IRAF *apphot* task. For targets with $\delta \geq -30^\circ$, photometry from the Pan-STARRS Stack Object catalog³ (Chambers et al. 2016; Flewelling et al. 2016) was used in calibrating the images, otherwise *Gaia* DR2 photometry (Gaia Collaboration et al. 2016, 2018; Riello et al. 2018) was used. When transforming reported magnitudes to other photometric systems, Tonry et al. (2012) and Evans et al. (2018) were used for Pan-STARRS and *Gaia*, respectively. The only exceptions to this procedure are the *B*-band FORS2/VLT images, which are calibrated using the reported photometric zeropoints⁴.

¹ <http://iraf.noao.edu/>

² <http://code.obs.carnegiescience.edu/mage-pipeline>

³ <http://archive.stsci.edu/panstarrs/stackobject/search.php>

⁴ <https://www.eso.org/observing/dfo/quality/FORS2/qc/zeropoints/zeropoints.html>

2.2 Archival Spectra and Photometry

The primary sources of our archival spectra and photometry are the Berkeley SuperNova Ia Program⁵ (BSNIP, Silverman et al. 2012, 2013), the Center for Astrophysics (CfA) Supernova Data Archive⁶ (Riess et al. 1999; Jha et al. 2006; Matheson et al. 2008; Blondin et al. 2012), the Carnegie Supernova Project⁷ (CSP, Hamuy et al. 2006; Folatelli et al. 2010a; Contreras et al. 2010; Stritzinger et al. 2011; Folatelli et al. 2013; Krisciunas et al. 2017; Phillips et al. 2019), the 100IAs project (Dong et al. 2018a), the ANU WiFeS SuperNova Program (AWSNAP; Childress et al. 2016), and the All-Sky Automated Survey for SuperNovae (ASAS-SN, Shappee et al. 2014a; Holoiu et al. 2017a,b,c, 2019, Valdely et al., Chen et al., in prep). The majority of the publicly available data were retrieved using the Open Supernova Catalog (OSC, Guillochon et al. 2017) and the Weizmann Interactive Supernova data REPOSITORY (WISEREP, Yaron & Gal-Yam 2012). All data provided by these sources are already reduced with the exception of precise spectral flux calibration, which we outline in §2.3. Additionally, we supplement these sources with archival data obtained from telescope databases, including the Keck Observatory Archive⁸ (KOA), the ESO Science Archive Facility⁹ (ESO SAF), the Isaac Newton Group Archive¹⁰ and the Gemini Observatory Archive¹¹ (GOA). Information on all the spectra in this study is presented in Table B4.

Data reduction and calibration was performed as uniformly as possible across all sources of spectra. Data retrieved from public archives were already reduced, with the exception of absolute flux calibration. The reduction of data retrieved from telescope archives was generally less complete. All spectra retrieved from the ESO SAF were already reduced (excluding flux corrections) with the exception of FORS1/2 data. For any ESO SAF data reduction, both spectroscopy and photometry, we used the ESO SAF esorex data reduction pipeline (Freudling et al. 2013).

Spectra obtained from the KOA and GOA were not reduced prior to retrieval and had to be manually reduced. Recent LRIS spectra were reduced using Lpipe¹², while older LRIS and DEIMOS data were reduced using the LowRedux/XIDL pipeline¹³. Gemini North/South GMOS spectra were reduced with the GMOS Data Reduction Cookbook¹⁴.

We manually reduced any unreduced spectra for which no pipeline exists using standard IRAF procedures. Images were flat-fielded and bias-subtracted using archival calibration images taken near the epoch of observation, and wavelength calibrated with arc lamp exposures. Spectrophotometric standard star observations were used to correct for

⁵ <http://heracles.astro.berkeley.edu/snbd/>

⁶ <https://www.cfa.harvard.edu/supernova/SNarchive.html>

⁷ <http://csp.obs.carnegiescience.edu/>

⁸ <https://koa.ipac.caltech.edu/>

⁹ <http://archive.eso.org/cms.html>

¹⁰ <http://casu.ast.cam.ac.uk/casuadc/ingarch/query>

¹¹ <https://archive.gemini.edu/>

¹² <http://www.astro.caltech.edu/~dperley/programs/lpipe.html>

¹³ <http://www.ucolick.org/~xavier/LowRedux/>

¹⁴ <http://ast.noao.edu/sites/default/files/GMOS-Cookbook/>

Table 1. All telescopes and instruments utilised in this work. If a reference could not be found for a given instrument, the corresponding instrument website is provided in the table notes.

Telescope	Abbrev. ^a	Instrument	Abbrev. ^a	Ref.	N_{spec}
Australian National University 2.3m	ANU2.3m	Wide-Field Spectrograph	WiFeS	Dopita et al. (2007, 2010)	7
Calar Alto 2.2m	CA2.2m	Calar Alto Faint Object Spectrograph	CAFOS	... ^b	1
Calar Alto 3.5m	CA3.5m	Multi-Object Spectrograph at Calar Alto	MOSCA	... ^c	2
Danish 1.54m	D1.54m	Danish Faint Object Spectrograph and Camera	DFOSC	Andersen et al. (1995)	1
du Pont Telescope	duPont	Wide Field Reimaging CCD Camera Boller and Chivens Spectrograph	WFCCD BC	... ^d ... ^e	4 1
ESO 1.5m	ESO1.5m	Boller and Chivens Spectrograph	BC	... ^f	2
ESO 3.6m	ESO3.6m	ESO Faint Object Spectrograph and Camera	EFOSC1/2	Buzzoni et al. (1984)	11
Harlan J Smith Telescope	HJST	UltraViolet Image Tube Spectrograph	UVITS	Wills et al. (1980)	1
Himalayan Chandra Telescope	HCT	Himalayan Faint Object Spectrograph	HFOSC	... ^g	2
Hubble Space Telescope	HST	Faint Object Spectrograph	FOS	... ^h	1
Isaac Newton Telescope	INT	Faint Object Spectrograph (1st Gen.)	FOS1	Breare et al. (1987)	2
Gemini North/South	GN/S	Gemini Multi-Object Spectrograph	GMOS	Hook et al. (2004)	13
Gran Telescopio Canarias	GTC	Optical System for Imaging and low-Intermediate-Resolution Integrated Spectroscopy	OSIRIS	Cepa (2010)	1
Keck I	KeckI	Low Resolution Imaging Spectrograph	LRIS	Oke et al. (1995)	27
Keck II	KeckII	DEep Imaging Multi-Object Spectrograph	DEIMOS	Faber et al. (2003)	9
Large Binocular Telescope	LBT	Echelle Imager and Spectrograph	ESI	Sheinis et al. (2002)	3
Magellan Baade Telescope	Baade	Multi-Object Double Spectrograph Inamori-Magellan Areal Camera and Spectrograph	MODS1/2 IMACS	Pogge et al. (2010) Dressler et al. (2011)	10 3
Magellan Clay Telescope	Clay	Magellan Echelle Spectrograph	MagE	Marshall et al. (2008)	2
Multiple Mirror Telescope	MMT	Low Dispersion Survey Spectrograph	LDSS	... ⁱ	5
New Technology Telescope	NTT	Blue Channel Spectrograph ESO Multi-Mode Instrument	BCS EMMI	Angel et al. (1979) D'Odorico (1990)	6 1
Palomar 200-inch	P200	SOFI	... DBSP	Moorwood et al. (1998) Oke & Gunn (1982)	1 4
Shane 3m Telescope	Shane3m	Double Spectrograph	KAST	Silverman et al. (2013)	11
Southern African Large Telescope	SALT	Kast Spectrograph	RSS	Buckley et al. (2006)	3
Subaru	Sub	Robert Stobie Spectrograph	CISCO	Motohara et al. (2002)	3
Tillinghast 1.5m	Till	OH-Airglow Suppressor/Cooled Infrared Spectrograph and Camera for OHS	FOCAS	Kashikawa et al. (2002)	2
Telescopio Nazionale Galileo Very Large Telescope	TNG VLT	Faint Object Spectrograph and Camera FAst Spectrograph for the Tillinghast telescope Device Optimized for LOw RESolution FOcal Reducer and low dispersion Spectrograph	FAST DOLORES FORS1/2	Fabricant et al. (1998) Molinari et al. (1999) Appenzeller et al. (1998)	7 2 43
William Herschel Telescope	WHT	Multi-Unit Spectroscopic Explorer XSHOOTER Intermediate dispersion Spectrograph and Imaging System ACAM Faint Object Spectrograph (2nd Gen.)	MUSE XSH ISIS ... FOS2	Bacon et al. (2010) Vernet et al. (2011) Jorden (1990) Benn et al. (2008) Breare et al. (1987)	8 16 5 1 6
Total	29		40		227

^a Abbreviations used in Table B4.^b http://w3.caha.es/CAHA/Instruments/CAFOS/cafos_overview.html^c <http://www.caha.es/CAHA/Instruments/MOSCA/index.html>^d <http://www.lco.cl/telescopes-information/lco/telescopes-information/irenee-du-pont/instruments/website/wfccd/wfccd-manuals>^e <http://www.lco.cl/telescopes-information/irenee-du-pont/instruments/website/boller-chivens-spectrograph-manuals/user-manual/the-boller-and-chivens-spectrograph>^f <http://www.ls.eso.org/lasilla/Telescopes/2p2/E1p5M/BC/BC.html>^g <https://www.iiap.res.in/iao/hfosc.html>^h http://stecf-poa.stsci.edu/poa/FDS/fos_doc_access.htmlⁱ <http://www.lco.cl/telescopes-information/magellan/instruments/ldss-3>

telescope/instrumental artefacts, atmospheric effects, and to place each spectrum on a reliable relative flux scale.

2.3 Accurate Flux Calibration

For our analysis in §3, the spectra must be on a reliable absolute flux scale. While calibrating spectra with spectrophotometric standard stars places these spectra on a dependable relative flux scale, slit losses, atmospheric conditions, and other effects can cause the resulting spectra to deviate from an absolute flux scale. To scale a spectrum to the absolute scale, we employed Eq. 7 from Fukugita et al. (1996) to calculate synthetic photometry from the spectra. The spectra are then scaled so that the synthetic photometry matches the observed photometry. There were several different sources of photometry used to calibrate the spectra. In order of preference and reliability, with accuracy estimates in given parentheses:

- (i) For spectra with acquisition images taken at the time of observation, we scale the entire spectrum to match these photometric observations, usually in the V or r filters ($\sim 5 - 10\%$).
- (ii) If acquisition images are unavailable, we next tried to use photometry within ± 5 d of the spectral observations. Photometry in all available filters within this temporal limit were used in the flux calibration ($\sim 10 - 15\%$).
- (iii) If no photometric data was available within ± 5 d, we searched for photometry within ± 50 d. If at least 3 photometric data points fell within this time span, we linearly interpolated to estimate the magnitude at the time of the spectral observation ($\sim 15 - 20\%$).
- (iv) If none of these were available, the nebular BVR magnitude was estimated with the NPPR and used to calibrate the spectrum (see Appendix A, $\sim 20\%$).

We required $> 90\%$ of the filter’s transmission curve be covered by the observed spectrum for viable calibrations. If only a single filter was available, the entire spectrum was scaled to match the observation. If two filters were available for flux calibration, a simple linear fit was applied to the scale factors. If > 3 filters were available, we use spline fits with fixed endpoints to ensure a robust flux correction across the entire spectrum. After placing the spectrum on an absolute flux scale, we correct for host galaxy and Milky Way reddening using the $E(B-V)_{\text{host}}$ derived from the light curve fits. We implement a Fitzpatrick (1999) extinction law and a Schlegel et al. (1998) Milky Way dust map for our reddening corrections. We assume $R_V = 3.1$ unless stated otherwise (see Appendix B).

2.4 Sample Demographics

After collecting all nebular spectra that meet our temporal and calibration requirements, our sample consists of 111 SNe Ia (Table B2). Due to the comprehensive nature of our search for nebular spectra, our sample is inherently biased towards brighter or peculiar SNe Ia as these objects have a higher likelihood of being observed in the nebular phase. This effect is readily apparent in Fig. 1 where the $\Delta m_{15}(B)$ values of SNe Ia in our sample are compared to a purely photometric sample from the Lick Observatory Supernova Search (LOSS, Li

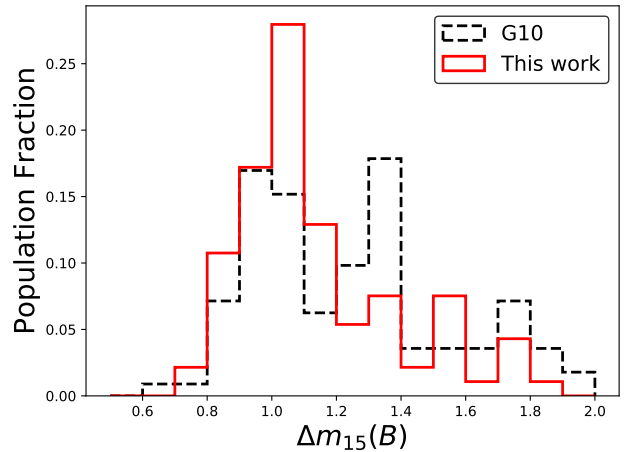


Figure 1. Distribution of $\Delta m_{15}(B)$ in our sample compared to the photometric sample from LOSS (Ganeshalingam et al. 2010). As expected, the nebular sample is biased towards brighter and broader SNe Ia.

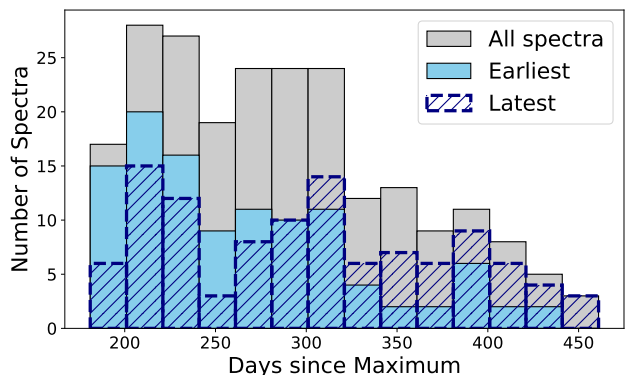


Figure 2. The number of spectra per days since maximum for 3 distributions, 1) all spectra in our sample (gray), 2) the earliest spectrum for each SN Ia (light blue), and 3) the latest spectrum for each SN Ia (dark blue, hatched).

et al. 2000; Ganeshalingam et al. 2010). Similar to the luminosity bias, we are biased to lower redshift SNe Ia with a median redshift of $z_{\text{med}} \approx 0.015$. We provide the temporal distribution for our set of nebular spectra in Fig. 2, including distributions for the earliest and latest spectra for each SN Ia. As expected, the number of spectra generally decline at later phases due to the supernovae fading from view.

3 SEARCHING FOR EMISSION FROM STRIPPED COMPANION MATERIAL

Prior to the work of Botyánszki et al. (2018), the majority of unbound mass limits in the literature utilised the work of Mattila et al. (2005) and Leonard (2007) to compute stripped mass limits from comparing observed spectra to expected H α luminosities. Several subsequent studies have adopted these methodologies in their work (e.g., Maguire et al. 2016; Graham et al. 2017) with notable success in ruling out hydrogen-rich companions. Yet the models of Mat-

Table 2. Line luminosities for both the hydrogen-rich (H-rich) model and the helium-rich (He-rich) model corresponding to the MS38 and helium models from Botyánszki et al. (2018). Helium lines are given letter designations to ease identification in Table B5. FWHM refers to the expected FWHM of a line profile broadened by $\sim 10^3$ km s $^{-1}$.

Line	λ	$L_{200}[10^{38} \text{ erg/s}]$	FWHM [Å]
H-rich Model			
H γ	4341Å	0.271	14.5
H β	4831Å	4.38	16.1
HeI-a	5875Å	4.27	19.6
H α	6563Å	68.0	21.9
HeI-b	6678Å	2.24	22.3
HeI-c	1.08μm	10.5	36.0
Pa β	1.281μm	14.6	42.7
Pa α	1.875μm	14.6	62.5
HeI-d	2.06μm	8.48	68.7
He-rich Model			
HeI-a	5875Å	8.26	19.6
HeI-b	6678Å	6.90	22.3
HeI-c	1.08μm	18.2	36.0
HeI-d	2.06μm	12.9	68.7

tila et al. (2005) had several shortcomings in observational implementation. In particular, Leonard (2007) assumed a linear scaling between the amount of unbound companion mass and the corresponding H α luminosity.

Botyánszki et al. (2018), using the MS38 model (a main-sequence star undergoing RLOF) from Boehner et al. (2017), instead found the emitted H α luminosity scales logarithmically with the amount of stripped mass. Additionally, Botyánszki et al. (2018) computed a simplified helium-star model, where all the stripped mass from the MS38 model is replaced with helium instead of Solar abundance material. This is not a true helium-star model, as helium-star companions are expected to have lower amounts of stripped mass than their hydrogen-rich counterparts and a modestly different velocity distribution (e.g. Pan et al. 2012), but it provides a starting point for calculating limits on the amount of unbound helium in a SN Ia spectrum.

While the models of Botyánszki et al. (2018) clarify the mass-luminosity scaling issue and expand to helium emission, they share two other shortcomings with the models of Mattila et al. (2005): the requirement of using H α to constrain the amount of unbound mass, and only calculating the expected H α luminosity at a single epoch (200 days post-explosion for Botyánszki et al. 2018 and 350 days post-maximum for Mattila et al. 2005). In the following subsections we discuss our stripped mass limits given these limitations.

3.1 Expanding on these Models

For SNe Ia with star-forming host galaxies, the region around H α can be contaminated by narrow host galaxy H α and NII emission lines which complicates setting limits on H α emission. However, the unbound material has emission lines besides H α , including H β , H γ , and the Paschen series. Assuming roughly Solar metallicity, the stripped material

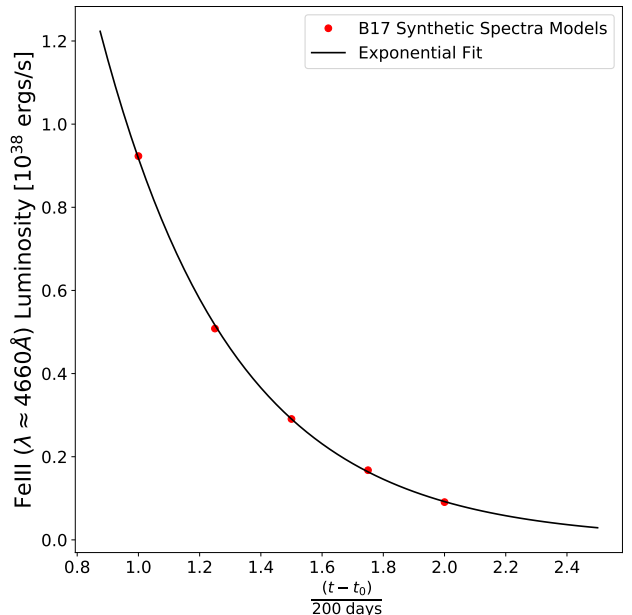


Figure 3. Peak luminosity of the FeIII line (red points) versus days since explosion ($t - t_0$) from the time-dependent SN Ia spectral models of Botyánszki & Kasen (2017) and the exponential fit (black line).

will also exhibit prominent HeI lines in the optical and NIR (Botyánszki et al. 2018). We provide the luminosities for each of these lines in Table 2 at $(t - t_0) = 200$ days from explosion for the hydrogen-rich (H-rich) model using the same MS38 model as Botyánszki et al. (2018). Additionally, we supply similar data for the simplified helium-star model from Botyánszki et al. (2018), which we refer to as the He-rich model.

Botyánszki et al. (2018) estimated the line luminosity at 200 days as a function of the amount of stripped mass (M_{st}). Table 2 provides the expected luminosity $L_{200}(M_{st})$ of various lines for $M_{st} = 0.25 M_\odot$. The dependence on the amount of stripped mass is well approximated by $\log_{10} L_{200}(M) \approx \log_{10} L_{200}(0.25M_\odot) + 0.17M - 0.2M^2$, where $M = \log_{10}(M_{st}/M_\odot)$. Botyánszki et al. (2018) do not provide the time dependence of the line emission specifically, but note that the H α emission is proportional to the FeIII emission over the $200 < (t - t_0) < 500$ day period they consider. Utilising the synthetic spectra models from Botyánszki & Kasen (2017), we find the FeIII emission is well fit by an exponential (Fig. 3), which leads to an estimate for the line luminosity of

$$\log_{10} L(M, t) = \log_{10} L_{200} + 0.17M - 0.20M^2 - \left(\frac{t - t_0}{200 \text{ days}} - 1 \right) \quad (1)$$

provided $M_{st} < 2M_\odot$. This should hold well for the Balmer lines, and is at least a better approximation for the Paschen and HeI lines than assuming their luminosities are temporally constant.

The models from Botyánszki & Kasen (2017) used to derive the luminosity decay in Fig. 3 are truncated at 400 days after explosion. However, the ratio between FeIII and

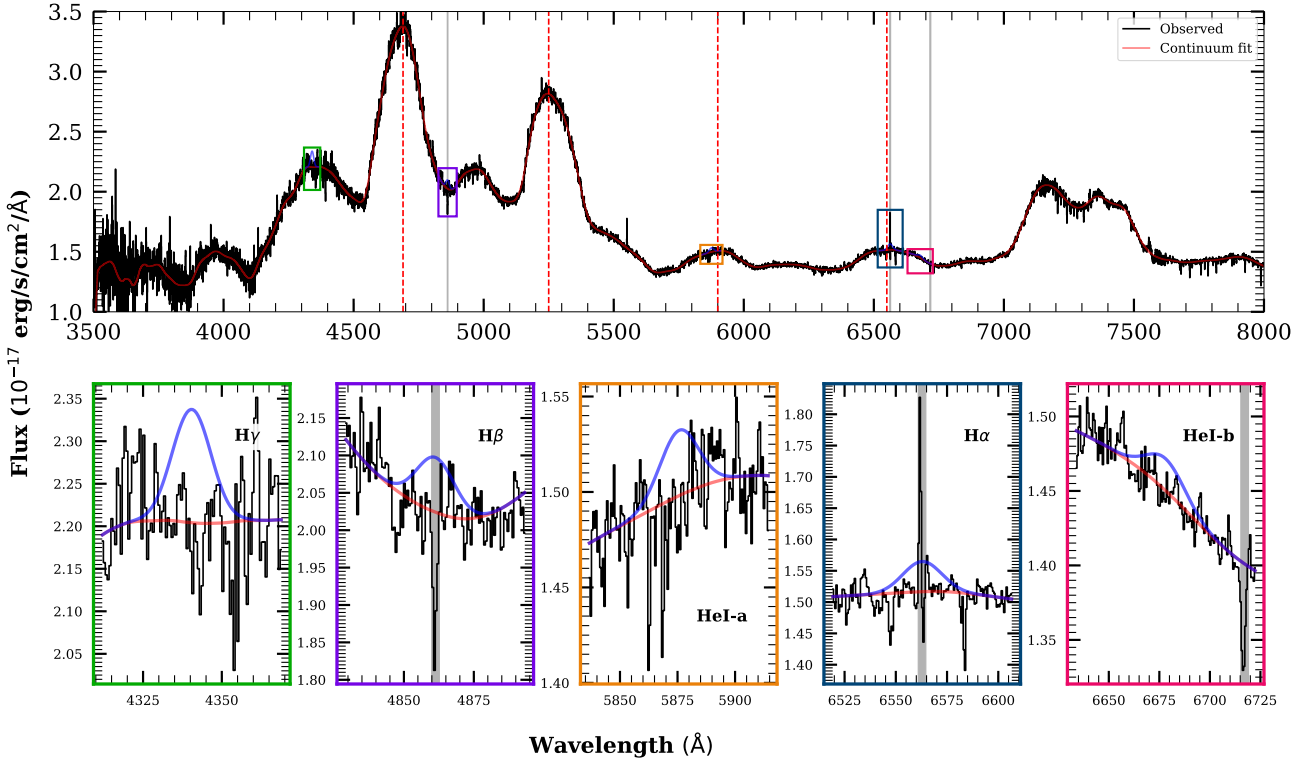


Figure 4. Nebular phase spectrum (black), continuum fit (red), and derived 10σ flux limits (blue) for the Baade/MagE +295 d spectrum of SN 2015F. The bottom panels show the regions near each possible emission line from Table 2 and correspond to the coloured boxes in the top panel. Gray shaded areas indicate masked spectral regions due to host galaxy contamination or instrumental effects, and vertical dashed lines indicate SNe Ia emission lines used to estimate the smoothing width for each spectrum (see §3). Similar spectral cutouts for all SNe Ia are included as supplementary figures (see Appendix B).

$H\alpha$ remains roughly constant out to 500 days after explosion (Botyánszki et al. 2018). To incorporate spectra taken between 400 – 500 days after explosion, we extrapolate the exponential fit to the later epoch. Since the models used to derive the FeIII emission decay are generalized to non-peculiar SNe Ia and independent of any possible H or He emission, we consider this assumption valid. However, we do not extrapolate to earlier epochs for two reasons. The onset of the nebular phase is not clearly defined in the literature (e.g., Black et al. 2016), leading to ambiguities in when stripped material might become visible. Additionally, the luminosities for stripped material given in Table 2 are taken from Botyánszki et al. (2018) who explicitly state that their models are valid in the regime of $200 \leq (t - t_0) \leq 500$ days. If these concerns are mitigated by future work our results can be expanded to include objects with earlier spectra.

3.2 Placing Statistical Limits on Stripped Mass

Once each spectrum is flux calibrated and corrected for the reddening, we place statistical limits on the presence of emission lines listed in Table 2, roughly following the methods of Leonard (2007). Each spectrum is rebinned to the approximate spectral resolution, and the spectral continuum is fit with a 2nd-order Savitsky-Golay polynomial (Press et al. 1992), excluding pixels within $2 \times \text{FWHM}$ of line centers to prevent biasing our continuum fit, as done in previous studies

(e.g., Maguire et al. 2016). However, since we are inspecting multiple lines for emission signatures, we apply our continuum model in velocity space instead of wavelength space to incorporate this modification.

No single continuum width adequately fits the continuum for all SNe Ia in our sample, especially considering the spectroscopic and temporal diversity. We tailored the continuum fit width for each spectrum based on the observed SN Ia expansion velocity, measured from the prominent emission lines in the spectrum. Since most of the major emission lines in nebular SNe Ia are blended to some extent (e.g., Mazzali et al. 2015, Fig. 5), we compute the weighted average from the fitted line profiles assuming a Gaussian emission profile + linear continuum. The lines considered for deriving the expansion velocity are the major FeII, FeIII, and CoIII lines indicated by the vertical dashed lines in Fig. 4. If the SNR of the spectrum is too low for the widths of at least 2 lines to be measured confidently, we assume a typical width of 3000 km s^{-1} . For velocities lower than this value, we risk biasing our continuum fit to include possible weak emission, and implement 3000 km s^{-1} as a strict lower bound. Additionally, since SNe Iax are known to have narrow line profiles in the nebular phase compared to typical SNe Ia (Foley et al. 2016), we adopt this lower bound for SNe-Iax as well. Because these velocities are simply a proxy for the width of the continuum fit, this method neglects the intricacies of SNe Ia emission profiles, especially since spectroscopically bi-modal SNe Ia are not uncommon (Dong et al. 2015a; Valley et al.

2019a). However, these complications are unimportant for our analysis, and we consider these simple velocity approximations adequate.

When applying the continuum fit to each spectrum, we minimize biasing our continuum by using 3σ clipping to exclude narrow host galaxy lines, telluric absorption, or instrumental artefacts. After fitting the continuum model to the data, we subtract off this continuum and inspect the residuals for emission-line signatures from unbound companion material. For each line in Table 2, we compute 10σ bounds on the integrated line flux in each region similar to Eq. 4 from Leonard & Filippenko (2001). However, for flux-calibrated spectra,

$$F(10\sigma) \equiv EW(10\sigma) \times C_\lambda = 10C_\lambda \Delta I \sqrt{W_{\text{line}} \Delta X} \quad (2)$$

where $F(10\sigma)$ is the 10σ upper limit on the integrated flux, $EW(10\sigma)$ is the corresponding upper limit on the equivalent width, C_λ is the continuum flux at wavelength λ , ΔI is the RMS scatter around a normalised continuum, W_{line} is the width of the line profile, and ΔX is the bin size of the spectrum. We assume W_{line} is equal to the FWHM of a $\sim 1000 \text{ km s}^{-1}$ emission line and provide these values in Table 2. Eq. 2 can be re-written as

$$F(10\sigma) = 10 \Delta f_\lambda \mathcal{F}^{-1} \sqrt{W_{\text{line}} \Delta X} \quad (3)$$

where Δf_λ is the 1σ RMS scatter of the spectrum around the continuum in flux units ($\text{erg s}^{-1} \text{ cm}^{-2} \text{ \AA}^{-1}$) and \mathcal{F}^{-1} is the correction term for masked pixels (see §3.3). Our 10σ statistical limit may seem overly conservative but it does correspond to a line profile that would be visibly obvious (e.g., Fig. 5). Additionally, other studies have run injection-recovery tests to determine the true detection threshold for $\sim 1000 \text{ km s}^{-1}$ emission lines in SNe Ia nebula spectra and a purely statistical $F(3\sigma)$ is difficult to recover (e.g., Sand et al. 2018a).

$F(10\sigma)$ is then converted into a luminosity via the distance moduli listed in Table B3. Distance moduli computed from the SN Ia light curves are used except where more reliable methods are available, such as Cepheid or Tip of the Red Giant Branch (TRGB) distances. Eq. 1 is inverted to numerically calculate a limit on M_{st} , which we consider a conservative upper bound on the amount of mass removed from a non-degenerate companion undergoing RLOF. This is done for each H/He line, retaining the best mass limit for both the H-rich and He-rich models. Note that the strictest mass limit for each model can come from different spectra, as each spectrum will have varying amounts of contamination from host galaxy and telluric lines.

3.3 Mitigating Host Galaxy Emission and Other Contaminants

Due to the comprehensive nature of our sample, some spectra have poor quality, significant host-galaxy emission and/or other contaminants. Pixels affected by host-galaxy emission, telluric absorption, or instrumental artefacts are masked in the ensuing flux limit calculation, ensuring only informative pixels are used in placing our flux upper limit. Masking these pixels also reduces the effective number of

pixels used in the non-detection limit calculation and weakens our statistical limit. In Eq. 3 we include the masked pixel correction term \mathcal{F}^{-1} from Tucker et al. (2018) to correct our limit to a more robust estimate. Concisely, the correction term \mathcal{F} is the fraction of unmasked line flux to total line flux ($\mathcal{F} \in [0, 1]$). Thus, masked pixels decrease \mathcal{F} and increase $F(10\sigma)$, but the effect is weighted by the location of the masked pixels relative to the line centre. For example, the masked narrow host galaxy H α and H β in the bottom panels of Fig. 4 have larger effects on \mathcal{F} than the masked [SII] line at 6713 \AA since [SII] is on the outskirts of the HeI-a line profile. Masking is only implemented when the derived $F(10\sigma)$ is not representative of the true flux limit due to contaminated pixels, we leave weak or minor contamination unmasked as it only solidifies our conservative flux limit and does not introduce extra steps in our analysis.

Another difficulty occurs when the expected emission line is blended with the edge of a steep SN spectral feature. This is especially problematic for 91bg-like and Iax SNe which have intrinsically narrow emission line profiles. If the continuum near H/He varies by more than the amplitude of our flux limit over its FWHM, we increase our flux limit to match the continuum level variation. This results in an unambiguous line profile that would be definitively detected and prevents questionable limits from being included in our statistical analysis.

Some spectra in our study have resolutions of order $\sim 500 \text{ km s}^{-1}$, which approaches the lower end of the expected stripped mass velocity distribution (e.g., Boehner et al. 2017). If broad, unresolved H emission was present in a spectrum, we confirm the host galaxy source with other typical galaxy emission lines such as [OII] (3727 \AA), [OIII] (4959, 5007 \AA), [NII] (6548, 6583 \AA), and [SII] (6713, 6731 \AA). Any unresolved H α emission with velocity widths $\gtrsim 300 \text{ km s}^{-1}$ had at least one other unresolved galaxy emission line in the spectrum, indicating the observed H emission was not from stripped material. Additionally, the recent discovery of broad H α emission in ATLAS18qtd (Prieto et al. 2019) affirms our treatment of galaxy emission lines, as none of the galaxy emission lines discussed previously were present in the discovery spectrum (see §5).

4 RESULTS

We find no evidence of emission from stripped/ablated companion material in any of our nebular phase spectra. Fig. 4 provides an example Baade/MagE spectrum of SN 2015F at +295 days after maximum light, including the observed spectrum, the continuum fit, and the 10σ flux limits for each line. We provide a random selection of H α flux limit cutouts in Fig. 5 and the spectral cutouts for all H and He lines are provided as supplementary material.

The distribution of stripped mass limits are shown for the H-rich and the He-rich cases in Figs. 6 and 7, respectively, with colour-shaded regions indicating the expected amounts of stripped mass from various studies in the literature. Fig. 8 shows the H-rich results using the methods and models of Mattila et al. (2005) and Leonard (2007) for comparison with previous estimates. Table B5 gives the phases, flux limits, and derived H-rich and He-rich mass limits for each SN Ia in our study.

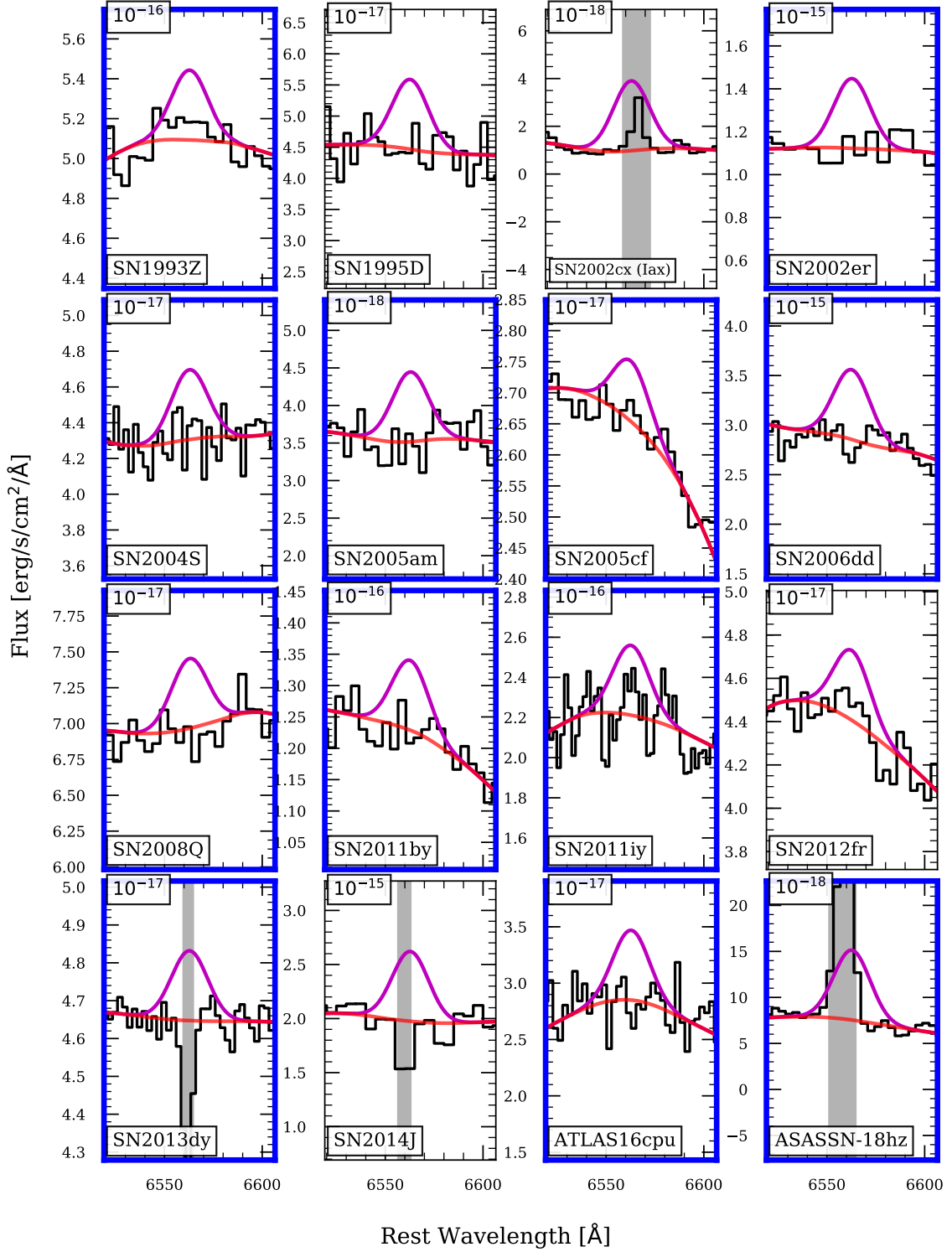


Figure 5. Randomly selected cutouts around H α for a portion of the SNe Ia in this work, including the observed spectrum (black), the continuum fit (red), and the empirical 10 σ line limit (purple). The scale for each spectrum is denoted in the top-left of each panel. Light grey areas mark masked regions (see text) and completely grey boxes signify SNe Ia with no spectra covering the wavelength range. Thick blue axes indicate this spectrum was used for the best M_{st} limit provided in Table B5. Cutouts for all SNe Ia and all H/He lines are provided as supplementary material (see Appendix B).

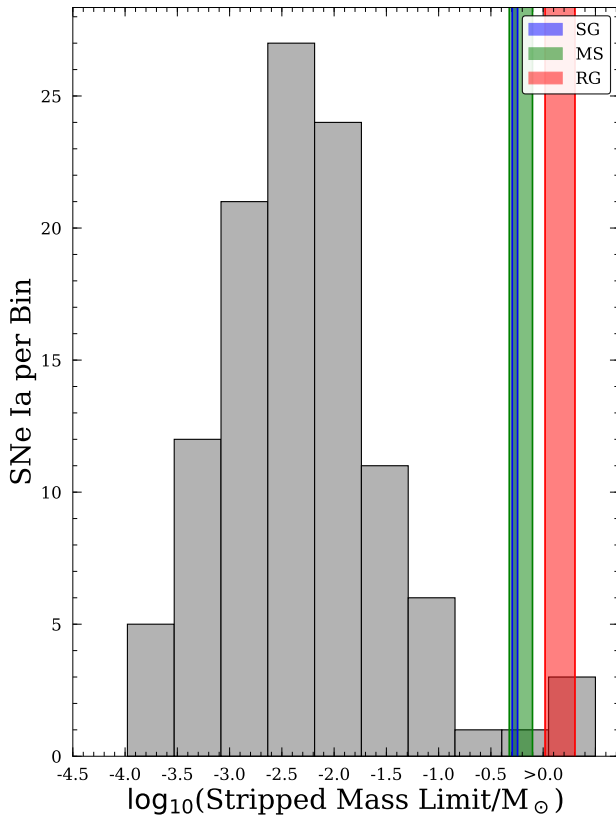


Figure 6. Distribution of mass limits on stripped H-rich material for all SNe Ia in our sample. Colour-shaded areas indicate expected amounts of unbound mass for sub-giant (SG, blue), main-sequence (MS, green), and red-giant (RG, red) companions, taken from Marietta et al. (2000), Pan et al. (2012), and Boehner et al. (2017).

We include the range of mass estimates from an H-rich RLOF companion in Figs. 6 and 8 as shaded regions for main-sequence (MS, blue), sub-giant (SG, green), and red giant (RG, red) companions taken from Marietta et al. (2000), Pan et al. (2012), and Boehner et al. (2017). We take $0.15 M_{\odot}$ as the minimum amount of mass stripped from a companion in the SD scenario, SNe Ia with $M_{st,H} < 0.15 M_{\odot}$ are considered unlikely to have an H-rich SD progenitor system.

For the He-rich SD channel, only Pan et al. (2012) and Liu et al. (2013a) have published models. We include their expected values for mass stripped from a RLOF helium-star companion in Fig. 7 as the magenta shaded area (Liu et al. 2012) and the cyan line (Pan et al. 2012). However, there are several caveats when considering the He-rich model. The expected line luminosities given in Table 2 are for $0.25 M_{\odot}$ of stripped He-rich material, more mass than expected for a true He-donor star. We compare our mass limits to the dedicated He-rich models from Pan et al. (2012), Liu et al. (2013a) and take a limit of $M_{st,He} < 0.023 M_{\odot}$ as our upper limit for He-rich SD systems.

If we assume SNe Ia with $M_{st,H} < 0.15 M_{\odot}$ and $M_{st,He} < 0.023 M_{\odot}$ exclude H-rich and He-rich SD progenitor systems, respectively, we can constrain the observed fraction of SD systems. Based on the non-detections in our sample, we can place observed upper limits on the fraction of SD SNe Ia.

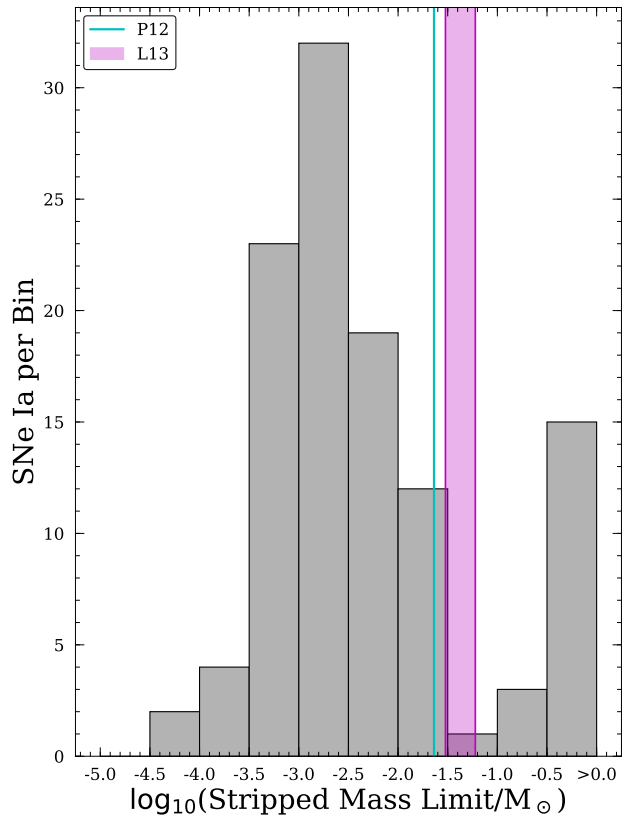


Figure 7. Similar to Fig. 6, except for the He-rich model. The magenta shaded region corresponds to stripped mass estimates from Liu et al. (2013a) and the cyan line marks the estimate from Pan et al. (2012).

For a binomial distribution with N trials and no successes, the upper limit f at a confidence level P can be expressed as

$$f < 1 - (1 - P)^{(N+1)^{-1}} \quad (4)$$

with the results for our sample provided in Table 3. $f_{1\sigma}$ and $f_{3\sigma}$ correspond to the 1σ and 3σ fractional upper limits on SD SNe Ia. For our null detections of unbound mass emission, we place statistical constraints on the fraction of SNe Ia that can form through the classical SD scenario for H-rich and He-rich companions. We do not consider SNe Ia with inadequate limits on M_{st} “successes”, as the spectra do not show any evidence of the expected emission signatures, so these objects are simply omitted from our statistical analysis.

5 DISCUSSION

5.1 Statistical Implications

With our updated modelling and comprehensive sample, we place strict constraints on the fraction of SNe Ia that can form through the classical SD scenario. At most, $\sim 6\%$ of SNe Ia (at 3σ confidence) can stem from the H-rich formation channel, placing the majority of the production of SNe Ia on the DD channel, unless a modification on the

Table 3. Statistics for each sample considered in our study (see §4). N is the number of SNe Ia with $M_{st} < M_{cut}$ and $f_{n\sigma}$ is the $n\sigma$ fractional upper limit on their occurrence. N_{tot} refers to the total number of SNe Ia in that sample.

Sample	N_{tot}	H-rich ($M_{st,H} < 0.15 M_\odot$)			He-rich ($M_{st,He} < 0.023 M_\odot$)		
		N	$f_{1\sigma}$	$f_{3\sigma}$	N	$f_{1\sigma}$	$f_{3\sigma}$
<i>Normal</i>	90	86	< 1.3%	< 6.6%	73	< 1.5%	< 7.7%
<i>91T-like</i>	5	5	< 17.4%	< 62.7%	4	< 20.5%	< 69.4%
<i>91bg-like</i>	8	8	< 12.0%	< 48.2%	7	< 13.4%	< 52.3%
<i>SC</i>	4	4	< 20.5%	< 69.4%	4	< 20.5%	< 69.4%
<i>Iax</i>	4	4	< 20.5%	< 69.4%	4	< 20.5%	< 69.4%
<i>Normal+91T</i>	95	91	< 1.2%	< 6.2%	77	< 1.5%	< 7.3%
<i>Normal+91bg</i>	98	94	< 1.2%	< 6.0%	80	< 1.4%	< 7.0%
<i>Normal+91T+91bg</i>	103	99	< 1.1%	< 5.7%	84	< 1.3%	< 6.7%
<i>Normal+91T+91bg+SC</i>	107	103	< 1.1%	< 5.5%	88	< 1.3%	< 6.4%
<i>All</i>	111	107	< 1.1%	< 5.3%	92	< 1.2%	< 6.2%

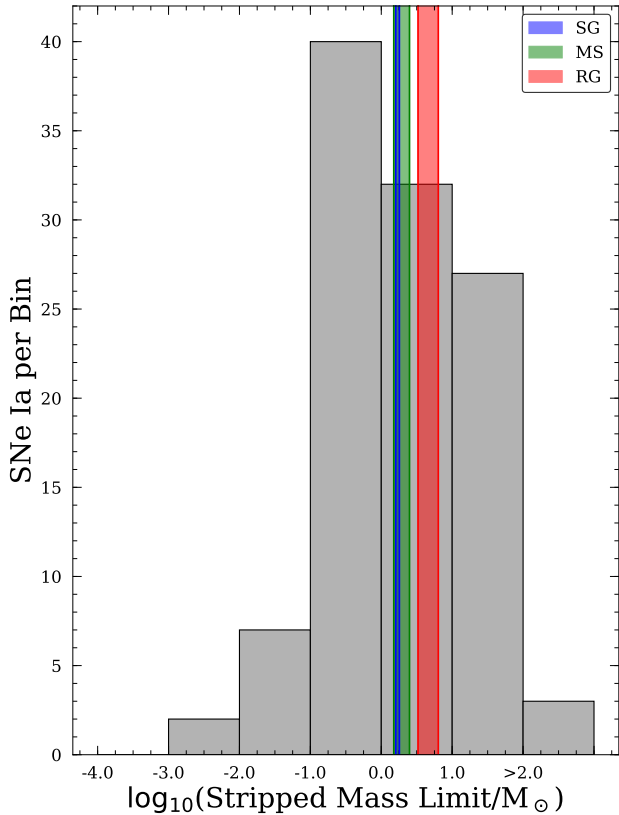


Figure 8. Similar to Fig. 6, except using the models of Mattila et al. (2005). The assumed linear scaling between luminosity and stripped mass leads to higher derived M_{st} .

SD scenario can prevent nearly all SNe Ia from exhibiting these expected H and He emission signatures such as the spin-up/spin-down scenario (Justham 2011; Di Stefano et al. 2011; Meng & Podsiadlowski 2013). Considering the simplest case of only spectroscopically normal SNe Ia, we place a 1σ (3σ) upper limit on SD progenitors of $< 1.3\%$ ($< 6.6\%$). The full statistical results are provided in Table 3, and we use the *Normal+91T+91bg+SC* sample as the most representative sample from our survey. Unfortunately, our sample prevents an analysis of under- versus over-luminous SNe Ia, as we

are biased towards brighter SNe Ia (Fig. 1). This highlights the importance of volume-limited surveys such as 100IAs (Dong et al. 2015a). Still, these stringent constraints on the observed rate of SD SNe Ia provide strong evidence for the DD channel producing the majority of SNe Ia.

We separately consider spectroscopic sub-classes at the extreme edges of the Phillips Relation. Because these SNe Ia are thought to be on the edges of typical SN Ia formation, we compare the derived stripped mass limits to the same expected stripped mass values as normal SNe Ia. Our sample has 8 91bg-like and 5 91T-like SNe Ia, for which we place 1σ (3σ) upper limits on H-rich SD progenitors at $< 12.0\%$ ($< 48.2\%$) and $< 17.4\%$ ($< 62.7\%$), respectively. It is worth mentioning that the stripped mass models assume a normal SN Ia explosion and the effects of under- and over-luminous SNe Ia on the amount of stripped material has yet to be investigated.

For SNe Iax and “Super Chandrasekhar” (SC) SNe Ia, it is worth discussing their characteristics and applicability to our study. The Iax sub-type (Foley et al. 2013) is thought to stem from an entirely different formation mechanism and are not observed to enter a nebular phase but instead have photospheric properties (Foley et al. 2016). Our study includes 4 such systems: SNe 2002cx, 2005hk, 2008A, and 2012Z. Liu et al. (2013b) investigated the expected values of unbound mass for these systems if in a SD system, finding significantly lower values of $M_{st,H} \approx 0.013 - 0.016 M_\odot$ compared to the typical $\sim 0.1 - 0.5 M_\odot$ range. All Iax SNe Ia in our sample have $M_{st,H} < 0.013 M_\odot$, so the statistics are unchanged if the more stringent mass limit is employed. However, even if material is unbound from non-degenerate donor stars in these SNe Ia, it is unclear if this material would be visible at late times. For these reasons, our main statistical analysis excludes these objects.

Our sample also includes 4 “Super Chandrasekhar” (SC) SNe Ia explosions (SNe 2006gz, 2007if, 2009dc, and SNF 20080723-012), where the inferred ejecta mass, M_{ej} , is higher than the Chandrasekhar mass of $\approx 1.4 M_\odot$ (e.g., Howell et al. 2006; Scalzo et al. 2019) although the nomenclature is currently debated (Chen et al. 2019). The preferred formation theory of SC SNe Ia involves a DD merger of two WDs with a combined mass above the Chandrasekhar mass (Tutukov & Yungelson 1994; Howell 2001), although SD progenitors have also been proposed (Yoon & Langer

2005). Because these objects do enter a nebular phase and have possible SD progenitors, we include these SNe Ia in our preferred sample.

For completeness and comparison to the literature, we also derive mass limits using the prior models of Marietta et al. (2000) and Mattila et al. (2005) which are shown in Fig. 8. Considering the same preferred *Normal+91T+91bg+SC* sample, we still rule out H-rich non-degenerate companions ($M_{st,H} < 0.15 M_\odot$) for 60 SNe Ia, corresponding to a 1σ (3σ) fractional upper limit of $< 1.9\%$ ($< 9.2\%$). This result differs slightly from the upper limit provided in Table 3 due to the assumed linear scaling between stripped mass and emitted luminosity (e.g., Leonard 2007).

In addition to the observational limitations discussed in §3, the models used in this work are developed for normal SNe Ia. Over- and under-luminous explosions will likely differ in the amount of stripped material from a companion star due to the differing expansion velocities (e.g., Benetti et al. 2005; Blondin et al. 2012; Folatelli et al. 2013) and amount of ejecta mass (e.g., Cappellaro et al. 1997; Scalzo et al. 2014, 2019). Additionally, the SN luminosity depends on the amount of Ni synthesized in the explosion (e.g., Arnett 1982; Cappellaro et al. 1997; Stritzinger et al. 2006b), indicating SNe Ia with lower Ni mass will have less gamma-ray production to power the $\text{H}\alpha$ emission (i.e., a reduced $L_{\text{H}\alpha}$). These effects likely superimpose, as under-luminous SNe Ia will strip less mass and synthesize less Ni, but the magnitude of these effects is currently unexplored in the literature. We encourage the modeling of other SNe Ia subtypes in future works.

5.2 The Exclusion of SNe Ia-CSM

SNe Ia-CSM, which show interaction with a nearby circumstellar environment, are a rare class of thermonuclear explosions for which SN 2002ic is the prototype (Wang et al. 2004). These events preferentially occur in star-forming host galaxies and generally have broad, over-luminous light curves ($M_R \sim -20$ mag, Silverman et al. 2013). The observed $\text{H}\alpha$ emission in SNe Ia-CSM usually appears near maximum light, has luminosities of $L_{\text{H}\alpha} \sim 10^{40-41} \text{ ergs s}^{-1}$, and have velocity widths on the order of $\sim 2000 \text{ km s}^{-1}$. SNe Ia-CSM are broadly thought to stem from SD progenitor systems (e.g., Han & Podsiadlowski 2006), although DD progenitors have also been proposed (Livio & Riess 2003).

Even among this rare class of SNe Ia there are peculiar events that do not conform to the “standard” properties. In particular, ASASSN-18tb (Kollmeier et al. 2019; Valley et al. 2019b) was an under-luminous explosion, occurred in an elliptical host galaxy with little star formation, and had (comparatively) weak $\text{H}\alpha$ emission ($L_{\text{H}\alpha} \sim 10^{38} \text{ ergs s}^{-1}$), inconsistent with typical SNe Ia-CSM. Additionally, there are cases where the $\text{H}\alpha$ emission does not appear until later in the SN’s evolution, referred to as “delayed-onset” SNe Ia-CSM (e.g., Graham et al. 2019).

$\text{H}\alpha$ emission is also expected for material stripped from a companion, therefore differentiating between SNe Ia-CSM and SNe Ia with stripped material emission is an important distinction. Stripped companion material will have significantly lower velocities than the expanding SN ejecta ($v_{\text{strip}} \sim 10^3 \text{ km s}^{-1}$ versus $v_{\text{ej}} \sim 10^4 \text{ km s}^{-1}$), shrouding the H-emitting material with the optically-thick photosphere until

the SN enters the nebular phase ($\sim 150-180$ days after maximum light). Thus, we exclude all objects with broad $\text{H}\alpha$ detected < 100 days after maximum light. The only SN Ia-CSM that passes this criterion is SN 2015cp, a delayed-onset SN Ia-CSM (Graham et al. 2019).

While it is possible that the $\text{H}\alpha$ emission observed in SN 2015cp is from material stripped from a companion, we find this scenario unlikely. The classification spectrum taken by PESSTO (Smartt et al. 2015b) at ~ 45 days after maximum excludes the presence of PTF11kx-like $\text{H}\alpha$ emission at 10σ (Graham et al. 2019). The next spectrum was acquired at ~ 700 days after maximum light and exhibited broad $\text{H}\alpha$ emission with $v_{\text{FWHM}} \approx 2400 \text{ km s}^{-1}$ and $L_{\text{H}\alpha} \approx 10^{38} \text{ ergs s}^{-1}$. This measured $L_{\text{H}\alpha}$ is an order of magnitude higher than the $\text{H}\alpha$ luminosity extrapolated from Eq. 1 at ~ 710 days after explosion, although the models have not been tested at these epochs. Additionally, the $\text{H}\alpha$ flux decreases sharply at ~ 730 days after peak by a factor of ≈ 3 over the span of ~ 90 days, inconsistent with $\text{H}\alpha$ emission powered by radioactively-decaying SN ejecta which would roughly follow the SN bolometric luminosity. These properties are consistent with CSM interaction, attributing the abrupt flux decrement to the shock passing through the CSM material. For these reasons we consider SN 2015cp a likely SN Ia-CSM and exclude it from our analysis, although further modeling is encouraged to definitively determine mass estimates.

5.3 Time-Varyable and Blue-Shifted Sodium Absorption

Another subset of SNe Ia with interesting properties are objects with time-varying and blue-shifted NaID absorption, for which SN 2006X is the prototype (Patat et al. 2007). The NaID absorption is thought to stem from NaID material near the explosion that photo-ionizes during the early phases of the explosion and produces the absorption lines as the NaID material cools and recombines (e.g., Simon et al. 2009). However, the origin of the NaID material is unclear and proposed sources include wind from a SD progenitor system (e.g., Patat et al. 2007), circumstellar debris from a DD merger (e.g., Raskin & Kasen 2013), or even nearby gas clouds within the host galaxy (Chugai 2008).

Sternberg et al. (2011) analyzed a set of 35 SNe Ia and found 22 exhibit some form of NaID absorption profiles, with 12 having blue-shifted (relative the host-galaxy velocity) NaID profiles. However, comparing their SNe Ia sample to a sample of core collapse (CC) SNe could not statistically confirm the two sets come from different parent populations (i.e., the source for SNe Ia and CC SNe NaID absorption could be the same). Additionally, the blue-shifted NaID profiles are preferentially observed in spiral galaxies, indicating age or host-galaxy environment may play a role in the NaID interpretation.

Another prediction for NaID absorption associated with the SN Ia progenitor system is a time-variable NaID equivalent width, as the NaID material will recombine at different times depending on the distance from the explosion. Sternberg et al. (2014) searched for time-varying NaID absorption in a sample of 14 objects and found 3 SNe Ia that meet this criterion (PTF11kx, SNe 2006X and 2007le). With these detections, Sternberg et al. (2014) found $18 \pm 11\%$ of SNe Ia have variable NaID profiles and thus could be produced by a

SD progenitor system, in conflict with the results presented here. One of these objects is a known SNe Ia-CSM that we exclude from the sample (PTF11kx, [Dilday et al. 2012](#)), but SNe 2006X and 2007le are both in our nebular sample and have strict constraints on stripped companion material ($M_{st} < 4 \times 10^{-5} M_\odot$ for SN 2006X and $M_{st} < 3 \times 10^{-3} M_\odot$ for SN 2007le). We discuss these discrepancies further in §5.4.

5.4 The Lack of a Consistent Theory for SNe Ia Progenitors

Besides this work, there are several other studies which place quantitative or qualitative limits on the fraction of SD progenitor systems using a range of wavelengths and techniques (e.g., [Gilfanov & Bogdán 2010](#); [Hayden et al. 2010](#); [Bianco et al. 2011](#); [Brown et al. 2012](#); [Chomiuk et al. 2016](#)). Most of these studies focus on WD+RG systems, as these are the easiest to observationally detect. Each study individually does not definitively rule out SD SNe Ia progenitors, however, when considered as a whole it is clear that most SNe Ia cannot form through the classical SD scenario. Thus, the DD scenario likely account for the majority of normal SNe Ia. However, detecting and characterising double WD binaries is exceptionally difficult (e.g., [Rebassa-Mansergas et al. 2018](#)).

Reconciling limits on SD progenitors with SD-favored SNe (i.e., SNe Ia-CSM and SNe Ia with variable NaID) has long been a difficulty for the community. Especially interesting are the systems with conflicting interpretations, such as SN 2007le and ASASSN-18bt. SN 2007le exhibits time-variable, blue-shifted NaID absorption ([Sternberg et al. 2014](#)) but has stringent limits on stripped material emission (this work, Table B5). Similarly, ASASSN-18bt showed a two-component rising light curve ([Shappee et al. 2019](#); [Dimitriadis et al. 2019b](#)), a potential signature for SN ejecta impacting a nearby companion ([Kasen 2010](#)). However, nebular spectra rule out any stripped material emission with strict upper limits ([Tucker et al. 2018](#); [Dimitriadis et al. 2019a](#), this work). While the discrepancies for both SNe Ia can also be explained with alternative theories (e.g., Ni⁵⁶ mixing for the two-component rise in ASASSN-18bt and DD merger debris for the NaID absorption in SN 2007le), these objects highlight the uncertainties that still surround SN Ia progenitors.

Recently, ATLAS18qtd (SN 2018cqj) was discovered to exhibit time-variable H α emission in the nebular phase ([Prieto et al. 2019](#)). The spectra were posted after the submission of this manuscript, however, it warrants a brief discussion here. The classification spectrum taken at 19 days after maximum has no evidence for H emission, and the next spectrum was not acquired until ~ 190 days after maximum. The measured H α luminosity declines contemporaneously with the SN Ia luminosity, a key expectation for material stripped from a SD progenitor. However, there are only two measurements of the H α emission and the inferred mass of the stripped material ($M_{st} \approx 10^{-3} M_\odot$) is far lower than expected ($\sim 0.1 - 0.5 M_\odot$). ATLAS18qtd is an under-luminous explosion, so it is possible the stripped material will be lower than expected from simulations in the literature, but the extent of these effects is still unexplored. Late-time observations of this unique object may yet further constrain the evolution of the H α emission and help elucidate its origin. If

we assume ATLAS18qtd is indeed a SD progenitor system, this discovery highlights the inherent rarity of such events compared to the typical SN Ia population.

There is also the possibility that stripped material does exist in our sample but is invisible due to observational factors. The radioactively-decaying SN Ia ejecta provides a power source for the stripped material, namely gamma-ray deposition. Since we only analyze spectra that are in the nebular phase we are probing the innermost regions of the explosion. SNe Ia at these epochs essentially have no photosphere, and thus have no way of shrouding the H α -emitting material. No such mechanism or process has been proposed to suppress the expected H α emission, so we consider this possibility unlikely. We conclude most SNe Ia cannot have formed from a classical SD progenitor system based on this work.

6 CONCLUSION

We present a large, comprehensive search for emission expected from stripped companion material in the SD formation scenario of SNe Ia. Using 227 spectra of 111 SNe Ia from a variety of telescopes and instruments, we find no evidence for any stripped material emission in our sample. Using these null detections, we place statistical constraints on the fraction of SNe Ia that can form through the classical RLOF SD scenario, finding $< 5.5\%$ and $< 6.4\%$ of SNe Ia can form through the H-rich and He-rich channels, respectively, at 3σ confidence. The lack of emission is difficult to reconcile with the classical SD formation scenario for SNe Ia, and provides unique constraints on the production mechanism of these phenomena.

Thus far, there has not been a proposed formation mechanism that adequately reproduces all aspects of SN Ia properties. There seems to be contributions from both SD and DD progenitors to the total SN Ia rate (e.g., Sec. 4.1 from [Maoz et al. 2014](#)), yet the exact distribution is widely debated. Reconciling seemingly conflicting results (e.g., this work versus [Sternberg et al. 2014](#)) has long been a difficulty. Any unifying theory for SNe Ia formation must account for all the observed characteristics of these phenomena and the seemingly conflicting results across various methodologies. If the SD channel does produce a significant fraction of SNe Ia, there must be an unincorporated physical process in previous modeling efforts to explain our non-detections of stripped material. Alternatively, most SNe Ia must form from DD systems to match the results presented here.

Facilities: duPont, Magellan, Very Large Telescope
Software: Python2.7, astropy ([The Astropy Collaboration et al. 2018](#)), astroquery ([Ginsburg et al. 2019](#)) numpy, scipy, PyMUSE ([Pessa et al. 2018](#)), SpectRes ([Carnall 2017](#)), extinction¹⁵, SExtractor ([Bertin & Arnouts 1996](#)), Montage¹⁶, Lpipe, IDL8.6, LowRedux, IRAF, SNooPy ([Burns et al. 2011](#))

¹⁵ <https://github.com/kbarbary/extinction>

¹⁶ <http://montage.ipac.caltech.edu/>

ACKNOWLEDGEMENTS

We thank K. Maguire, K. Graham, K. Motohara, K. Maeda, S. Taubenberger, T. Diamond, G. Dimitriadis, C. Ashall, and D. Sand for supplying nebular spectra. We thank A. Laity for assisting with the KOA data search and retrieval. Additionally, we thank C. Auge, G. Anand, A. Payne, and O. Graur for useful conversations about the project. We thank P. Chen from providing several SNe Ia light curves prior to publication. Also, many thanks to Bev Wills for her help tracking down the information regarding the nebular spectrum of SN 1981B.

M.A.T. acknowledges support from the United States Department of Energy through the Computational Sciences Graduate Fellowship (DOE CSGF) through grant DE-SC0019323. B.J.S is supported by NSF grants AST-1908952, AST-1920392, and AST-1911074. M.D.S. is supported in part by a generous grant (13261) from VILLUM FONDEN and a project grant from the Independent Research Fund Denmark. Support for J.L.P. is provided in part by FONDECYT through the grant 1191038 and by the Ministry of Economy, Development, and Tourism's Millennium Science Initiative through grant IC120009, awarded to The Millennium Institute of Astrophysics, MAS. P.J.V. is supported by the National Science Foundation Graduate Research Fellowship Program Under Grant No. DGE-1343012. C.S.K. is supported by NSF grants AST-1515876, AST-1515927 and AST-181440. C.S.K. is also supported by a fellowship from the Radcliffe Institute for Advanced Studies at Harvard University.

This work is Based on (in part) observations collected at the European Organisation for Astronomical Research in the Southern Hemisphere under ESO programmes 0100.D-0191(A), 0101.D-0173(A), 0102.D-0287(A), and 096.D-0296(A). This paper includes data gathered with the 6.5 meter Magellan Telescopes located at Las Campanas Observatory, Chile. The CSP has been supported by the National Science Foundation under grants AST0306969, AST0607438, AST1008343, AST1613426, and AST1613472.

This paper made use of the modIDL spectral data reduction reduction pipeline developed in part with funds provided by NSF Grant AST-1108693.

This research made use of Montage. It is funded by the National Science Foundation under Grant Number ACI-1440620, and was previously funded by the National Aeronautics and Space Administration's Earth Science Technology Office, Computation Technologies Project, under Cooperative Agreement Number NCC5-626 between NASA and the California Institute of Technology.

This work has made use of data from the European Space Agency (ESA) mission *Gaia* (<https://www.cosmos.esa.int/gaia>), processed by the *Gaia* Data Processing and Analysis Consortium (DPAC, <https://www.cosmos.esa.int/web/gaia/dpac/consortium>). Funding for the DPAC has been provided by national institutions, in particular the institutions participating in the *Gaia* Multilateral Agreement.

The Pan-STARRS1 Surveys (PS1) and the PS1 public science archive have been made possible through contributions by the Institute for Astronomy, the University of Hawaii, the Pan-STARRS Project Office, the Max-Planck Society and its participating institutes, the Max Planck In-

stitute for Astronomy, Heidelberg and the Max Planck Institute for Extraterrestrial Physics, Garching, The Johns Hopkins University, Durham University, the University of Edinburgh, the Queen's University Belfast, the Harvard-Smithsonian Center for Astrophysics, the Las Cumbres Observatory Global Telescope Network Incorporated, the National Central University of Taiwan, the Space Telescope Science Institute, the National Aeronautics and Space Administration under Grant No. NNX08AR22G issued through the Planetary Science Division of the NASA Science Mission Directorate, the National Science Foundation Grant No. AST-1238877, the University of Maryland, Eotvos Lorand University (ELTE), the Los Alamos National Laboratory, and the Gordon and Betty Moore Foundation.

Based on observations obtained at the Gemini Observatory acquired through the Gemini Observatory Archive and processed with the Gemini PyRAF package, which is operated by the Association of Universities for Research in Astronomy, Inc., under a cooperative agreement with the NSF on behalf of the Gemini partnership: the National Science Foundation (United States), the National Research Council (Canada), CONICYT (Chile), Ministerio de Ciencia, Tecnología e Innovación Productiva (Argentina), and Ministério da Ciência, Tecnologia e Inovação (Brazil).

This paper makes use of data obtained from the Isaac Newton Group of Telescopes Archive which is maintained as part of the CASU Astronomical Data Centre at the Institute of Astronomy, Cambridge.

The LBT is an international collaboration among institutions in the United States, Italy and Germany. LBT Corporation partners are: The University of Arizona on behalf of the Arizona Board of Regents; Istituto Nazionale di Astrofisica, Italy; LBT Beteiligungsgesellschaft, Germany, representing the Max-Planck Society, The Leibniz Institute for Astrophysics Potsdam, and Heidelberg University; The Ohio State University, and The Research Corporation, on behalf of The University of Notre Dame, University of Minnesota and University of Virginia.

REFERENCES

- Abazajian K., et al., 2005, *AJ*, **129**, 1755
- Abolfathi B., et al., 2018, *The Astrophysical Journal Supplement Series*, **235**, 42
- Adelman-McCarthy J. K., et al., 2008, *The Astrophysical Journal Supplement Series*, **175**, 297
- Akerlof C., et al., 2007, Central Bureau Electronic Telegrams, **1059**, 2
- Aksenov E. P., 1981, International Astronomical Union Circular, **3580**, 1
- Altavilla G., et al., 2004, *MNRAS*, **349**, 1344
- Amanullah R., et al., 2014, *ApJ*, **788**, L21
- Andersen J., et al., 1995, *The Messenger*, **79**, 12
- Angel J. R. P., et al., 1979, in *The MMT and the Future of Ground-Based Astronomy*, Proceedings of a Symposium held to mark the dedication of the Multiple Mirror Telescope at the Mount Hopkins Observatory, Arizona on May 9, 1979. Edited by Trevor C. Weekes. SAO Special Report #385, 1979., p.87. p. 87
- Antognini J. M., et al., 2014, *MNRAS*, **439**, 1079
- Anupama G. C., et al., 2005, *A&A*, **429**, 667
- Appenzeller I., et al., 1998, *The Messenger*, **94**, 1

- Arbour R., et al., 1999, International Astronomical Union Circular, [7156](#), 1
- Arbour R., et al., 2004, International Astronomical Union Circular, [8406](#), 1
- Arcavi I., et al., 2014, The Astronomer's Telegram, [6661](#), 1
- Ardeberg A., et al., 1973, A&A, [28](#), 295
- Argyle R. W., et al., 1994, International Astronomical Union Circular, [5976](#), 3
- Armstrong M., et al., 1999, International Astronomical Union Circular, [7108](#), 1
- Arnett W. D., 1982, ApJ, [253](#), 785
- Ayani K., et al., 1998, International Astronomical Union Circular, [6878](#), 2
- Ayani K., et al., 1998, International Astronomical Union Circular, [6905](#), 1
- Bacon R., et al., 2010, in Proceedings of the SPIE, Volume 7735, id. 773508 (2010).., doi:[10.1117/12.856027](#)
- Barbon R., et al., 1972, International Astronomical Union Circular, [2411](#), 1
- Barbon R., et al., 1982, A&A, [116](#), 35
- Barbon R., et al., 1990, A&A, [237](#), 79
- Benetti S., et al., 1995, International Astronomical Union Circular, [6135](#), 1
- Benetti S., et al., 2004, MNRAS, [348](#), 261
- Benetti S., et al., 2005, ApJ, [623](#), 1011
- Benetti S., et al., 2017, The Astronomer's Telegram, [11036](#), 1
- Benn C., et al., 2008, in Ground-based and Airborne Instrumentation for Astronomy II. Edited by McLean, Ian S.; Casali, Mark M. Proceedings of the SPIE, Volume 7014, article id. 70146X, 12 pp. (2008).., doi:[10.1117/12.788694](#)
- Bertin E., et al., 1996, *Astronomy and Astrophysics Supplement Series*, [117](#), 393
- Beutler B., et al., 2003, International Astronomical Union Circular, [8197](#), 1
- Bianco F. B., et al., 2011, ApJ, [741](#), 20
- Black C. S., et al., 2016, MNRAS, [462](#), 649
- Blakeslee J. P., et al., 2010, ApJ, [724](#), 657
- Blanco V. M., et al., 1980, International Astronomical Union Circular, [3556](#), 2
- Blanco V. M., et al., 1986, International Astronomical Union Circular, [4224](#), 1
- Blondin S., et al., 2008, Central Bureau Electronic Telegrams, [1198](#), 1
- Blondin S., et al., 2012, AJ, [143](#)
- Boehner P., et al., 2017, MNRAS, [465](#), 2060
- Botyánszki J., et al., 2017, ApJ, [845](#)
- Botyánszki J., et al., 2018, ApJ, [852](#)
- Branch D., et al., 1993, AJ, [106](#), 2383
- Breare J. M., et al., 1987, MNRAS, [227](#), 909
- Brimacombe J., et al., 2011, Central Bureau Electronic Telegrams, [2928](#), 1
- Brimacombe J., et al., 2014a, The Astronomer's Telegram, [6737](#), 1
- Brimacombe J., et al., 2014b, The Astronomer's Telegram, [6803](#), 1
- Brimacombe J., et al., 2015, The Astronomer's Telegram, [6950](#), 1
- Brimacombe J., et al., 2016, The Astronomer's Telegram, [8979](#), 1
- Brimacombe J., et al., 2017, The Astronomer's Telegram, [10108](#), 1
- Brimacombe J., et al., 2018, The Astronomer's Telegram, [11521](#), 1
- Brown P. J., et al., 2012, ApJ, [749](#)
- Brown P. J., et al., 2014, Ap&SS, [354](#), 89
- Brown P. J., et al., 2015, ApJ, [805](#), 74
- Brown J. S., et al., 2016, The Astronomer's Telegram, [9666](#), 1
- Brown J. S., et al., 2018, The Astronomer's Telegram, [11253](#), 1
- Buckley D. A. H., et al., 2006, in Society of Photo-Optical Instrumentation Engineers (SPIE) Conference Series. p. 62690A,
- doi:[10.1117/12.673838](#)
- Bues I., et al., 1986, International Astronomical Union Circular, [4215](#), 2
- Bureau M., et al., 1996, ApJ, [463](#), 60
- Burns C. R., et al., 2011, AJ, [141](#)
- Burns C. R., et al., 2014, ApJ, [789](#), 32
- Busko I., et al., 1981, International Astronomical Union Circular, [3589](#), 2
- Buta R. J., et al., 1983, *Publications of the Astronomical Society of the Pacific*, [95](#), 72
- Buzzoni B., et al., 1984, The Messenger, [38](#), 9
- Cacella P., et al., 2002, International Astronomical Union Circular, [7847](#), 1
- Canal R., et al., 2001, ApJ, [550](#), L53
- Candia P., et al., 2003, *Publications of the Astronomical Society of the Pacific*, [115](#), 277
- Cappellari M., et al., 2011, MNRAS, [413](#), 813
- Cappellaro E., et al., 1997, A&A, [328](#), 203
- Cappellaro E., et al., 2001, ApJ, [549](#), L215
- Carnall A. C., 2017, preprint, p. arXiv:[1705.05165](#) (arXiv:1705.05165)
- Casper C., et al., 2013, Central Bureau Electronic Telegrams, [3588](#), 1
- Catinella B., et al., 2005, AJ, [130](#), 1037
- Cenko S. B., et al., 2011, The Astronomer's Telegram, [3583](#), 1
- Cenko S. B., et al., 2012, Central Bureau Electronic Telegrams, [3014](#), 1
- Cepa J., 2010, *Astrophysics and Space Science Proceedings*, [14](#), 15
- Challis P., et al., 2009, Central Bureau Electronic Telegrams, [2025](#), 1
- Chambers K. C., et al., 2016, preprint, p. arXiv:[1612.05560](#) (arXiv:1612.05560)
- Chen P., et al., 2019, ApJ, [880](#), 35
- Childress M. J., et al., 2015, MNRAS, [454](#), 3816
- Childress M. J., et al., 2016, *Publications of the Astronomical Society of Australia*, [33](#), e055
- Chomiuk L., et al., 2016, ApJ, [821](#), 119
- Chornock R., et al., 2000, International Astronomical Union Circular, [7463](#), 1
- Christensen L., et al., 2003, A&A, [401](#), 479
- Chugai N. N., 1986, Soviet Ast., [30](#), 563
- Chugai N. N., 2008, *Astronomy Letters*, [34](#), 389
- Colless M., et al., 2003, arXiv e-prints, pp astro-ph/0306581
- Collobert M., et al., 2006, MNRAS, [370](#), 1213
- Contreras C., et al., 2010, AJ, [139](#), 519
- Corsini E. M., et al., 2003, ApJ, [599](#), L29
- Cortini G., et al., 2014, Central Bureau Electronic Telegrams, [3911](#), 1
- Cousins A. W. J., 1972, *Information Bulletin on Variable Stars*, [700](#), 1
- Cox L., et al., 2010, Central Bureau Electronic Telegrams, [2612](#), 1
- Cox L., et al., 2011, Central Bureau Electronic Telegrams, [2676](#), 1
- Cragg T., et al., 1981, International Astronomical Union Circular, [3583](#), 1
- Cristiani S., et al., 1992, A&A, [259](#), 63
- Cumming R. J., et al., 1994, International Astronomical Union Circular, [5951](#), 1
- D'Odorico S., 1990, The Messenger, [61](#), 51
- D'Onofrio M., et al., 1995, A&A, [296](#), 319
- Delgado A., et al., 2016, Transient Name Server Discovery Report, [2016-485](#), 1
- Di Stefano R., et al., 2011, ApJ, [738](#), L1
- Dilday B., et al., 2012, Science, [337](#), 942
- Dimitriadis G., et al., 2014, The Astronomer's Telegram, [6749](#), 1
- Dimitriadis G., et al., 2019a, ApJ, [870](#), L14

- Dimitriadis G., et al., 2019b, *ApJ*, **870**, L1
 Dong S., et al., 2015a, *MNRAS*, **454**, L61
 Dong S., et al., 2015b, The Astronomer's Telegram, **7447**, 1
 Dong S., et al., 2018a, *MNRAS*, **479**, L70
 Dong S., et al., 2018b, The Astronomer's Telegram, **11346**, 1
 Dopita M., et al., 2007, *Ap&SS*, **310**, 255
 Dopita M., et al., 2010, *Ap&SS*, **327**, 245
 Downes D., et al., 1993, *ApJ*, **414**, L13
 Drake A. J., et al., 2011a, Central Bureau Electronic Telegrams, **2636**, 1
 Drake A. J., et al., 2011b, Central Bureau Electronic Telegrams, **2703**, 1
 Drescher C., et al., 2012, Central Bureau Electronic Telegrams, **3346**, 1
 Dressler A., et al., 2003, International Astronomical Union Circular, **8198**, 2
 Dressler A., et al., 2011, *Publications of the Astronomical Society of the Pacific*, **123**, 288
 Elias J. H., et al., 1983, *ApJ*, **268**, 718
 Elias-Rosa N., et al., 2005, International Astronomical Union Circular, **8479**, 3
 Elias-Rosa N., et al., 2006, *MNRAS*, **369**, 1880
 Epinat B., et al., 2008, *MNRAS*, **388**, 500
 Evans R., et al., 1986, International Astronomical Union Circular, **4208**, 1
 Evans R., et al., 2003, International Astronomical Union Circular, **8171**, 1
 Evans D. W., et al., 2018, preprint, p. arXiv:1804.09368
 (arXiv:1804.09368)
 Everson R. W., et al., 2017, The Astronomer's Telegram, **10518**, 1
 Faber S. M., et al., 2003, in Instrument Design and Performance for Optical/Infrared Ground-based Telescopes. Edited by Iye, Masanori; Moorwood, Alan F. M. Proceedings of the SPIE, Volume 4841, pp. 1657–1669 (2003).. pp 1657–1669, doi:10.1117/12.460346
 Fabricant D., et al., 1998, *Publications of the Astronomical Society of the Pacific*, **110**, 79
 Falco E. E., et al., 1999, *Publications of the Astronomical Society of the Pacific*, **111**, 438
 Feast M. W., et al., 1986, International Astronomical Union Circular, **4210**, 1
 Filippenko A. V., et al., 1999, International Astronomical Union Circular, **7108**, 2
 Filippenko A. V., et al., 2007, Central Bureau Electronic Telegrams, **1101**, 1
 Fink M., et al., 2010, *A&A*, **514**, A53
 Firth R. E., et al., 2015, *MNRAS*, **446**, 3895
 Fitzpatrick E. L., 1999, *Publications of the Astronomical Society of the Pacific*, **111**, 63
 Flewelling H. A., et al., 2016, preprint, p. arXiv:1612.05243
 (arXiv:1612.05243)
 Folatelli G., et al., 2010a, *AJ*, **139**, 120
 Folatelli G., et al., 2010b, Central Bureau Electronic Telegrams, **2390**, 1
 Folatelli G., et al., 2013, *ApJ*, **773**
 Foley R. J., et al., 2013, *ApJ*, **767**, 57
 Foley R. J., et al., 2014, *MNRAS*, **443**, 2887
 Foley R. J., et al., 2015, *ApJ*, **798**, L37
 Foley R. J., et al., 2016, *MNRAS*, **461**, 433
 Foley R. J., et al., 2018, *MNRAS*, **475**, 193
 Ford C. H., et al., 1993, *AJ*, **106**, 1101
 Fossey S. J., et al., 2014, Central Bureau Electronic Telegrams, **3792**, 1
 Freedman W. L., et al., 2001, *ApJ*, **553**, 47
 Freudling W., et al., 2013, *A&A*, **559**, A96
 Friedman A. S., et al., 2015, *The Astrophysical Journal Supplement Series*, **220**
 Frieman J., et al., 2006, International Astronomical Union Circular, **8754**, 1
 Frohmaier C., et al., 2015, The Astronomer's Telegram, **7452**, 1
 Frye R., et al., 1972, International Astronomical Union Circular, **2398**, 1
 Fukugita M., et al., 1996, *AJ*, **111**, 1748
 Gagliano R., et al., 2016, Transient Name Server Discovery Report, **2016-761**, 1
 Gagliano R., et al., 2017, Transient Name Server Discovery Report, **2017-961**, 1
 Gaia Collaboration et al., 2016, *A&A*, **595**, A1
 Gaia Collaboration et al., 2018, preprint, p. arXiv:1804.09365
 (arXiv:1804.09365)
 Galbany L., et al., 2014, *A&A*, **572**, A38
 Galbany L., et al., 2016, *MNRAS*, **457**, 525
 Gall C., et al., 2018, *A&A*, **611**, A58
 Ganeshalingam M., et al., 2010, *The Astrophysical Journal Supplement Series*, **190**, 418
 Gao J., et al., 2015, *ApJ*, **807**, L26
 Garnavich P. M., et al., 2004, *ApJ*, **613**, 1120
 Garradd G. J., et al., 1996, International Astronomical Union Circular, **6380**, 1
 Gaskell C. M., et al., 1989, International Astronomical Union Circular, **4761**, 2
 Gerardy C., et al., 1999, International Astronomical Union Circular, **7158**, 2
 Gilfanov M., et al., 2010, *Nature*, **463**, 924
 Gilmore A. C., 1991, International Astronomical Union Circular, **5309**, 3
 Ginsburg A., et al., 2019, arXiv e-prints, p. arXiv:1901.04520
 Giovanelli R., et al., 1997, *AJ*, **113**, 22
 Gomez G., et al., 1996, *AJ*, **112**, 2094
 Gonzalez S., et al., 2004, International Astronomical Union Circular, **8409**, 2
 Goobar A., et al., 2014, *ApJ*, **784**
 Graham D. A., et al., 1978, *A&A*, **70**, L69
 Graham A. W., et al., 1998, *Astronomy and Astrophysics Supplement Series*, **133**, 325
 Graham M. L., et al., 2017, *MNRAS*, **472**, 3437
 Graham M. L., et al., 2019, *ApJ*, **871**, 62
 Grogin N. A., et al., 1998, *The Astrophysical Journal Supplement Series*, **119**, 277
 Guillochon J., et al., 2017, *ApJ*, **835**
 Guthrie B. N. G., et al., 1996, *A&A*, **310**, 353
 Gutierrez C. P., et al., 2016, *A&A*, **590**, A5
 Halevi G., et al., 2016, The Astronomer's Telegram, **9309**, 1
 Hamuy M., et al., 1991, *AJ*, **102**, 208
 Hamuy M., et al., 1996, *AJ*, **112**, 2408
 Hamuy M., et al., 2006, *Publications of the Astronomical Society of the Pacific*, **118**, 2
 Han Z., et al., 2006, *MNRAS*, **368**, 1095
 Harutyunyan A., et al., 2007, Central Bureau Electronic Telegrams, **1021**, 1
 Harutyunyan A., et al., 2009, Central Bureau Electronic Telegrams, **1768**, 1
 Hayden B. T., et al., 2010, *ApJ*, **722**, 1691
 Heraudeau P., et al., 1994, International Astronomical Union Circular, **5952**, 3
 Herbig G. H., et al., 1972, International Astronomical Union Circular, **2407**, 1
 Hernandez M., et al., 2000, *MNRAS*, **319**, 223
 Hicken M., et al., 2007, *ApJ*, **669**, L17
 Hicken M., et al., 2009, *ApJ*, **700**, 331
 Hicken M., et al., 2012, *The Astrophysical Journal Supplement Series*, **200**
 Ho W. C. G., et al., 2001, *Publications of the Astronomical Society of the Pacific*, **113**, 1349
 Höflich P., et al., 2004, *ApJ*, **617**, 1258

- Holberg J., et al., 1991, International Astronomical Union Circular, [5270](#), 3
- Holmbo S., et al., 2018, arXiv e-prints, p. [arXiv:1809.01359](#)
- Holoien T. W. S., et al., 2014, The Astronomer's Telegram, [6637](#), 1
- Holoien T. W. S., et al., 2017a, *MNRAS*, [464](#), 2672
- Holoien T. W. S., et al., 2017b, *MNRAS*, [467](#), 1098
- Holoien T. W. S., et al., 2017c, *MNRAS*, [471](#), 4966
- Holoien T. W. S., et al., 2019, *MNRAS*, p. 93
- Holtzman J. A., et al., 2008, *AJ*, [136](#), 2306
- Hook I. M., et al., 2004, *Publications of the Astronomical Society of the Pacific*, [116](#), 425
- Hosseinzadeh G., et al., 2017a, The Astronomer's Telegram, [10164](#), 1
- Hosseinzadeh G., et al., 2017b, The Astronomer's Telegram, [10639](#), 1
- Howell D. A., 2001, *ApJ*, [554](#), L193
- Howell D. A., et al., 2006, *Nature*, [443](#), 308
- Howerton S., et al., 2011, Central Bureau Electronic Telegrams, [2658](#), 1
- Howerton S., et al., 2013, Central Bureau Electronic Telegrams, [3533](#), 1
- Hoyle F., et al., 1960, *ApJ*, [132](#), 565
- Huang X., et al., 2017, *ApJ*, [836](#), 157
- Huchra J. P., et al., 1999, *The Astrophysical Journal Supplement Series*, [121](#), 287
- Hurst G. M., et al., 1998, International Astronomical Union Circular, [6875](#), 1
- Hutchings D., et al., 2002, International Astronomical Union Circular, [7918](#), 1
- Iben I., et al., 1984, *The Astrophysical Journal Supplement Series*, [54](#), 335
- Iijima T., et al., 1994, International Astronomical Union Circular, [6108](#), 1
- Inserra C., et al., 2013, *ApJ*, [770](#)
- Itagaki K., et al., 2014, Central Bureau Electronic Telegrams, [3792](#), 2
- Jha S., et al., 1999, *The Astrophysical Journal Supplement Series*, [125](#), 73
- Jha S., et al., 2006, *AJ*, [131](#), 527
- Jha S. W., et al., 2017, The Astronomer's Telegram, [10261](#), 1
- Jha S. W., et al., 2019, *Nature Astronomy*, [3](#), 706
- Jones D. H., et al., 2006, *MNRAS*, [369](#), 25
- Jones D. H., et al., 2009, *MNRAS*, [399](#), 683
- Jones S., et al., 2017, The Astronomer's Telegram, [11092](#), 1
- Jorden P. R., 1990, in Proc. SPIE Vol. 1235, p. 790–798, Instrumentation in Astronomy VII, David L. Crawford; Ed.. pp 790–798, doi:[10.1117/12.19163](#)
- Justham S., 2011, *ApJ*, [730](#), L34
- Kand rashoff M., et al., 2012, Central Bureau Electronic Telegrams, [3111](#), 1
- Karamehmetoglu E., et al., 2015, The Astronomer's Telegram, [7476](#), 1
- Kasen D., 2010, *ApJ*, [708](#), 1025
- Kashikawa N., et al., 2002, *Publications of the Astronomical Society of Japan*, [54](#), 819
- Katz B., et al., 2012, preprint, p. [arXiv:1211.4584](#) ([arXiv:1211.4584](#))
- Kawakita H., et al., 2002, International Astronomical Union Circular, [7848](#), 2
- Kelson D. D., 2003, *Publications of the Astronomical Society of the Pacific*, [115](#), 688
- Kelson D. D., et al., 2000, *ApJ*, [531](#), 159
- Kent B. R., et al., 2008, *AJ*, [136](#), 713
- Khan R., et al., 2011, *ApJ*, [726](#), 106
- Kim H., et al., 2013, Central Bureau Electronic Telegrams, [3743](#), 1
- Kirshner R. P., et al., 1975, *ApJ*, [200](#), 574
- Kirshner R., et al., 1991, International Astronomical Union Circular, [5403](#), 2
- Kirshner R. P., et al., 1993, *ApJ*, [415](#), 589
- Kiyota S., et al., 2014a, The Astronomer's Telegram, [6594](#), 1
- Kiyota S., et al., 2014b, The Astronomer's Telegram, [6683](#), 1
- Kiyota S., et al., 2014c, The Astronomer's Telegram, [6802](#), 1
- Kiyota S., et al., 2014d, The Astronomer's Telegram, [6809](#), 1
- Kleiser I., et al., 2009, Central Bureau Electronic Telegrams, [1918](#), 1
- Klotz A., et al., 2012, Central Bureau Electronic Telegrams, [3277](#), 2
- Kollmeier J. A., et al., 2019, arXiv e-prints, p. [arXiv:1902.02251](#)
- Koribalski B. S., et al., 2004, *AJ*, [128](#), 16
- Kosai H., et al., 1991, International Astronomical Union Circular, [5400](#), 1
- Kotak R., et al., 2003a, International Astronomical Union Circular, [8099](#), 1
- Kotak R., et al., 2003b, International Astronomical Union Circular, [8122](#), 3
- Kotak R., et al., 2005, *A&A*, [436](#), 1021
- Kowal C. T., 1972, International Astronomical Union Circular, [2405](#), 1
- Kowalski M., et al., 2008, *ApJ*, [686](#)
- Krisciunas K., et al., 2000, *ApJ*, [539](#), 658
- Krisciunas K., et al., 2003, *AJ*, [125](#), 166
- Krisciunas K., et al., 2004, *AJ*, [128](#), 3034
- Krisciunas K., et al., 2007, *AJ*, [133](#), 58
- Krisciunas K., et al., 2009, *AJ*, [138](#), 1584
- Krisciunas K., et al., 2017, *AJ*, [154](#), 211
- Kromer M., et al., 2010, *ApJ*, [719](#), 1067
- Krumm N., et al., 1980, *AJ*, [85](#), 1312
- Lair J. C., et al., 2006, *AJ*, [132](#), 2024
- Lanz T., et al., 2005, *ApJ*, [619](#), 517
- Larsen S. S., et al., 2001, *AJ*, [121](#), 2974
- Lauberts A., et al., 1989, The surface photometry catalogue of the ESO-Uppsala galaxies
- Lavery R. J., 1989, International Astronomical Union Circular, [4743](#), 2
- Leadbeater R., 2016, Transient Name Server Classification Report, [2016-793](#), 1
- Leadbeater R., 2018, Transient Name Server Classification Report, [2018-159](#), 1
- Lee T. A., et al., 1972, *ApJ*, [177](#), L59
- Leibengut B., et al., 1993, *AJ*, [105](#), 301
- Leloudas G., et al., 2009, *A&A*, [505](#), 265
- Leonard D. C., 2007, *ApJ*, [670](#), 1275
- Leonard D. C., et al., 2001, *Publications of the Astronomical Society of the Pacific*, [113](#), 920
- Li W. D., et al., 1999, *AJ*, [117](#), 2709
- Li W. D., et al., 2000, in Holt S. S., et al., eds, American Institute of Physics Conference Series Vol. 522, American Institute of Physics Conference Series. pp 103–106 ([arXiv:astro-ph/9912336](#)), doi:[10.1063/1.1291702](#)
- Li W., et al., 2001, *Publications of the Astronomical Society of the Pacific*, [113](#), 1178
- Li W., et al., 2003a, *Publications of the Astronomical Society of the Pacific*, [115](#), 453
- Li W., et al., 2003b, International Astronomical Union Circular, [8245](#), 1
- Li W., et al., 2019, *ApJ*, [870](#), 12
- Liller W., et al., 1992, International Astronomical Union Circular, [5431](#), 3
- Liller W., et al., 1992, International Astronomical Union Circular, [5428](#), 1
- Lira P., et al., 1998, *AJ*, [115](#), 234
- Liu Z. W., et al., 2012, *A&A*, [548](#), A2
- Liu Z.-W., et al., 2013a, *ApJ*, [774](#), 37
- Liu Z.-W., et al., 2013b, *ApJ*, [778](#), 121

- Livio M., et al., 2018, *Phys. Rep.*, **736**, 1
- Livio M., et al., 2003, *ApJ*, **594**, L93
- Livne E., 1990, *ApJ*, **354**, L53
- Livne E., et al., 1995, *ApJ*, **452**, 62
- Longhetti M., et al., 1998, *Astronomy and Astrophysics Supplement Series*, **130**, 251
- Lundqvist P., et al., 2013, *MNRAS*, **435**, 329
- Lundqvist P., et al., 2015, *A&A*, **577**, A39
- Maeda K., et al., 2009, *ApJ*, **690**, 1745
- Maguire K., et al., 2014, *MNRAS*, **444**, 3258
- Maguire K., et al., 2016, *MNRAS*, **457**, 3254
- Maguire K., et al., 2018, *MNRAS*, **477**, 3567
- Malesani D., et al., 2018, The Astronomer's Telegram, **11516**, 1
- Maoz D., et al., 2014, *Annual Review of Astronomy and Astrophysics*, **52**, 107
- Marietta E., et al., 2000, *The Astrophysical Journal Supplement Series*, **128**, 615
- Marion G. H., et al., 2012, Central Bureau Electronic Telegrams, **3146**, 2
- Marshall J. L., et al., 2008, in *Ground-based and Airborne Instrumentation for Astronomy II*. Edited by McLean, Ian S.; Casali, Mark M. Proceedings of the SPIE, Volume 7014, article id. 701454, 10 pp. (2008).. doi:[10.1117/12.789972](https://doi.org/10.1117/12.789972)
- Martin R., et al., 2004, International Astronomical Union Circular, **8282**, 1
- Martin R., et al., 2005, International Astronomical Union Circular, **8490**, 1
- Matheson T., et al., 2002, International Astronomical Union Circular, **7903**, 2
- Matheson T., et al., 2008, *AJ*, **135**, 1598
- Mathewson D. S., et al., 1992, *The Astrophysical Journal Supplement Series*, **81**, 413
- Mattila S., et al., 2005, *A&A*, **443**, 649
- Mattila S., et al., 2016, The Astronomer's Telegram, **8992**, 1
- Maury A., et al., 1990, International Astronomical Union Circular, **5039**, 1
- Maza J., et al., 2010, Central Bureau Electronic Telegrams, **2388**, 1
- Mazzali P. A., et al., 2015, *MNRAS*, **450**, 2631
- McCully C., et al., 2014, *Nature*, **512**, 54
- Meng X., et al., 2013, *ApJ*, **778**, L35
- Menzies J., et al., 1991, International Astronomical Union Circular, **5246**, 2
- Meyer M. J., et al., 2004, *MNRAS*, **350**, 1195
- Mikuz H., 1994, International Astronomical Union Circular, **5958**, 3
- Mikuz H., 1995, International Astronomical Union Circular, **6166**, 2
- Misra K., et al., 2005, *MNRAS*, **360**, 662
- Modjaz M., et al., 2005a, Central Bureau Electronic Telegrams, **160**, 1
- Modjaz M., et al., 2005b, International Astronomical Union Circular, **8491**, 2
- Molinari E., et al., 1999, in *Looking Deep in the Southern Sky, Proceedings of the ESO/Australia Workshop held at Sydney, Australia, 10-12 December 1997*. Edited by Faffaella Morganti and Warrick J. Couch. Berlin: Springer- Verlag, 1999. p. 157.. p. 157
- Monard L. A. G., et al., 2010, Central Bureau Electronic Telegrams, **2434**, 1
- Monard L. A. G., et al., 2001, International Astronomical Union Circular, **7720**, 1
- Monard L. A. G., et al., 2007, Central Bureau Electronic Telegrams, **1100**, 1
- Monard L. A. G., et al., 2011, Central Bureau Electronic Telegrams, **2635**, 1
- Monard L. A. G., et al., 2015, Central Bureau Electronic Telegrams, **4081**, 1
- Moorwood A., et al., 1998, *The Messenger*, **91**, 9
- Morrell N., et al., 2016, *The Astronomer's Telegram*, **9170**, 1
- Morrell N., et al., 2007, Central Bureau Electronic Telegrams, **1131**, 1
- Morrell N., et al., 2014a, *The Astronomer's Telegram*, **6508**, 1
- Morrell N., et al., 2014b, *The Astronomer's Telegram*, **6765**, 1
- Morrell N., et al., 2015, *The Astronomer's Telegram*, **6988**, 1
- Motohara K., et al., 2002, *Publications of the Astronomical Society of Japan*, **54**, 315
- Motohara K., et al., 2006, *ApJ*, **652**, L101
- Munari U., et al., 2013, *New Astron.*, **20**, 30
- Munch G., et al., 1986, *International Astronomical Union Circular*, **4183**, 1
- Nakano S., et al., 2007, Central Bureau Electronic Telegrams, **863**, 1
- Nakano S., et al., 1995, International Astronomical Union Circular, **6134**, 1
- Nakano S., et al., 2003, International Astronomical Union Circular, **8097**, 1
- Nakano S., et al., 2005, International Astronomical Union Circular, **8475**, 1
- Nakano S., et al., 2007, Central Bureau Electronic Telegrams, **1017**, 1
- Nakano S., et al., 2008, Central Bureau Electronic Telegrams, **1193**, 1
- Nakano S., et al., 2011, Central Bureau Electronic Telegrams, **2783**, 1
- Nakano S., et al., 2012, Central Bureau Electronic Telegrams, **3209**, 1
- Nakano S., et al., 2015, Central Bureau Electronic Telegrams, **4106**, 1
- Nicolas J., et al., 2014, *The Astronomer's Telegram*, **6500**, 1
- Nishiyama K., et al., 2012, Central Bureau Electronic Telegrams, **3349**, 1
- Noguchi T., et al., 2011a, Central Bureau Electronic Telegrams, **2940**, 1
- Noguchi T., et al., 2011b, Central Bureau Electronic Telegrams, **2943**, 1
- Nomoto K., 1982, *ApJ*, **253**, 798
- Nucita A. A., et al., 2017, *ApJ*, **850**, 111
- Nugent P. E., et al., 2011a, *Nature*, **480**, 344
- Nugent P., et al., 2011b, *The Astronomer's Telegram*, **3581**, 1
- Nyholm A., et al., 2017, *The Astronomer's Telegram*, **10131**, 1
- Ochner P., et al., 2016, *The Astronomer's Telegram*, **9018**, 1
- Ogando R. L. C., et al., 2008, *AJ*, **135**, 2424
- Oke J. B., et al., 1982, *Publications of the Astronomical Society of the Pacific*, **94**, 586
- Oke J. B., et al., 1995, *Publications of the Astronomical Society of the Pacific*, **107**, 375
- Olszewski E. W., 1982, *Information Bulletin on Variable Stars*, **2065**, 1
- Osmer P. S., et al., 1972, *Nature Physical Science*, **238**, 21
- Pakmor R., et al., 2012, *ApJ*, **747**, L10
- Pan K.-C., et al., 2012, *ApJ*, **750**, 151
- Pan Y. C., et al., 2015, *MNRAS*, **452**, 4307
- Pan Y. C., et al., 2017, *The Astronomer's Telegram*, **10225**, 1
- Parker S., 2016, *Transient Name Server Discovery Report*, **2016-304**, 1
- Parker S., 2017, *Transient Name Server Discovery Report*, **2017-700**, 1
- Parker S., et al., 2013a, Central Bureau Electronic Telegrams, **3416**, 1
- Parker P., et al., 2013b, Central Bureau Electronic Telegrams, **3539**, 1
- Pastorello A., et al., 2007, *MNRAS*, **376**, 1301
- Patat F., et al., 2007, *Science*, **317**, 924
- Paturel G., et al., 2003, *A&A*, **412**, 57
- Pejcha O., et al., 2013, *MNRAS*, **435**, 943

- Pessa I., et al., 2018, preprint, p. arXiv:1803.05005 ([arXiv:1803.05005](#))
- Petrushevska T., et al., 2016, The Astronomer's Telegram, 9049, 1
- Phillips M. M., et al., 1987, *Publications of the Astronomical Society of the Pacific*, 99, 592
- Phillips M. M., et al., 2006, *AJ*, 131, 2615
- Phillips M. M., et al., 2007, *Publications of the Astronomical Society of the Pacific*, 119, 360
- Phillips M. M., et al., 2013, *ApJ*, 779, 38
- Phillips M. M., et al., 2019, *Publications of the Astronomical Society of the Pacific*, 131, 014001
- Pignata G., et al., 2004, *MNRAS*, 355, 178
- Pignata G., et al., 2008, *MNRAS*, 388, 971
- Pignata G., et al., 2009, Central Bureau Electronic Telegrams, 2022, 1
- Pignata G., et al., 2010, Central Bureau Electronic Telegrams, 2344, 1
- Pisano D. J., et al., 2011, *The Astrophysical Journal Supplement Series*, 197, 28
- Pogge R. W., et al., 2010, in Proceedings of the SPIE, Volume 7735, id. 77350A (2010).., doi:10.1117/12.857215
- Pollas C., et al., 2007, Central Bureau Electronic Telegrams, 1121, 1
- Pollas C., et al., 1989, International Astronomical Union Circular, 4742, 2
- Ponticello N. J., et al., 2006, International Astronomical Union Circular, 8667, 1
- Prentice S., et al., 2017, Transient Name Server Classification Report, 2017-978, 1
- Press W. H., et al., 1992, Numerical recipes in FORTRAN. The art of scientific computing
- Prieto J. L., et al., 2011, Central Bureau Electronic Telegrams, 2613, 1
- Prieto J. L., et al., 2006, Central Bureau Electronic Telegrams, 651, 1
- Prieto J. L., et al., 2010, Central Bureau Electronic Telegrams, 2453, 1
- Prieto J. L., et al., 2019, arXiv e-prints, p. arXiv:1909.05267
- Przybylski A., 1972, International Astronomical Union Circular, 2434, 1
- Puckett T., et al., 2009, Central Bureau Electronic Telegrams, 1762, 1
- Pugh H., et al., 2005, Central Bureau Electronic Telegrams, 158, 1
- Quimby R., et al., 2005, International Astronomical Union Circular, 8625, 2
- Quimby R., et al., 2006a, Central Bureau Electronic Telegrams, 393, 1
- Quimby R., et al., 2006b, International Astronomical Union Circular, 8723, 2
- Rand R. J., 1995, *AJ*, 109, 2444
- Raskin C., et al., 2013, *ApJ*, 772, 1
- Rebassa-Mansergas A., et al., 2018, preprint, p. arXiv:1809.07158 ([arXiv:1809.07158](#))
- Rhee M. H., et al., 1996, *Astronomy and Astrophysics Supplement Series*, 115, 407
- Richmond M. W., et al., 2012, *Journal of the American Association of Variable Star Observers (AAVSO)*, 40, 872
- Richmond M. W., et al., 1995, *AJ*, 109, 2121
- Riello M., et al., 2002, International Astronomical Union Circular, 7919, 2
- Riello M., et al., 2018, preprint, p. arXiv:1804.09367 ([arXiv:1804.09367](#))
- Riess A. G., et al., 1999, *AJ*, 117, 707
- Riess A. G., et al., 2005, *ApJ*, 627, 579
- Riess A. G., et al., 2016, *ApJ*, 826
- Romero-Canizales C., et al., 2014, The Astronomer's Telegram, 6618, 1
- Röpke F. K., et al., 2012, *ApJ*, 750, L19
- Rothberg B., et al., 2006, *AJ*, 131, 185
- Rudy R. J., et al., 2015, The Astronomer's Telegram, 7825, 1
- Ruffini N. J., et al., 2019, *MNRAS*, 489, 420
- Saha A., et al., 2006, *The Astrophysical Journal Supplement Series*, 165, 108
- Sahu D. K., et al., 2008, *ApJ*, 680, 580
- Sako M., et al., 2014, preprint, ([arXiv:1401.3317](#))
- Salgado F., et al., 2007, Central Bureau Electronic Telegrams, 865, 1
- Salvo M. E., et al., 2001, *MNRAS*, 321, 254
- Salvo M., et al., 2006, Central Bureau Electronic Telegrams, 557, 1
- Sand D. J., et al., 2017, The Astronomer's Telegram, 10569, 1
- Sand D. J., et al., 2018a, preprint, p. arXiv:1804.03666 ([arXiv:1804.03666](#))
- Sand D., et al., 2018b, The Astronomer's Telegram, 11328, 1
- Sand D., et al., 2018c, The Astronomer's Telegram, 11330, 1
- Sand D., et al., 2018d, The Astronomer's Telegram, 11371, 1
- Sand D. J., et al., 2019, *ApJ*, 877, L4
- Saulder C., et al., 2016, *A&A*, 596, A14
- Scalzo R. A., et al., 2010, *ApJ*, 713, 1073
- Scalzo R. A., et al., 2014, *MNRAS*, 445, 2535
- Scalzo R. A., et al., 2019, *MNRAS*, 483, 628
- Schaefer B., 1987, International Astronomical Union Circular, 4421, 1
- Schlegel D. J., et al., 1998, *ApJ*, 500, 525
- Schmidt B. P., et al., 1994, *ApJ*, 434, L19
- Schneider S. E., et al., 1990, *The Astrophysical Journal Supplement Series*, 72, 245
- Schneider S. E., et al., 1992, *The Astrophysical Journal Supplement Series*, 81, 5
- Schwartz M., et al., 2003, International Astronomical Union Circular, 8121, 1
- Serduke F. J. D., et al., 2005, Central Bureau Electronic Telegrams, 269, 1
- Shappee B. J., et al., 2013, *ApJ*, 766
- Shappee B. J., et al., 2013a, *ApJ*, 762
- Shappee B. J., et al., 2013b, *ApJ*, 765, 150
- Shappee B. J., et al., 2014a, *ApJ*, 788, 48
- Shappee B. J., et al., 2014b, The Astronomer's Telegram, 6812, 1
- Shappee B. J., et al., 2015, The Astronomer's Telegram, 6882, 1
- Shappee B. J., et al., 2017, *ApJ*, 841, 48
- Shappee B. J., et al., 2018, *ApJ*, 855, 6
- Shappee B. J., et al., 2019, *ApJ*, 870, 13
- Sheinis A. I., et al., 2002, *Publications of the Astronomical Society of the Pacific*, 114, 851
- Shen K. J., et al., 2018, preprint, p. arXiv:1804.11163 ([arXiv:1804.11163](#))
- Silverman J. M., et al., 2011, *MNRAS*, 410, 585
- Silverman J. M., et al., 2012, *MNRAS*, 425, 1789
- Silverman J. M., et al., 2013, *MNRAS*, 430, 1030
- Simon J. D., et al., 2009, *ApJ*, 702, 1157
- Smartt S. J., et al., 2002, International Astronomical Union Circular, 7961, 2
- Smartt S. J., et al., 2015a, *A&A*, 579
- Smartt S. J., et al., 2015b, *A&A*, 579, A40
- Smith R. J., et al., 2000, *MNRAS*, 313, 469
- Smoker J. V., et al., 2000, *A&A*, 361, 19
- Sollerman J., et al., 2001, International Astronomical Union Circular, 7723, 2
- Sollerman J., et al., 2004, *A&A*, 428, 555
- Springob C. M., et al., 2014, *MNRAS*, 445, 2677
- Spyromilio J., et al., 2004, *A&A*, 426, 547
- Srivastav S., et al., 2016, *MNRAS*, 457, 1000

- Stanek K. Z., 2018, Transient Name Server Discovery Report, [2018-234](#), 1
- Stanek K. Z., et al., 2014, The Astronomer's Telegram, [6830](#), 1
- Stanishev V., et al., 2008, Central Bureau Electronic Telegrams, [1232](#), 1
- Stanishev V., et al., 2007, *A&A*, [469](#), 645
- Sternberg A., et al., 2011, *Science*, [333](#), 856
- Sternberg A., et al., 2014, *MNRAS*, [443](#), 1849
- Stone G., et al., 2018, The Astronomer's Telegram, [11343](#), 1
- Strauss M. A., et al., 1992, *The Astrophysical Journal Supplement Series*, [83](#), 29
- Stritzinger M., 2010, Central Bureau Electronic Telegrams, [2346](#), 1
- Stritzinger M., et al., 2006a, *A&A*, [460](#), 793
- Stritzinger M., et al., 2006b, *A&A*, [460](#), 793
- Stritzinger M., et al., 2010, *AJ*, [140](#), 2036
- Stritzinger M. D., et al., 2011, *AJ*, [142](#)
- Stritzinger M. D., et al., 2015, *A&A*, [573](#), A2
- Strohmayer T., et al., 1996, International Astronomical Union Circular, [6484](#), 1
- Suntzeff N., et al., 1989, International Astronomical Union Circular, [4728](#), 1
- Suntzeff N., et al., 1992, International Astronomical Union Circular, [5432](#), 2
- Suntzeff N. B., et al., 1996, International Astronomical Union Circular, [6381](#), 1
- Suntzeff N. B., et al., 1999, *AJ*, [117](#), 1175
- Suntzeff N., et al., 2004, International Astronomical Union Circular, [8283](#), 1
- Szabó G. M., et al., 2003, *A&A*, [408](#), 915
- Taam R. E., 1980, *ApJ*, [237](#), 142
- Tartaglia L., et al., 2017a, The Astronomer's Telegram, [10158](#), 1
- Tartaglia L., et al., 2017b, The Astronomer's Telegram, [10260](#), 1
- Tartaglia L., et al., 2017c, The Astronomer's Telegram, [10439](#), 1
- Tartaglia L., et al., 2017d, The Astronomer's Telegram, [10629](#), 1
- Taubenberger S., et al., 2013a, *MNRAS*, [432](#), 3117
- Taubenberger S., et al., 2013b, *ApJ*, [775](#), L43
- Taubenberger S., et al., 2015, *MNRAS*, [448](#), L48
- Terreran G., et al., 2016, The Astronomer's Telegram, [9403](#), 1
- The Astropy Collaboration et al., 2018, preprint, p. [arXiv:1801.02634](#) ([arXiv:1801.02634](#))
- Theureau G., et al., 1998, *Astronomy and Astrophysics Supplement Series*, [130](#), 333
- Theureau G., et al., 2007, *A&A*, [465](#), 71
- Thompson T. A., 2011, *ApJ*, [741](#), 82
- Tinella V., 2016, Transient Name Server Discovery Report, [2016-305](#), 1
- Tonry J. L., et al., 2001, *ApJ*, [546](#), 681
- Tonry J. L., et al., 2012, *ApJ*, [750](#), 99
- Tonry J., et al., 2016, Transient Name Server Discovery Report, [2016-583](#), 1
- Tonry J., et al., 2017a, Transient Name Server Discovery Report, [2017-1371](#), 1
- Tonry J., et al., 2017b, Transient Name Server Discovery Report, [2017-1431](#), 1
- Tonry J., et al., 2017c, Transient Name Server Discovery Report, [2017-361](#), 1
- Tonry J., et al., 2017d, Transient Name Server Discovery Report, [2017-860](#), 1
- Toth I., et al., 2000, *A&A*, [361](#), 63
- Treffers R. R., et al., 1993, International Astronomical Union Circular, [5870](#), 3
- Treffers R. R., et al., 1994, International Astronomical Union Circular, [5946](#), 2
- Tsvetkov D. Y., 1982, Soviet Astronomy Letters, [8](#), 115
- Tsvetkov D. Y., 1986, *Peremennye Zvezdy*, [22](#), 279
- Tsvetkov D. Y., et al., 1997, *Astronomy Letters*, [23](#), 26
- Tsvetkov D. Y., et al., 1990, *A&A*, [236](#), 133
- Tsvetkov D. Y., et al., 2013, Contributions of the Astronomical Observatory Skalnate Pleso, [43](#), 94
- Tsvetkov D. Y., et al., 2014, Contributions of the Astronomical Observatory Skalnate Pleso, [44](#), 67
- Tucker M. A., et al., 2018, arXiv e-prints, p. [arXiv:1811.09635](#)
- Tully R. B., et al., 2008, *ApJ*, [676](#), 184
- Tully R. B., et al., 2013, *AJ*, [146](#), 86
- Turatto M., et al., 1990, *AJ*, [100](#), 771
- Turatto M., et al., 1996, *MNRAS*, [283](#), 1
- Tutukov A. V., et al., 2007, *Astronomy Reports*, [51](#), 291
- Tutukov A. V., et al., 1979, *Acta Astron.*, [29](#), 665
- Tutukov A. V., et al., 1994, *MNRAS*, [268](#), 871
- Tutukov A., et al., 1996, *MNRAS*, [280](#), 1035
- Uddin S., et al., 2017, The Astronomer's Telegram, [10605](#), 1
- Valenti S., et al., 2017, Transient Name Server Classification Report, [2017-613](#), 1
- Valentini G., et al., 2003, *ApJ*, [595](#), 779
- Vallely P. J., et al., 2019a, arXiv e-prints, p. [arXiv:1902.00037](#)
- Vallely P. J., et al., 2019b, *MNRAS*, [487](#), 2372
- Vannmunder T., et al., 1994, International Astronomical Union Circular, [6115](#), 3
- Verheijen M. A. W., et al., 2001, *A&A*, [370](#), 765
- Vernet J., et al., 2011, *A&A*, [536](#)
- Vettolani G., et al., 1981, International Astronomical Union Circular, [3584](#), 1
- Villegas D., et al., 2010, *ApJ*, [717](#), 603
- Villi M., et al., 1998, International Astronomical Union Circular, [6899](#), 1
- Villi M., et al., 2008, Central Bureau Electronic Telegrams, [1228](#), 1
- Vinkó J., et al., 2003, *A&A*, [397](#), 115
- Vladimirov V., et al., 2015, The Astronomer's Telegram, [7732](#), 1
- Volkov I. M., 1991, Information Bulletin on Variable Stars, [3581](#), 1
- Waagen E., et al., 1991, International Astronomical Union Circular, [5239](#), 1
- Walker A., et al., 1994, International Astronomical Union Circular, [5950](#), 1
- Walker E. S., et al., 2015, *The Astrophysical Journal Supplement Series*, [219](#)
- Wang L., et al., 2004, *ApJ*, [604](#), L53
- Wang X., et al., 2008, *ApJ*, [675](#), 626
- Webbink R. F., 1984, *ApJ*, [277](#), 355
- Wells L. A., et al., 1994, *AJ*, [108](#), 2233
- Weyant A., et al., 2018, *AJ*, [155](#)
- Wheeler J. C., et al., 1975, *ApJ*, [200](#), 145
- Whelan J., et al., 1973, *ApJ*, [186](#), 1007
- Wiethoff W., et al., 2017, The Astronomer's Telegram, [10521](#), 1
- Wills B. J., et al., 1980, *ApJ*, [237](#), 319
- Wood-Vasey W. M., et al., 2002a, International Astronomical Union Circular, [7902](#), 3
- Wood-Vasey W. M., et al., 2002b, International Astronomical Union Circular, [7959](#), 1
- Woods D. F., et al., 2006, *AJ*, [132](#), 197
- Woods T. E., et al., 2018, *ApJ*, [863](#), 120
- Woosley S. E., et al., 1994, *ApJ*, [423](#), 371
- Wyrzykowski L., et al., 2015, The Astronomer's Telegram, [8484](#), 1
- Yamanaka M., et al., 2015, *ApJ*, [806](#), 191
- Yaron O., et al., 2012, *Publications of the Astronomical Society of the Pacific*, [124](#), 668
- Yoon S. C., et al., 2003, *A&A*, [412](#), L53
- Yoon S. C., et al., 2005, *A&A*, [435](#), 967
- Yu C., et al., 2000, International Astronomical Union Circular, [7458](#), 1
- Zhai Q., et al., 2016, *AJ*, [151](#)
- Zhang J., et al., 2014, The Astronomer's Telegram, [6813](#), 1
- Zhang T., et al., 2010, *PASP*, [122](#), 1

- Zhang T., et al., 2011, Central Bureau Electronic Telegrams, **2708**, 3
 Zhang J.-J., et al., 2014, *AJ*, **148**
 Zhang J., et al., 2018, Transient Name Server Classification Report, **2018-293**, 1
 Zheng W., et al., 2013, The Astronomer’s Telegram, **5637**, 1
 de Vaucouleurs G., et al., 1991, Third Reference Catalogue of Bright Galaxies
 van Driel W., et al., 2001, *A&A*, **378**, 370
 van Dyk S. D., et al., 1994, International Astronomical Union Circular, **6105**, 1
 van Genderen A. M., 1975, *A&A*, **45**, 429

APPENDIX A: A NEBULAR PHASE PHILLIP’S RELATION

In most SNe Ia, the peak luminosity and photospheric phase decline rate (e.g., Δm_{15}) are correlated with the amount of ^{56}Ni produced in the explosion (e.g., Stritzinger et al. 2006a; Scalzo et al. 2019). Therefore, these same observables should also correlate with the magnitude of SNe Ia as they enter the nebular phase. For SNe Ia with nebular spectra but no usable nebular photometry, this relation provides a method for estimating the nebular magnitude using near-peak photometry.

The photometric sample used in deriving the Nebular Phase Phillips Relation (NPPR) excludes Iax, CSM, and SC SNe Ia. Although 91T- and 91bg-like do not strictly follow the relation between luminosity and decline rate of normal SNe Ia, they are powered by the radioactive decay of ^{56}Ni to stable ^{56}Fe . As mentioned before, Δm_{15} is indicative of the amount of ^{56}Ni synthesised in the explosion, and therefore our parameterization described below still accurately models 91T- and 91bg-like SNe Ia. However, SC and Iax SNe Ia have unique ionisation properties, which is further exemplified by their nebular spectra which lack the prominent [FeII/III] and [CoII/III] emission features of their normal, 91T-, and 91bg-like counterparts (e.g., Taubenberger et al. 2013a; Foley et al. 2016). It is possible that the photometric intricacies of 91T- and 91bg-like SNe Ia are washed out by our heterogeneous sample, and more precise results can be attained with distinct samples of SNe Ia spectral types.

Taking all available nebular phase photometry of viable SNe Ia from this work and the literature, we derive an approximate functional form for calculating the apparent magnitude of a SN Ia with a measured m_{\max} and Δm_{15} . Since SNe Ia have nearly linear decays in magnitude space at nebular epochs, we use the functional form

$$m_{\lambda,\text{neb}}(t_p) = m_{\lambda,\max} + \Delta m_{\lambda}(t_p), \quad (\text{A1})$$

where $m_{\lambda,\text{neb}}(t_p)$ is the nebular magnitude in filter λ at phase $t_p = t - t_{\max}$, $m_{\lambda,\max}$ the magnitude at peak in filter λ , and Δm_{λ} is the change in brightness between maximum light and t_p for that filter. By formulating our relation for individual filters, we can neglect extinction from the Milky Way and the host galaxy since the maximum light and nebular magnitude of a SN Ia will be affected equally. Thus, we parameterize Δm_{λ} as a function of a SN Ia’s Δm_{15} ,

$$\Delta m_{\lambda} = A_{\lambda}(\Delta m_{15}) \times (t_p - 250 \text{ d}) + B_{\lambda}(\Delta m_{15}), \quad (\text{A2})$$

where

$$A_{\lambda}(\Delta m_{15}) = a_{\lambda}(\Delta m_{15} - 1.1 \text{ mag}) + b_{\lambda}, \quad (\text{A3})$$

and

$$B_{\lambda}(\Delta m_{15}) = c_{\lambda}(\Delta m_{15} - 1.1 \text{ mag}) + d_{\lambda}. \quad (\text{A4})$$

Here, $m_{\lambda,\max}$ is the apparent magnitude at maximum light in filter λ , $m_{\lambda}(t)$ is the nebular magnitude, t_p is the phase of the observations, Δm_{15} the decline rate, and measured coefficients $\{a, b, c, d\}$ which are provided in Table A1. t_p and Δm_{15} are offset by typical values to reduce their covariance in the fitting process.

The coefficients in Table A1 were computed using all

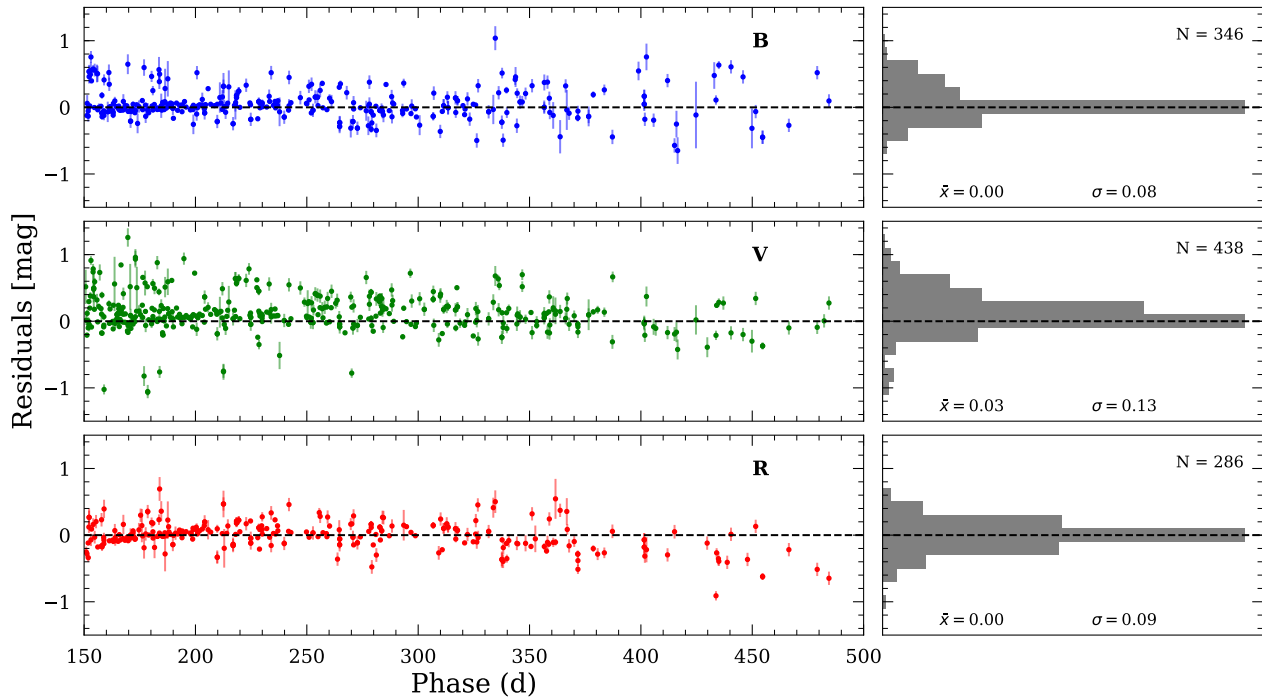


Figure A1. *Left:* Residuals of the late-time relation bootstrap fit from Eqs. A2–A4 using the values in Table A1. *Right:* Collapsed residual distribution of the best-fit solution.

Table A1. Values of the coefficients for Eqs. A2–A4 and fit statistics. N_{tot} is the total number of photometric points used in each filter from N_{SN} SNe Ia.

Filter	a_λ [10^{-3} day $^{-1}$]	b_λ [10^{-2} mag day $^{-1}$]	c_λ	d_λ [mag]	N_{SN}	N_{tot}	\bar{x}	σ
B	$-7.66^{+0.53}_{-0.62}$	$1.443^{+0.005}_{-0.005}$	$0.48^{+0.04}_{-0.04}$	$6.168^{+0.003}_{-0.004}$	42	346	0.00	0.08
V	$-13.68^{+0.33}_{-0.37}$	$1.620^{+0.003}_{-0.003}$	$2.58^{+0.02}_{-0.02}$	$6.050^{+0.002}_{-0.002}$	67	438	0.03	0.13
R	$4.22^{+0.41}_{-0.33}$	$1.650^{+0.004}_{-0.003}$	$1.00^{+0.03}_{-0.03}$	$6.776^{+0.002}_{-0.002}$	34	286	0.00	0.09

available nebular photometry between 150–500 d after maximum light. The coefficients were first approximated using a sample of well-studied SNe Ia with ≥ 5 measurements in a given filter in the temporal bounds listed above, such as SNe 2011fe, 2012fr, 2013gy, and 2015F, then expanded to include all photometric points. The SNe Ia used in deriving the NPPR have decline rates that span $\Delta m_{15} \sim 0.8 – 1.8$ mag and are denoted with a $*$ in Table B7. For publicly available photometry for which there are no reported uncertainties, we assign a nominal uncertainty of 0.1 mag. In fitting the data, we implement non-linear least squares fitting coupled with a bootstrap-resampling technique to derive reasonable estimates for the uncertainties. The residuals of the best-fit solution are shown in the left panel of Fig. A1, and the collapsed distribution is provided in the right panel.

For SNe Ia with a measured peak magnitude and Δm_{15} , we show the nebular *BVR* magnitude can be approximated to $\sim 20\%$. These results were derived using a heterogeneous data set and likely can be improved with a consistent photometric system and targeted observations across a reasonable

span of Δm_{15} . This technique can also be used in identifying peculiar or strange SNe Ia that deviate from their expected brightness at a given epoch, such as “late-onset” CSM interaction (e.g., Graham et al. 2019). Additionally, we attempted to expand this methodology to other photometric filters (e.g., *g*, *r*), but there were too few observations to build a quality model.

APPENDIX B: SUPPLEMENTARY TABLES AND FIGURES

In Table B2, we provide the name of the SN Ia, redshift, and references for discovery and classification. Table B3 provides the parameters from the light curve fits, including time of maximum light, Δm_{15} , and the distance modulus. We also include the total number of nebular phase spectra for that SN Ia and the corresponding phases. For information on each spectrum, including the date, telescope, instrument, and reference, see Table B4. Flux limits and derived mass limits are given in Table B5. New photometry presented in this work

is provided in Table B6 and all photometry references are given in Table B7.

B1 Data Tables

For SNe Ia with redshifts measured from the supernova lines near maximum light, we tweak the redshift using host galaxy emission lines when necessary. Major host galaxy lines such as H α , H β , [NII], and [OIII] are fit with Gaussian line profiles to estimate the line centre and then used to measure the host redshift.

For SNe Ia with insufficient photometry for a reliable light curve fit in **SNooPy**, we consider two approaches. If there are ≥ 3 photometric points near maximum light, we use linear least-squares coupled with bootstrap-resampling to fit a quadratic curve to the data and estimate t_{\max} and the associated uncertainty. Otherwise, the value for t_{\max} is taken from the spectroscopic classification reference given in Table B2 and assigned a nominal uncertainty of ± 5 d.

SNe-Iax do not conform to the standard SNe Ia templates utilised by **SNooPy** and other SN Ia light curve fitters. Thus, we compute Δm_{15} and t_{\max} using spline fits in the **SNooPy** environment. This prevents us from deriving the host reddening $E(B-V)_{\text{host}}$, however, the Iax SNe in our sample have negligible reddening (Li et al. 2003a; Phillips et al. 2007; McCully et al. 2014; Stritzinger et al. 2015; Foley et al. 2015).

The ‘‘Quality’’ column in Table B4 provides a rough estimate of the quality of the spectrum. This is mostly qualitative, and intended to provide readers with an estimate of the spectral quality for each SN Ia in our sample. The rankings are as follows:

High: The spectrum clearly shows the major Fe and Co emission lines between $\sim 4000 - 7000\text{\AA}$. The spectrum exhibits little to no host contamination or instrumental artefacts.

Med(ium): The major Fe lines are visible, while the Co lines are noisy or absent. The spectrum may also suffer from minor to moderate host galaxy contamination and/or instrumental artefacts.

Low: The major Fe lines are barely detectable above the spectral noise, and the Co lines mostly below the detection threshold. This category also includes overall medium-quality spectra with significant host galaxy contamination and/or instrumental artefacts.

B2 Special Cases

We discuss any extenuating circumstances or any other relevant details about specific SNe Ia that differ from the general methodology described in §2. Examples include alternative flux calibration methods, spectroscopic oddities noticed in our analysis, and spectrum reference discrepancies. SNe Ia with R_V values known to deviate from the standard $R_V = 3.1$ are listed in Table B1. For ensemble studies (e.g., Phillips et al. 2013; Burns et al. 2014), we require a $\geq 3\sigma$ deviation from $R_V = 3.1$ to include the value in our calculation. When drawing R_V values from Burns et al. (2014), we implement the F99+uniform prior results.

SN1998bu: The two nebular spectra from Cappellaro et al. (2001) do not have any specific mention in that

Table B1. R_V values and references for SNe Ia with $\geq 3\sigma$ deviations from the assumed $R_V = 3.1$.

Name	R_V	Ref.
SN2002bo	1.2	Phillips et al. (2013)
SN2004eo	0.8	Burns et al. (2014)
SN2006X	1.5	Wang et al. (2008); Phillips et al. (2013); Burns et al. (2014)
SN2007le	1.6	Phillips et al. (2013); Burns et al. (2014)
SN2014J	1.5	Amanullah et al. (2014); Foley et al. (2014); Gao et al. (2015); Brown et al. (2015)

manuscript, however, the reference on WiseRep points to this paper. Thus, we include the reference, but acknowledge we could not verify this paper was the true source for these spectra.

SN2002bo: The OSC and WiseRep also report several nebular phase NIR spectra for this SN. However, cross-referencing the reported spectra with the observational parameters given in Benetti et al. (2004), we believe the dates provided for the NIR spectra are off by a year, and these spectra are closer to a few months after maximum light instead of several hundred days after maximum light. We exclude these spectra from our sample.

B3 Supplementary Figures

We provide cutouts around each spectral line inspected for H/He emission (Table 2) for the spectrum used in calculating the limits provided in Table B5 for each SN Ia as supplementary figures. An example of the format of these figures is provided in Fig. 5. The black line is the observed spectrum, with the continuum fit and flux upper limit in red and purple, respectively. Gray shaded areas indicate masked spectral regions and completely gray boxes indicate that particular SN Ia had no spectra covering that spectral region. When multiple nebular spectra of a SN Ia cover the same expected H/He line, we provide the spectrum corresponding to the best mass limit *for that line*. Therefore, the panel for H α may show a different spectrum than the panel for H β for the same SN Ia. This ensures all adequate spectra are presented, even when some spectra do not cover all the optical and NIR lines considered in this study. The border colour of a given panel indicates whether it is used in the final stripped mass determination, the results of which are provided in Table B5. Blue borders indicate the panels used in the H-rich mass limit, red borders indicate He-rich limits, and purple borders indicate He lines used for both H- and He-rich limits.

Table B2. All SNe Ia studied in this work.

Disc. Name	IAU Name	Pec?	z	Redshift Ref.	Discovery	Classification
...	ASASSN-14hr	N	0.03362	Jones et al. (2009)	Nicolas et al. (2014)	Morrell et al. (2014a)
...	ASASSN-14jc	N	0.01132	Jones et al. (2009)	Kiyota et al. (2014a)	Romero-Canizales et al. (2014)
...	ASASSN-14jg	N	0.01483	Jones et al. (2009)	Holoien et al. (2014)	Arcavi et al. (2014)
...	ASASSN-14jz	N	0.01550	This Work	Kiyota et al. (2014b)	Dimitriadis et al. (2014)
...	ASASSN-14kq	N	0.03360	Jones et al. (2009)	Brimacombe et al. (2014a)	Morrell et al. (2014b)
...	ASASSN-14lt	N	0.03205	Springob et al. (2014)	Kiyota et al. (2014c)	Zhang & Wang (2014)
...	ASASSN-14lu	N	0.02700	Collobert et al. (2006)	Brimacombe et al. (2014b)	Shappee et al. (2014b)
...	ASASSN-14lv	N	0.04919	Jones et al. (2006)	Kiyota et al. (2014d)	Shappee et al. (2015)
...	ASASSN-14me	N	0.01800	Shappee et al. (2015)	Stanek et al. (2014)	Shappee et al. (2015)
...	ASASSN-15be	N	0.02190	Colless et al. (2003)	Brimacombe et al. (2015)	Morrell et al. (2015)
...	ASASSN-15hx	N	0.00810	This Work	Dong et al. (2015b)	Frohmaier et al. (2015)
...	PSN J1149 ^a	N	0.00560	Meyer et al. (2004)	Vladimirov et al. (2015)	Rudy et al. (2015)
...	SN1972E	N	0.00136	Koribalski et al. (2004)	Kowal (1972)	Herbig et al. (1972)
...	SN1981B	N	0.00603	Grogan et al. (1998)	Aksenov (1981)	Vettolani et al. (1981)
...	SN1986G	91bg-like	0.00182	Graham et al. (1978)	Evans et al. (1986)	Feast et al. (1986)
...	SN1990N	N	0.00340	Meyer et al. (2004)	Maury et al. (1990)	Maury et al. (1990)
...	SN1991T	91T-like	0.00579	Strauss et al. (1992)	Waagen et al. (1991)	Waagen et al. (1991)
...	SN1991bg	91bg-like	0.00339	Cappellari et al. (2011)	Kosai et al. (1991)	Kirshner et al. (1991)
...	SN1992A	N	0.00626	D'Onofrio et al. (1995)	Liller et al. (1992)	Liller et al. (1992)
...	SN1993Z	N	0.00450	Epinat et al. (2008)	Treffers et al. (1993)	Treffers et al. (1993)
...	SN1994ae	N	0.00427	Krumm & Salpeter (1980)	van Dyk et al. (1994)	Iijima et al. (1994)
...	SN1995D	N	0.00656	Cappellari et al. (2011)	Nakano et al. (1995)	Benetti et al. (1995)
...	SN1996X	N	0.00694	Ogando et al. (2008)	Garradd et al. (1996)	Suntzeff et al. (1996)
...	SN1998aq	N	0.00370	de Vaucouleurs et al. (1991)	Hurst et al. (1998)	Ayani & Yamaoka (1998)
...	SN1998bu	N	0.00299	de Vaucouleurs et al. (1991)	Villi et al. (1998)	Ayani et al. (1998)
...	SN1999aa	91T-like	0.01444	de Vaucouleurs et al. (1991)	Armstrong & Schwartz (1999)	Filippenko et al. (1999)
...	SN1999by	91bg-like	0.00213	de Vaucouleurs et al. (1991)	Arbour et al. (1999)	Gerardy & Fesen (1999)
...	SN2000cx	91T-like	0.00802	Cappellari et al. (2011)	Yu et al. (2000)	Chornock et al. (2000)
...	SN2001el	N	0.00389	Koribalski et al. (2004)	Monard et al. (2001)	Sollerman et al. (2001)
...	SN2002bo	N	0.00424	Theureau et al. (1998)	Cacella et al. (2002)	Kawakita et al. (2002)
...	SN2002cx	Iax	0.02396	Falco et al. (1999)	Wood-Vasey et al. (2002a)	Matheson et al. (2002)
...	SN2002dj	N	0.00939	Rothberg & Joseph (2006)	Hutchings & Li (2002)	Riello et al. (2002)
...	SN2002er	N	0.00857	de Vaucouleurs et al. (1991)	Wood-Vasey et al. (2002b)	Smartt et al. (2002)
...	SN2003cg	N	0.00413	van Driel et al. (2001)	Nakano et al. (2003)	Kotak et al. (2003a)
...	SN2003du	N	0.00638	Schneider et al. (1992)	Schwartz & Holvorcem (2003)	Kotak et al. (2003b)
...	SN2003gs	91bg-like	0.00477	Smith et al. (2000)	Evans et al. (2003)	Evans et al. (2003)
...	SN2003hv	N	0.00562	Ogando et al. (2008)	Beutler & Li (2003)	Dressler et al. (2003)
...	SN2003kf	N	0.00739	Theureau et al. (1998)	Li et al. (2003b)	Li et al. (2003b)
...	SN2004S	N	0.00936	Theureau et al. (2007)	Martin & Biggs (2004)	Suntzeff et al. (2004)
...	SN2004eo	N	0.01570	Theureau et al. (1998)	Arborea et al. (2004)	Gonzalez et al. (2004)
...	SN2005W	N	0.00889	de Vaucouleurs et al. (1991)	Nakano et al. (2005)	Elias-Rosa et al. (2005)
...	SN2005am	N	0.00790	Theureau et al. (1998)	Martin et al. (2005)	Modjaz et al. (2005b)
...	SN2005cf	N	0.00646	de Vaucouleurs et al. (1991)	Pugh & Li (2005)	Modjaz et al. (2005a)
...	SN2005hk	Iax	0.01299	Abolfathi et al. (2018)	Quimby et al. (2005)	Serdeke et al. (2005)
...	SN2006X	N	0.00524	Rand (1995)	Ponticello et al. (2006)	Quimby et al. (2006a)
...	SN2006dd	N	0.00587	Longhetti et al. (1998)	Quimby et al. (2006b)	Salvo et al. (2006)
...	SN2006gz	SC	0.02800	Falco et al. (1999)	Frieman et al. (2006)	Prieto et al. (2006)
...	SN2007af	N	0.00546	Koribalski et al. (2004)	Nakano & Itagaki (2007)	Salgado et al. (2007)
...	SN2007gi	N	0.00462	Cappellari et al. (2011)	Nakano et al. (2007)	Harutyunyan et al. (2007)
...	SN2007if	SC	0.07416	Scalzo et al. (2010)	Akerlof et al. (2007)	Akerlof et al. (2007)
...	SN2007le	N	0.00672	Koribalski et al. (2004)	Monard et al. (2007)	Filippenko et al. (2007)
...	SN2007on	N	0.00649	Graham et al. (1998)	Pollas & Klotz (2007)	Morrell et al. (2007)
...	SN2008A	Iax	0.01643	Theureau et al. (1998)	Nakano et al. (2008)	Blondin & Berlind (2008)
...	SN2008Q	N	0.00802	Cappellari et al. (2011)	Villi et al. (2008)	Stanishev & Pursimo (2008)
...	SN2009dc	SC	0.02139	Falco et al. (1999)	Puckett et al. (2009)	Harutyunyan et al. (2009)
...	SN2009ig	N	0.00877	Meyer et al. (2004)	Kleiser et al. (2009)	Kleiser et al. (2009)
...	SN2009le	N	0.01779	Theureau et al. (1998)	Pignata et al. (2009)	Challis & Berlind (2009)
...	SN2010ev	N	0.00921	Meyer et al. (2004)	Pignata et al. (2010)	Stritzinger (2010)
...	SN2010gp	N	0.02450	Downes et al. (1993)	Maza et al. (2010)	Folatelli et al. (2010b)
...	SN2010hg	N	0.00822	Meyer et al. (2004)	Monard & Africa (2010)	Prieto et al. (2010)
...	SN2010lp	91bg-like	0.01015	Huchra et al. (1999)	Cox et al. (2010)	Prieto & Morrell (2011)

Table B2 – continued All SNe Ia studied in this work.

Disc. Name	IAU Name	Pec?	z	Redshift Ref.	Discovery	Classification
...	SN2011K	N	0.01450	Monard et al. (2011)	Drake et al. (2011a)	Drake et al. (2011a)
SNhunt37	SN2011ae	N	0.00605	Meyer et al. (2004)	Howerton et al. (2011)	Howerton et al. (2011)
...	SN2011at	N	0.00676	Theureau et al. (1998)	Cox et al. (2011)	Cox et al. (2011)
...	SN2011by	N	0.00284	Verheijen & Sancisi (2001)	Drake et al. (2011b)	Zhang et al. (2011)
...	SN2011ek	N	0.00503	Rhee & van Albada (1996)	Nakano et al. (2011)	Nakano et al. (2011)
PTF11kly	SN2011fe	N	0.00080	Maguire et al. (2014)	Nugent et al. (2011b)	Cenko et al. (2011)
...	SN2011im	N	0.01623	Catinella et al. (2005)	Brimacombe et al. (2011)	Brimacombe et al. (2011)
...	SN2011iv	N	0.00649	Graham et al. (1998)	Noguchi et al. (2011a)	Noguchi et al. (2011)
...	SN2011iy	N	0.00427	Corsini et al. (2003)	Noguchi et al. (2011b)	Noguchi et al. (2011)
...	SN2012Z	Iax	0.00712	Koribalski et al. (2004)	Cenko et al. (2012)	Cenko et al. (2012)
...	SN2012cg	N	0.00146	Kent et al. (2008)	Kand rashoff et al. (2012)	Kand rashoff et al. (2012)
SNhunt136	SN2012cu	N	0.00347	de Vaucouleurs et al. (1991)	Marion et al. (2012)	Marion et al. (2012)
...	SN2012ei	N	0.00672	Galbany et al. (2014)	Nakano et al. (2012)	Nakano et al. (2012)
...	SN2012fr	N	0.00546	Bureau et al. (1996)	Klotz et al. (2012)	Klotz et al. (2012)
...	SN2012hr	N	0.00756	Tully et al. (2008)	Drescher et al. (2012)	Drescher et al. (2012)
...	SN2012ht	N	0.00356	Guthrie & Napier (1996)	Nishiyama et al. (2012)	Nishiyama et al. (2012)
...	SN2013aa	N	0.00400	Huchra et al. (1999)	Parker et al. (2013a)	Parker et al. (2013a)
SNhunt196	SN2013cs	N	0.00924	Pisano et al. (2011)	Howerton et al. (2013)	Howerton et al. (2013)
...	SN2013ct	N	0.00384	Smoker et al. (2000)	Parker et al. (2013b)	Parker et al. (2013b)
...	SN2013dy	N	0.00389	Pan et al. (2015)	Casper et al. (2013)	Casper et al. (2013)
...	SN2013gy	N	0.01402	Catinella et al. (2005)	Kim et al. (2013)	Kim et al. (2013)
...	SN2014J	N	0.00068	de Vaucouleurs et al. (1991)	Fossey et al. (2014)	Itagaki et al. (2014)
...	SN2014bv	N	0.00559	de Vaucouleurs et al. (1991)	Cortini et al. (2014)	Cortini et al. (2014)
...	SN2015F	N	0.00489	Meyer et al. (2004)	Monard et al. (2015)	Monard et al. (2015)
...	SN2015I	N	0.00759	Giovanelli et al. (1997)	Nakano et al. (2015)	Karamahmetoglu et al. (2015)
...	SN2016brx	91bg-like	0.01017	Jones et al. (2009)	Parker (2016)	Morrell & Shappee (2016)
...	SN2016bry	N	0.01602	Rhee & van Albada (1996)	Tinella (2016)	Ochner et al. (2016)
ASASSN-16eq	SN2016bsa	N	0.01431	Paturel et al. (2003)	Brimacombe et al. (2016)	Mattila et al. (2016)
Gaia16avm	SN2016ehy	N	0.04500	Halevi et al. (2016)	Delgado et al. (2016)	Halevi et al. (2016)
ATLAS16cpu	SN2016ffh	N	0.01820	Abazajian et al. (2005)	Tonry et al. (2016)	Terraran et al. (2016)
...	SN2016gxp	91T-like	0.01785	Huchra et al. (1999)	Gagliano et al. (2016)	Leadbeater (2016)
ASASSN-17cs	SN2017azw	N	0.02000	Nyholm et al. (2017)	Brimacombe et al. (2017)	Nyholm et al. (2017)
DLT17u	SN2017cbv	N	0.00399	Koribalski et al. (2004)	Tartaglia et al. (2017a)	Hosseinzadeh et al. (2017)
ATLAS17dfo	SN2017ckq	N	0.00989	Mathewson et al. (1992)	Tonry et al. (2017c)	Pan et al. (2017)
DLT17ar	SN2017cyy	N	0.00978	Meyer et al. (2004)	Tartaglia et al. (2017b)	Jha et al. (2017)
DLT17bk	SN2017ejb	91bg-like	0.00987	de Vaucouleurs et al. (1991)	Tartaglia et al. (2017c)	Valenti et al. (2017)
ASASSN-18hz	SN2017evn	N	0.01716	Adelman-McCarthy et al. (2008)	Wiethoff et al. (2017)	Everson et al. (2017)
...	SN2017ezd	N	0.01808	Jones et al. (2009)	Parker (2017)	Uddin et al. (2017)
DLT17bx	SN2017fgc	N	0.00772	Cappellari et al. (2011)	Sand et al. (2017)	Sand et al. (2017)
DLT17cd	SN2017fzw	91bg-like	0.00540	de Vaucouleurs et al. (1991)	Tartaglia et al. (2017d)	Hosseinzadeh et al. (2017)
ATLAS17jiv	SN2017gah	N	0.00891	Lauberts & Valentijn (1989)	Tonry et al. (2017d)	Hosseinzadeh et al. (2017)
...	SN2017glq	N	0.01176	Woods et al. (2006)	Gagliano et al. (2017)	Prentice & Ashall (2017)
ATLAS17nmh	SN2017isq	N	0.00939	Benetti et al. (2017)	Tonry et al. (2017a)	Benetti et al. (2017)
ATLAS17nse	SN2017iyb	N	0.01011	Meyer et al. (2004)	Tonry et al. (2017b)	Jones et al. (2017)
ASASSN-18hb	SN2018aqi	N	0.01251	Theureau et al. (1998)	Malesani et al. (2018)	Brimacombe et al. (2018)
ASASSN-18bt	SN2018oh	N	0.01098	Schneider et al. (1990)	Brown et al. (2018)	Leadbeater (2018)
ASASSN-18da	SN2018vw	91T-like	0.02000	Dong et al. (2018b)	Stanek (2018)	Stone et al. (2018)
DLT18h	SN2018xx	N	0.00999	Smith et al. (2000)	Sand et al. (2018b)	Sand et al. (2018c)
DLT18i	SN2018yu	N	0.00811	de Vaucouleurs et al. (1991)	Sand et al. (2018d)	Zhang et al. (2018)
...	SNF-012 ^b	SC	0.07454	Taubenberger et al. (2013a)

^aPSN J1149 = PSN J11492548-0507138^bSNF-012 = SNF20080723-012

Table B3. SNe Ia light curve parameters, number of late-time spectra and the corresponding phases, ordered by t_{\max} . See §3 for fitting methods.

SN	t_{\max}^a (MJD)	$\Delta m_{15}(B)$ (mag)	μ (mag)	E(B-V)	N_{spec}	Phase (days)
SN1972E	41445.9 ± 0.4	0.93 ± 0.06	27.75 ± 0.06 ¹	-0.03 ± 0.06	4	205 – 418
SN1981B	44672.7 ± 0.4	1.12 ± 0.06	30.91 ± 0.05 ²	0.06 ± 0.06	1	267
SN1986G	46561.0 ± 0.4	1.57 ± 0.07	27.82 ± 0.06 ¹	0.91 ± 0.06	4	256 – 325
SN1990N	48082.5 ± 0.3	1.09 ± 0.06	31.53 ± 0.07 ²	0.02 ± 0.06	5	186 – 333
SN1991T	48374.5 ± 0.3	0.97 ± 0.06	30.67 ± 0.09 ¹	0.17 ± 0.06	6	258 – 552
SN1991bg	48604.1 ± 0.4	1.76 ± 0.06	31.07 ± 0.06 ³	0.07 ± 0.07	2	198 – 202
SN1992A	48639.3 ± 0.3	1.27 ± 0.06	31.22 ± 0.06 ³	0.04 ± 0.06	1	292
SN1993Z	49247.1 ± 0.8	0.87 ± 0.06	33.10 ± 0.17	0.00 ± 0.06	2	181 – 213
SN1994ae	49685.3 ± 0.3	1.04 ± 0.06	32.07 ± 0.05 ²	0.05 ± 0.06	2	219 – 369
SN1995D	49767.4 ± 0.4	0.90 ± 0.06	32.67 ± 0.18	0.01 ± 0.06	2	278 – 286
SN1996X	50189.8 ± 0.3	1.20 ± 0.06	32.29 ± 0.25	-0.02 ± 0.06	2	247 – 299
SN1998aq	50930.8 ± 0.3	1.11 ± 0.07	31.74 ± 0.07 ²	0.01 ± 0.06	3	210 – 240
SN1998bu	50951.9 ± 0.3	1.05 ± 0.06	30.11 ± 0.06 ⁴	0.41 ± 0.06	11	191 – 341
SN1999aa	51232.5 ± 0.3	0.90 ± 0.06	34.19 ± 0.23	-0.01 ± 0.06	2	258 – 284
SN1999by	51308.9 ± 0.3	1.76 ± 0.06	30.75 ± 0.06 ⁵	0.05 ± 0.06	1	185
SN2000cx	51752.8 ± 0.3	1.27 ± 0.06	32.14 ± 0.09 ⁶	0.02 ± 0.06	2	182 – 451
SN2001el	52182.3 ± 0.4	1.12 ± 0.06	31.31 ± 0.05 ²	0.22 ± 0.06	3	310 – 398
SN2002bo	52356.8 ± 0.3	1.10 ± 0.06	31.73 ± 0.09 ¹	0.36 ± 0.06	2	227 – 311
SN2002cx	52415.1 ± 0.3	1.13 ± 0.06	35.31 ± 0.15 ⁷	0.07 ± 0.06	4	232 – 317
SN2002dj	52451.3 ± 0.4	1.02 ± 0.08	33.23 ± 0.16	0.03 ± 0.07	2	220 – 273
SN2002er	52525.3 ± 0.3	1.23 ± 0.06	33.15 ± 0.17	0.16 ± 0.06	1	214
SN2003cg	52729.2 ± 0.3	1.14 ± 0.06	31.83 ± 0.10 ¹	1.32 ± 0.06	1	385
SN2003du	52766.6 ± 0.3	1.02 ± 0.06	32.92 ± 0.06 ²	0.00 ± 0.06	6	194 – 375
SN2003gs	52842.2 ± 0.4	1.59 ± 0.06	32.13 ± 0.20	0.00 ± 0.06	1	207
SN2003hv	52891.5 ± 0.3	1.55 ± 0.06	31.51 ± 0.20	0.00 ± 0.06	2	319 – 393
SN2003kf	52980.3 ± 0.3	1.03 ± 0.06	32.43 ± 0.10 ¹	-0.03 ± 0.06	1	401
SN2004S	53039.7 ± 0.4	1.06 ± 0.06	33.41 ± 0.18	0.00 ± 0.06	1	315
SN2004eo	53278.7 ± 0.3	1.31 ± 0.06	34.03 ± 0.15	0.01 ± 0.06	1	227
SN2005W	53412.6 ± 0.3	1.02 ± 0.06	33.01 ± 0.20	0.23 ± 0.06	1	213
SN2005am	53435.0 ± 0.3	1.30 ± 0.06	32.66 ± 0.17	0.03 ± 0.06	2	300 – 383
SN2005cf	53534.3 ± 0.3	1.11 ± 0.06	32.26 ± 0.10 ²	-0.02 ± 0.06	4	266 – 383
SN2005hk	53684.8 ± 0.3	1.58 ± 0.10	33.91 ± 0.15 ⁷	...	2	378 – 408
SN2006X	53786.3 ± 0.3	1.08 ± 0.06	30.72 ± 0.06 ¹	1.38 ± 0.06	3	277 – 360
SN2006dd	53918.6 ± 0.3	1.05 ± 0.06	31.52 ± 0.13	0.00 ± 0.06	2	188 – 195
SN2006gz	54021.7 ± 0.1	0.88 ± 0.06	35.22 ± 0.15 ⁷	0.20 ± 0.06	1	339
SN2007af	54174.0 ± 0.3	1.08 ± 0.06	31.79 ± 0.05 ²	0.12 ± 0.06	1	302
SN2007gi	54327.9 ± 0.3	1.21 ± 0.06	32.17 ± 0.12	0.12 ± 0.06	1	223
SN2007if	54340.3 ± 0.4	0.88 ± 0.06	37.55 ± 0.15 ⁷	-0.03 ± 0.06	2	393 – 421
SN2007le	54399.0 ± 0.3	1.05 ± 0.06	32.44 ± 0.10	0.30 ± 0.06	1	307
SN2007on	54419.8 ± 0.3	1.81 ± 0.06	31.34 ± 0.07 ³	...	3	286 – 381
SN2008A	54478.0 ± 0.4	1.55 ± 0.09	34.26 ± 0.15 ⁷	...	3	204 – 288
SN2008Q	54505.6 ± 0.3	1.09 ± 0.06	32.66 ± 0.18	0.06 ± 0.06	1	200
SNF-012	54682.1 ± 1.1	1.29 ± 0.16	37.66 ± 0.15 ⁷	...	3	265 – 319
SN2009dc	54946.4 ± 0.4	0.80 ± 0.06	35.07 ± 0.15 ⁷	...	2	287 – 380
SN2009ig	55080.1 ± 0.3	0.88 ± 0.06	32.50 ± 0.08 ²	0.12 ± 0.06	1	405
SN2009le	55165.6 ± 0.4	0.91 ± 0.06	34.47 ± 0.17	0.20 ± 0.06	1	317
SN2010ev	55384.8 ± 0.3	1.12 ± 0.06	33.47 ± 0.20	0.19 ± 0.06	1	270
SN2010gp	55406.0 ± 0.4	1.10 ± 0.06	34.61 ± 0.36	0.44 ± 0.08	1	276
SN2010hg	55451.0 ± 5.0	...	32.82 ± 0.50 ⁸	...	1	203
SN2010lp	55568.0 ± 5.0	...	33.04 ± 0.40 ⁸	...	1	264
SN2011K	55577.9 ± 0.3	1.30 ± 0.06	33.95 ± 0.09	0.01 ± 0.06	1	344
SNhunt37	55620.1 ± 0.6	1.03 ± 0.07	32.16 ± 0.08	0.05 ± 0.13	1	306
SN2011at	55625.0 ± 0.4	0.92 ± 0.06	32.63 ± 0.16	0.17 ± 0.06	1	359
SN2011by	55690.5 ± 0.5	1.11 ± 0.08	31.59 ± 0.07 ²	0.09 ± 0.07	1	207
SN2011ek	55788.8 ± 0.4	1.00 ± 0.07	32.47 ± 0.44	0.59 ± 0.06	1	422
PTF11kly	55815.1 ± 0.3	1.18 ± 0.06	29.14 ± 0.05 ²	0.04 ± 0.06	9	204 – 346
SN2011iy	55893.2 ± 0.4	1.03 ± 0.08	31.33 ± 0.17	0.25 ± 0.06	1	205
SN2011im	55902.3 ± 0.4	1.06 ± 0.07	34.83 ± 0.15	0.11 ± 0.06	1	313
SN2011iv	55906.0 ± 0.3	1.63 ± 0.05	31.53 ± 0.07 ⁹	0.01 ± 0.06	5	244 – 304
SN2012Z	55967.7 ± 0.1	1.43 ± 0.01	32.52 ± 0.06 ²	...	4	193 – 254

Table B3 – continued Basic SNe Ia light curve parameters, number of late-time spectra and the corresponding phases. See §3 for fitting methods.

SN	t_{\max}^a (MJD)	$\Delta m_{15}(B)$ (mag)	μ (mag)	E(B-V)	N_{spec}	Phase (days)
SN2012cg	56082.1 ± 0.3	0.98 ± 0.06	31.03 ± 0.15	0.20 ± 0.06	3	286 – 342
SNhunt136	56105.1 ± 0.1	...	31.11 ± 0.15 ¹⁰	...	1	319
SN2012ei	56160.0 ± 5.0	...	32.01 ± 0.46 ¹¹	...	1	254
SN2012fr	56244.0 ± 0.3	0.90 ± 0.06	31.31 ± 0.06 ²	-0.02 ± 0.06	8	222 – 415
SN2012hr	56287.0 ± 0.3	1.07 ± 0.06	33.19 ± 0.16	0.00 ± 0.06	3	284 – 458
SN2012ht	56296.0 ± 0.3	1.56 ± 0.06	31.91 ± 0.04 ²	0.00 ± 0.06	1	422
SN2013aa	56343.2 ± 0.4	0.90 ± 0.06	30.60 ± 0.22	0.02 ± 0.06	6	189 – 426
SN2013ct	56416.1 ± 5.0	...	30.27 ± 0.20 ¹	...	1	229
SNhunt196	56437.2 ± 0.3	1.07 ± 0.06	32.78 ± 0.17	0.14 ± 0.06	3	263 – 304
SN2013dy	56501.0 ± 0.3	0.94 ± 0.06	31.50 ± 0.08 ²	0.10 ± 0.06	4	334 – 480
SN2013gy	56648.9 ± 0.3	1.10 ± 0.06	33.75 ± 0.15 ¹²	0.20 ± 0.06	4	235 – 424
SN2014J	56690.3 ± 0.3	1.01 ± 0.06	27.74 ± 0.08 ¹	1.22 ± 0.06	4	212 – 350
SN2014bv	56840.3 ± 0.4	1.79 ± 0.06	31.66 ± 0.36	0.46 ± 0.06	1	294
ASASSN-14hr	56937.4 ± 1.7	...	35.70 ± 0.36 ⁷	...	1	468
ASASSN-14jg	56959.7 ± 0.4	0.89 ± 0.06	34.00 ± 0.16	0.03 ± 0.06	3	223 – 325
ASASSN-14jc	56960.3 ± 4.0	...	33.44 ± 0.15 ⁷	...	1	390
ASASSN-14jz	56979.0 ± 2.6	...	33.50 ± 0.50 ⁷	...	1	204
ASASSN-14kq	56991.1 ± 1.5	...	35.69 ± 0.15 ⁷	...	1	413
ASASSN-14lv	56995.1 ± 1.7	...	36.57 ± 0.15 ⁷	...	1	398
ASASSN-14lu	57000.7 ± 4.8	...	34.46 ± 0.46 ¹³	...	1	477
ASASSN-14lt	57011.1 ± 2.1	...	35.76 ± 0.50 ¹⁴	...	1	389
ASASSN-14me	57023.1 ± 0.5	...	34.42 ± 0.15 ⁷	...	2	304 – 362
ASASSN-15be	57052.5 ± 0.6	...	34.97 ± 0.15 ⁷	...	1	265
SN2015F	57106.7 ± 0.3	... ^a	... ^a	... ^a	7	193 – 295
ASASSN-15hx	57152.2 ± 0.3	... ^a	... ^a	... ^a	3	250 – 445
SN2015I	57157.4 ± 0.4	... ^a	... ^a	... ^a	1	269
PSN J1149	57216.6 ± 0.4	... ^a	... ^a	... ^a	1	205
SN2016brx	57497.0 ± 5.0	...	33.01 ± 0.40 ⁸	...	1	184
SN2016bry	57506.4 ± 0.0	... ^a	... ^a	... ^a	1	206
ASASSN-16eq	57507.1 ± 0.5	... ^a	... ^a	... ^a	1	202
Gaia16avm	57584.8 ± 0.4	... ^a	... ^a	... ^a	1	229
ATLAS16cpu	57632.0 ± 0.4	... ^a	... ^a	... ^a	1	182
SN2016gxp	57682.1 ± 0.4	... ^a	... ^a	... ^a	1	218
ASASSN-17cs	57817.2 ± 0.3	... ^a	... ^a	... ^a	1	220
DLT17u	57842.3 ± 0.3	... ^a	... ^a	... ^a	1	316
ATLAS17dfo	57850.3 ± 0.3	... ^a	... ^a	... ^a	1	288
DLT17ar	57870.7 ± 0.4	... ^a	... ^a	... ^a	1	228
DLT17bk	57911.1 ± 0.4	... ^a	... ^a	... ^a	1	284
ASASSN-18hz	57935.7 ± 0.4	... ^a	... ^a	... ^a	1	229
SN2017ezd	57941.3 ± 0.4	... ^a	... ^a	... ^a	1	255
DLT17bx	57959.9 ± 0.3	... ^a	... ^a	... ^a	1	379
ATLAS17jiv	57985.4 ± 0.3	... ^a	... ^a	... ^a	1	295
DLT17cd	57989.5 ± 0.3	... ^a	... ^a	... ^a	1	229
SN2017glq	58016.0 ± 0.4	... ^a	... ^a	... ^a	1	331
ATLAS17nmh	58058.4 ± 1.4	... ^a	... ^a	... ^a	1	195
ATLAS17nse	58118.4 ± 0.3	... ^a	... ^a	... ^a	2	253 – 307
ASASSN-18bt	58163.3 ± 0.3	... ^a	... ^a	... ^a	3	236 – 267
ASASSN-18da	58178.8 ± 0.4	... ^a	... ^a	... ^a	1	220
DLT18h	58185.3 ± 0.4	... ^a	... ^a	... ^a	1	336
DLT18i	58195.2 ± 0.3	... ^a	... ^a	... ^a	1	237
ASASSN-18hb	58222.9 ± 0.4	... ^a	... ^a	... ^a	1	237

References: (1) Tully et al. (2013); (2) Riess et al. (2016); (3) Villegas et al. (2010); (4) Freedman et al. (2001); (5) Saha et al. (2006); (6) Larsen et al. (2001); (7) Derived from redshift; (8) Theureau et al. (2007); (9) Blakeslee et al. (2010); (10) Huang et al. (2017); (11) Tonry et al. (2001); (12) Holmbo et al. (2018); (13) Saulder et al. (2016); (14) Springob et al. (2014); (15) Li et al. (2019).

^a To be presented in P. Chen et al. (in prep.).

Table B4. Spectra observations.

SN	Obs. Date (MJD)	Phase ^a (days)	Telescope ^b	Instrument ^b	Range (Å)	Expt. (s)	v_{exp} [km s ⁻¹]	Qual.	Ref.
SN1972E	41651.00	205.1	P200	DBSP	4000 – 10000	...	5100 ± 800	Med	Kirshner & Oke (1975)
	41682.00	236.1	P200	DBSP	3300 – 10300	...	5900 ± 400	Med	Kirshner & Oke (1975)
	41795.00	349.1	P200	DBSP	3400 – 10200	...	6300 ± 100	Med	Kirshner & Oke (1975)
	41864.00	418.1	P200	DBSP	3400 – 9200	...	6600 ± 200	Med	Kirshner & Oke (1975)
SN1981B	44940.00	267.3	HJST	UVITS	3400 – 7100	3600	6200 ± 300	Med	Branch et al. (1993)
SN1986G	46816.50	255.5	ESO2.2m	BC	4500 – 6800	...	5500 ± 100	Med	Cristiani et al. (1992)
	46817.50	256.5	ESO3.6m	EFOSC	3700 – 9500	...	4900 ± 100	High	Cristiani et al. (1992)
	46818.50	257.5	ESO3.6m	EFOSC	4000 – 9300	...	5000 ± 200	High	Cristiani et al. (1992)
	46885.50	324.5	ESO3.6m	EFOSC	3800 – 7000	...	5100 ± 400	Med	Cristiani et al. (1992)
SN1990N	48268.50	186.0	WHT	FOS	3400 – 9700	1880	5000 ± 700	High	Gomez et al. (1996)
	48309.50	227.0	WHT	FOS	3500 – 9700	1800	5800 ± 600	High	Gomez et al. (1996)
	48337.50	255.0	WHT	FOS	3500 – 9700	1800	5800 ± 800	Med	Gomez et al. (1996)
	48362.50	280.0	WHT	FOS	3500 – 9700	1800	5500 ± 500	Med	Gomez et al. (1996)
	48415.50	333.0	WHT	FOS	3600 – 9700	2000	6100 ± 400	Med	Gomez et al. (1996)
SN1991T	48632.50	258.0	WHT	ISIS	3200 – 8500	1800	7100 ± 400	High	Gomez et al. (1996)
	48658.50	284.0	INT	FOS1	3800 – 8800	3600	6500 ± 100	Med	Gomez et al. (1996)
	48690.50	316.0	INT	FOS1	3800 – 9900	1800	6200 ± 1000	Med	Gomez et al. (1996)
	48694.93	320.4	Shane3m	KAST	3300 – 10100	3600	6500 ± 700	Med	BSNIP
	48723.86	349.3	Shane3m	KAST	3300 – 10400	3600	6600 ± 200	Med	BSNIP
SN1991bg	48802.50	198.4	WHT	FOS2	4900 – 9700	2000	(3 000)	Low	Gomez et al. (1996)
	48806.50	202.4	ESO3.6m	EFOSC2	3800 – 6800	...	1100 ± 100	Med	Turatto et al. (1996)
SN1992A	48931.00	291.7	HST	FOS	1600 – 4800	2000	(3 000)	Low	Kirshner et al. (1993)
SN1993Z	49428.50	181.4	Shane3m	KAST	3100 – 10300	1800	6700 ± 400	Med	BSNIP
	49460.00	212.9	Shane3m	KAST	3100 – 10400	2700	6200 ± 800	Med	BSNIP
SN1994ae	49904.71	219.4	Shane3m	KAST	3600 – 10400	1800	5900 ± 500	Med	BSNIP
	50053.97	368.7	MMT	BCS	3200 – 8600	1200	6000 ± 200	Med	CfA
SN1995D	50045.00	277.6	MMT	BCS	3200 – 8200	1200	7000 ± 200	Med	CfA
	50053.00	285.6	MMT	BCS	3200 – 8800	1200	5800 ± 400	Med	CfA
SN1996X	50437.00	247.2	ESO1.5m	BC	3500 – 9200	...	4100 ± 100	Low	Salvo et al. (2001)
	50489.00	299.2	ESO3.6m	EFOSC2	3700 – 6900	...	6200 ± 200	High	Salvo et al. (2001)
SN1998aq	51141.00	210.2	Till	FAST	3700 – 7500	2100	5900 ± 300	Med	CfA
	51161.00	230.2	Till	FAST	3700 – 7500	2400	6100 ± 100	Med	CfA
	51171.00	240.2	Till	FAST	3700 – 7500	2400	6200 ± 300	Med	CfA
	51143.04	191.2	Till	FAST	3700 – 7500	2400	6000 ± 500	High	CfA
	51161.04	209.2	Till	FAST	3700 – 7500	2400	6200 ± 200	High	CfA
SN1998bu	51169.98	218.1	Till	FAST	3700 – 7500	2400	6100 ± 200	Med	CfA
	51188.88	237.0	Shane3m	KAST	3400 – 10200	1800	6300 ± 200	High	BSNIP
	51195.96	244.1	Till	FAST	3700 – 7500	2400	6100 ± 200	Med	CfA
	51201.96	250.1	D1.54m	DFOSC	3000 – 8500	...	6300 ± 1500	Med	Cappellaro et al. (2001)
	51204.96	253.1	NTT	SOFI	9400 – 25400	4800	3000 ± 700	Med	Spyromilio et al. (2004)
	51232.92	281.0	Shane3m	KAST	3400 – 10500	1800	6100 ± 100	High	BSNIP
	51281.50	329.6	ESO3.6m	EFOSC2	3400 – 7500	...	5900 ± 100	Med	Cappellaro et al. (2001)
	51292.78	340.9	Shane3m	KAST	3300 – 10500	1800	6400 ± 200	Med	BSNIP
SN1999aa	51491.00	258.5	KeckI	LRIS	4100 – 9500	600	5700 ± 1400	Med	BSNIP
	51517.00	284.5	KeckI	LRIS	3900 – 9900	600	6500 ± 100	Med	BSNIP
SN1999by	51494.14	185.2	KeckI	LRIS	4000 – 9700	100	2100 ± 900	High	BSNIP
SN2000cx	51935.00	182.2	MMT	BCS	3700 – 7100	2400	6300 ± 200	Med	CfA
	52204.00	451.2	KeckII	ESI	3900 – 10100	1800	11300 ± 1000	Low	BSNIP
SN2001el	52492.40	310.1	VLT	FORS1	6200 – 10000	1500	(3 000)	Med	PI-Sollerman
	52500.35	318.1	VLT	FORS1	6200 – 10000	2400	(3 000)	Med	PI-Sollerman
SN2002bo	52580.15	397.9	VLT	FORS1	3800 – 9300	3000	5300 ± 800	Med	Mattila et al. (2005)
	52584.00	227.2	KeckII	ESI	4000 – 10100	240	(3 000)	low	BSNIP
	52668.00	311.2	MMT	BCS	3200 – 8700	3600	5800 ± 400	Med	Blondin et al. (2012)
	52647.15	232.1	KeckI	LRIS	3200 – 9200	1800	(3 000)	Low	BSNIP
SN2002cx	52699.11	284.0	KeckI	LRIS	3100 – 9200	2200	(3 000)	Low	BSNIP
	52699.14	284.1	KeckI	LRIS	6100 – 7300	2200	(3 000)	Low	BSNIP
	52731.81	316.7	Clay	LDSS	3600 – 9300	3600	(3 000)	Low	CfA
	52671.00	219.7	NTT	EFOSC2	3400 – 7400	...	6400 ± 400	Med	Pignata et al. (2008)
SN2002dj	52724.00	272.7	VLT	FORS1	3600 – 8500	...	6500 ± 300	Med	Pignata et al. (2008)

Table B4 – continued Spectra observations.

SN	Obs. Date (MJD)	Phase ^a (days)	Telescope ^b	Instrument ^b	Range (Å)	Expt. (s)	v_{exp} [km s ⁻¹]	Qual.	Ref.
SN2002er	52739.00	213.7	TNG	DOLORES	3500 – 8000	...	5800 ± 100	Med	Kotak et al. (2005)
SN2003cg	53114.00	384.8	VLT	FORS1	3900 – 8000	3800	6000 ± 500	Med	Elias-Rosa et al. (2006)
SN2003du	52961.00	194.4	WHT	ISIS	4400 – 7000	...	5800 ± 100	Med	Stanishev et al. (2007)
	52974.00	207.4	CA3.5m	MOSCA	3200 – 9200	...	5500 ± 200	Med	Stanishev et al. (2007)
	52986.00	219.4	CA2.2m	CAFOS	3200 – 8700	...	6300 ± 900	Med	Stanishev et al. (2007)
	53037.00	270.4	CA2.5m	MOSCA	3200 – 9200	...	6600 ± 100	Med	Stanishev et al. (2007)
	53063.00	296.4	Sub	CISCO	10200 – 18900	4000	6700 ± 1700	Low	Höflich et al. (2004)
	53142.00	375.4	TNG	DOLORES	3400 – 8000	...	6300 ± 800	High	Stanishev et al. (2007)
	53049.30	207.1	KeckII	ESI	3900 – 10100	...	3900 ± 500	High	BSNIP
SN2003hv	53211.00	319.5	VLT	FORS1	3400 – 9800	...	6100 ± 100	High	Leloudas et al. (2009)
	53285.00	393.5	Sub	CISCO	10200 – 18900	12000	4900 ± 100	Med	Motohara et al. (2006)
SN2003kf	53381.00	400.7	Clay	LDSS	4000 – 8400	2400	6900 ± 200	Med	CfA
SN2004S	53355.00	315.3	KeckII	DEIMOS	4700 – 7100	1800	(3000)	Low	BSNIP
SN2004eo	53506.00	227.3	VLT	FORS1	3600 – 8700	2280	5600 ± 300	High	Pastorello et al. (2007)
SN2005W	53626.04	213.4	Sub	CISCO	10300 – 18900	4000	3900 ± 300	Med	Motohara et al. (2006)
SN2005am	53735.00	300.0	KeckI	LRIS	5400 – 7100	7200	6800 ± 600	Med	Leonard (2007)
	53818.00	383.0	GS	GMOS	5100 – 6800	10410	5700 ± 800	Med	Leonard (2007)
	53800.00	265.7	GN	GMOS	5500 – 7500	10800	5400 ± 600	High	Leonard (2007)
SN2005cf	53852.00	317.7	KeckI	LRIS	3200 – 9200	1200	5800 ± 300	Med	BSNIP
	53887.00	352.7	KeckI	LRIS	5800 – 7400	11000	5600 ± 800	Med	Leonard (2007)
	53917.00	382.7	KeckI	LRIS	5800 – 7400	6600	5900 ± 400	Med	Leonard (2007)
SN2005hk	54062.73	377.9	KeckI	LRIS	3100 – 9100	1800	(3000)	Low	McCully et al. (2014)
	54092.72	407.9	KeckII	DEIMOS	4900 – 9900	1800	(3000)	Low	McCully et al. (2014)
SN2006X	54063.14	276.9	KeckI	LRIS	3100 – 9200	500	7000 ± 1200	Med	BSNIP
	54093.15	306.9	KeckII	DEIMOS	4600 – 7200	600	(3000)	Low	BSNIP
	54146.00	359.7	KeckI	LRIS	3200 – 9200	1800	5500 ± 1400	Low	BSNIP
SN2006dd	54106.30	187.7	NTT	EMMI	4000 – 10100	600	6300 ± 100	Med	Stritzinger et al. (2010)
	54113.30	194.7	duPont	DPBC	3900 – 10000	2700	6800 ± 800	Med	Stritzinger et al. (2010)
SN2006gz	54360.70	339.0	Sub	FOCAS	3700 – 9900	3600	(3000)	Low	Maeda et al. (2009)
SN2007af	54476.00	302.0	MMT	BCS	3200 – 8300	2700	5400 ± 300	Med	CfA
SN2007gi	54551.00	223.1	GN	GMOS	4500 – 8700	1300	4400 ± 900	High	Sand et al. (2019)
SN2007if	54733.20	392.9	VLT	FORS2	3500 – 9000	5700	(3000)	Low	Taubenberger et al. (2013a)
SN2007le	54761.20	420.9	VLT	FORS2	3500 – 9000	8550	(3000)	Med	Taubenberger et al. (2013a)
SN2007on	54705.50	306.5	KeckI	LRIS	3300 – 9200	1200	6500 ± 200	Med	BSNIP
	54773.50	285.6	Clay	LDSS	4500 – 7000	7200	5500 ± 600	High	CSP
SN2008A	54800.50	353.7	GS	GMOS	3800 – 9900	1200	5700 ± 300	High	Gall et al. (2018)
	54681.63	380.7	GS	GMOS	3900 – 7900	1500	5600 ± 200	Med	Gall et al. (2018)
SN2008Q	54706.51	203.6	KeckI	LRIS	3400 – 9000	600	(3000)	Med	McCully et al. (2014)
	54766.28	228.5	KeckI	LRIS	3200 – 9100	1200	(3000)	Med	McCully et al. (2014)
	54973.50	288.3	KeckI	LRIS	3200 – 9100	1200	(3000)	Med	McCully et al. (2014)
SNF-012	54947.50	265.4	VLT	FORS2	3300 – 8900	...	7100 ± 100	Med	BSNIP
SN2009dc	54973.50	291.4	VLT	FORS2	3600 – 8900	...	6800 ± 100	Med	Taubenberger et al. (2013a)
	55001.50	319.4	VLT	FORS2	3600 – 8600	...	7300 ± 400	Med	Taubenberger et al. (2013a)
SN2009ig	55233.60	287.2	KeckI	LRIS	3400 – 9900	600	(3000)	Med	Silverman et al. (2011)
	55326.20	379.8	VLT	XSH	3300 – 13000	5400	(3000)	Med	Taubenberger et al. (2013a)
SN2009le	55485.27	405.1	VLT	FORS2	3500 – 10200	2400	7300 ± 2200	High	Maguire et al. (2016)
SN2009le	55482.14	316.5	VLT	FORS2	3400 – 10800	2700	7000 ± 200	Med	PI-Taubenberger
SN2010ev	55655.01	270.2	VLT	FORS2	4000 – 8400	2400	6500 ± 600	Med	PI-Taubenberger
SN2010gp	55682.29	276.2	VLT	FORS2	3400 – 9700	2700	6100 ± 200	High	Maguire et al. (2016)
SN2010hg	55654.16	203.2	VLT	FORS2	3500 – 10100	900	5900 ± 600	High	PI-Taubenberger
SN2010lp	55832.00	264.0	VLT	FORS2	3600 – 10200	8100	(3000)	High	Taubenberger et al. (2013b)
SN2011K	55922.10	344.2	VLT	FORS2	3400 – 6500	5400	5600 ± 300	Med	PI-Taubenberger
SNhun37	55926.31	306.2	VLT	FORS2	3600 – 8200	1200	7100 ± 800	Med	PI-Taubenberger
SN2011at	55984.10	359.1	VLT	FORS2	3600 – 10200	2400	6700 ± 400	Med	PI-Taubenberger
SN2011by	55897.60	207.1	KeckI	LRIS	3300 – 10100	450	5600 ± 800	High	Silverman et al. (2013)
SN2011ek	56211.21	422.4	VLT	FORS2	3400 – 10000	2700	5800 ± 100	Med	Maguire et al. (2016)
PTF11kly	56019.00	203.9	Shane3m	KAST	3500 – 10000	...	5700 ± 500	High	Mazzali et al. (2015)
	56040.00	224.9	Shane3m	KAST	3500 – 10000	...	5700 ± 300	High	Mazzali et al. (2015)

Table B4 – continued Spectra observations.

SN	Obs. Date (MJD)	Phase ^a (days)	Telescope ^b	Instrument ^b	Range (Å)	Expt. (s)	v_{exp} [km s ⁻¹]	Qual.	Ref.
	56044.00	228.9	LBT	MODS	3200 – 10000	...	5800 ± 300	High	Shappee et al. (2013a)
	56046.25	231.1	KeckI	LRIS	3100 – 7300	300	5900 ± 100	Med	PI-Filippenko
	56073.00	257.9	WHT	ISIS	3500 – 9500	...	5500 ± 100	High	Mazzali et al. (2015)
	56103.00	287.9	WHT	ISIS	3400 – 10000	...	5700 ± 200	High	Mazzali et al. (2015)
	56125.00	309.9	Shane3m	KAST	3500 – 10000	...	5800 ± 200	High	Mazzali et al. (2015)
	56128.00	312.9	GTC	OSIRIS	3600 – 10400	...	5800 ± 100	High	Taubenberger et al. (2015)
	56161.00	345.9	WHT	ISIS	3500 – 10000	...	5800 ± 300	High	Mazzali et al. (2015)
SN2011iy	56098.10	204.9	duPont	WFCCCD	3600 – 9200	1500	6300 ± 100	High	This work
SN2011im	56215.60	313.3	VLT	FORS2	3800 – 6300	5400	5900 ± 300	Med	PI-Taubenberger
SN2011iv	56149.50	243.5	duPont	WFCCCD	3600 – 9100	1000	5500 ± 400	Med	Gall et al. (2018)
	56166.30	260.3	NTT	EFOSC	3600 – 9200	1800	6400 ± 200	High	Gall et al. (2018)
	56181.30	275.3	duPont	WFCCCD	3600 – 9100	1200	7200 ± 600	Med	Gall et al. (2018)
	56210.37	304.4	VLT	FORS2	3400 – 10200	900	6800 ± 200	Med	Maguire et al. (2016)
SN2012Z	56161.00	193.3	SALT	RSS	3500 – 9300	...	(3 000)	Low	Stritzinger et al. (2015)
	56182.00	214.3	duPont	WFCCCD	3800 – 9100	...	(3 000)	Low	Stritzinger et al. (2015)
	56215.00	247.3	KeckII	DEIMOS	4600 – 9700	...	(3 000)	Low	Stritzinger et al. (2015)
	56222.00	254.3	Sub	FOCAS	4000 – 8000	...	(3 000)	Low	Yamanaka et al. (2015)
SN2012cg	56368.40	286.3	LBT	MODS	3400 – 10000	9600	6500 ± 200	High	Shappee et al. (2018)
	56420.20	338.1	VLT	XSH	3700 – 24800	4800	6300 ± 300	High	Maguire et al. (2016)
	56424.15	342.1	VLT	FORS2	3400 – 10600	600	5400 ± 1100	High	Maguire et al. (2016)
SNhunt136	56424.16	319.1	VLT	FORS2	3400 – 10600	1800	5600 ± 200	High	Maguire et al. (2016)
SN2012ei	56414.38	254.4	LBT	MODS	3400 – 8900	3600	5300 ± 200	Med	Vallely et al. (2019a)
SN2012fr	56466.26	222.2	ANU	WiFeS	3500 – 9500	4800	6200 ± 900	Med	Childress et al. (2015)
	56505.19	261.1	ANU	WiFeS	3500 – 9200	7200	6200 ± 400	Med	Childress et al. (2015)
	56533.50	289.5	GS	GMOS	4000 – 9500	3000	6100 ± 600	High	Graham et al. (2017)
	56581.81	337.8	NTT	EFOSC2	3600 – 9200	5400	5000 ± 700	Low	Smartt et al. (2015b)
	56584.37	340.3	SALT	RSS	3500 – 9300	2700	5900 ± 100	Med	Childress et al. (2015)
	56600.30	356.3	VLT	XSH	3700 – 24700	6000	4600 ± 1200	High	Maguire et al. (2016)
	56610.99	366.9	ANU	WiFeS	3500 – 9200	10800	6500 ± 200	Med	Childress et al. (2015)
	56659.50	415.5	GS	GMOS	4000 – 9500	12600	6300 ± 800	Med	Graham et al. (2017)
SN2012hr	56571.50	284.5	GS	GMOS	4000 – 9500	8000	5400 ± 300	High	Childress et al. (2015)
	56656.50	369.5	ANU	WiFeS	3500 – 9200	12000	5800 ± 100	Med	Childress et al. (2015)
	56745.50	458.5	GS	GMOS	4000 – 5800	7200	(3 000)	Low	Graham et al. (2017)
SN2012ht	56718.15	422.2	VLT	XSH	3700 – 24700	12600	(3 000)	Low	Maguire et al. (2016)
SN2013aa	56532.25	189.0	SALT	RSS	3500 – 9000	1350	5700 ± 900	High	Childress et al. (2015)
	56548.88	205.7	ANU	WiFeS	3500 – 9200	4800	5900 ± 700	Med	Childress et al. (2015)
	56689.08	345.9	ANU	WiFeS	3500 – 9200	10800	5800 ± 300	Med	Childress et al. (2015)
	56696.40	353.2	VLT	XSH	3700 – 10700	3800	6100 ± 100	High	Maguire et al. (2016)
	56743.50	400.3	GS	GMOS	4000 – 9500	4500	6000 ± 200	Med	Graham et al. (2017)
	56769.20	426.0	VLT	XSH	3700 – 24700	7500	4400 ± 700	High	Maguire et al. (2018)
SN2013ct	56645.05	228.9	VLT	XSH	3700 – 24700	1900	5500 ± 700	High	Maguire et al. (2016)
SNhunt196	56700.00	262.8	GS	GMOS	4000 – 9500	2700	5000 ± 700	Med	Graham et al. (2017)
	56738.00	300.8	ANU	WiFeS	3500 – 9200	10800	6500 ± 200	Low	Childress et al. (2015)
	56741.00	303.8	VLT	XSH	3700 – 24600	11700	5800 ± 1100	High	Maguire et al. (2016)
SN2013dy	56834.58	333.6	KeckII	DEIMOS	4500 – 9600	2400	7100 ± 200	High	Pan et al. (2015)
	56920.00	419.0	KeckII	DEIMOS	4000 – 7600	2400	6800 ± 100	Med	Childress et al. (2015)
	56924.34	423.4	KeckI	LRIS	3200 – 10100	2000	6400 ± 100	Med	Pan et al. (2015)
	56981.32	480.4	KeckI	LRIS	3200 – 10100	2000	(3 000)	Low	Pan et al. (2015)
SN2013gy	56883.50	234.6	Baade	IMACS	3000 – 8300	...	6600 ± 800	Med	Holmbo et al. (2018)
	56920.00	271.1	KeckII	DEIMOS	3900 – 7500	...	5300 ± 400	Med	Childress et al. (2015)
	56924.00	275.1	KeckI	LRIS	3200 – 10000	2400	5500 ± 500	Med	Childress et al. (2015)
	57073.00	424.1	KeckI	LRIS	3200 – 10000	2400	(3 000)	Low	Graham et al. (2017)
SN2014J	56902.00	211.7	WHT	ACAM	4900 – 9400	180	5500 ± 600	Med	Galbany et al. (2016)
	56920.00	229.7	KeckII	DEIMOS	4000 – 7600	...	5900 ± 600	High	Childress et al. (2015)
	56958.00	267.7	HCT	HFOSC	3700 – 9100	...	5500 ± 300	Med	Srivastav et al. (2016)
	57040.00	349.7	HCT	HFOSC	3700 – 9100	...	5600 ± 500	Med	Srivastav et al. (2016)
SN2014bv	57134.23	293.9	LBT	MODS	3400 – 9900	10800	5100 ± 400	Med	Vallely et al. (2019a)
ASASSN-14hr	57405.06	467.6	VLT	MUSE	4600 – 9000	2800	(3 000)	Low	This work
ASASSN-14jg	57182.27	222.5	Baade	IMACS	4000 – 8100	1800	6500 ± 300	High	This work

Table B4 – continued Spectra observations.

SN	Obs. Date (MJD)	Phase ^a (days)	Telescope ^b	Instrument ^b	Range (Å)	Expt. (s)	v_{exp} [km s ⁻¹]	Qual.	Ref.
	57228.15	268.4	GS	GMOS	4000 – 9400	14400	5900 ± 1000	Med	Graham et al. (2017)
	57285.20	325.5	VLT	XSH	3600 – 10100	2900	6300 ± 1100	Med	Maguire et al. (2018)
ASASSN-14jc	57350.26	390.0	VLT	MUSE	4700 – 9200	2465	(3000)	Low	This work
ASASSN-14jz	57182.56	203.5	Baade	IMACS	4000 – 8100	1800	6000 ± 900	High	This work
ASASSN-14kq	57404.02	412.9	VLT	MUSE	4600 – 9000	2450	(3000)	Low	This work
ASASSN-14lv	57393.04	398.0	VLT	MUSE	4500 – 8900	2460	(3000)	Low	This work
ASASSN-14lu	57477.30	476.6	VLT	MUSE	4600 – 9100	2475	(3000)	Low	This work
ASASSN-14lt	57400.05	388.9	VLT	MUSE	4600 – 9000	4960	(3000)	Low	This work
ASASSN-14me	57327.21	304.1	VLT	MUSE	4700 – 9200	2470	(3000)	Low	This work
	57385.11	362.0	VLT	MUSE	4700 – 9200	2460	(3000)	Low	This work
ASASSN-15be	57317.30	264.8	VLT	XSH	3600 – 10000	5800	6200 ± 200	Med	BSNIP
SN2015F	57299.24	192.5	NTT	EFOSC	5900 – 9900	2700	(3000)	Med	Smartt et al. (2015b)
	57302.33	195.6	NTT	EFOSC	3300 – 7400	5400	5300 ± 400	Med	Smartt et al. (2015b)
	57331.36	224.6	VLT	XSH	5800 – 10100	1200	(3000)	Med	PI-Cartier
	57345.24	238.5	VLT	XSH	5800 – 10100	3300	(3000)	Med	PI-Cartier
	57372.22	265.5	VLT	XSH	5800 – 10100	3700	(3000)	Med	PI-Cartier
	57386.00	279.3	GS	GMOS	4000 – 9500	6000	6000 ± 600	High	Graham et al. (2017)
	57402.18	295.5	Baade	MagE	3500 – 8200	32400	5200 ± 700	High	This work
ASASSN-15hx	57402.31	250.1	Baade	MagE	3100 – 8200	22800	6200 ± 500	High	This work
	57566.08	413.9	VLT	XSH	3000 – 24600	3000	(3000)	Med	Maguire et al. (2018)
	57597.00	444.8	VLT	XSH	3000 – 24600	3000	(3000)	Med	PI-Maguire
SN2015I	57426.00	268.6	LBT	MODS	3000 – 9900	10800	6400 ± 800	Med	Vallely et al. (2019a)
PSN J1149	57421.30	204.7	VLT	XSH	3700 – 24700	2900	5400 ± 600	High	Maguire et al. (2018)
SN2016brx	57681.00	184.0	Clay	LDSS	3700 – 9500	12600	3100 ± 700	High	Dong et al. (2018a)
SN2016bry	57712.14	205.7	LBT	MODS	3000 – 5700	...	(3000)	Low	Vallely et al. (2019a)
ASASSN-16eq	57709.19	202.1	LBT	MODS	3200 – 5400	...	6100 ± 300	Low	Vallely et al. (2019a)
Gaia16avm	57814.00	229.2	LBT	MODS	3200 – 8100	3600	7500 ± 600	Low	Vallely et al. (2019a)
ATLAS16cpu	57814.30	182.3	LBT	MODS	3000 – 10800	...	6100 ± 600	Med	Vallely et al. (2019a)
SN2016gxp	57900.43	218.3	LBT	MODS	3000 – 9800	...	5300 ± 1200	Med	Vallely et al. (2019a)
ASASSN-17cs	58037.00	219.8	VLT	FORS2	4200 – 9100	2600	6100 ± 600	Med	100IAs
DLT17u	58158.27	316.0	Clay	LDSS	3900 – 9200	1800	5500 ± 200	Med	This work
ATLAS17dfo	58138.29	288.0	VLT	FORS2	4200 – 9100	2600	5900 ± 300	Med	100IAs
DLT17ar	58098.28	227.6	VLT	FORS2	4200 – 9100	2600	5200 ± 800	Med	100IAs
DLT17bk	58195.36	284.3	VLT	FORS2	4100 – 9400	2600	4100 ± 300	Med	100IAs
ASASSN-18hz	58164.28	228.5	VLT	FORS2	4100 – 9400	2600	5500 ± 500	Med	100IAs
SN2017ezd	58196.36	255.1	VLT	FORS2	4100 – 9300	2600	5500 ± 900	Low	100IAs
DLT17bx	58339.27	379.3	VLT	FORS2	4200 – 9500	2600	5800 ± 1500	Med	100IAs
ATLAS17jiv	58280.27	294.9	VLT	FORS2	4100 – 9400	2600	4800 ± 600	Med	100IAs
DLT17cd	58218.04	228.5	VLT	FORS2	4200 – 9500	2600	5100 ± 300	High	100IAs
SN2017glq	58347.25	331.3	VLT	FORS2	4200 – 7500	2600	5700 ± 400	Med	100IAs
ATLAS17nmh	58253.17	194.8	VLT	FORS2	4200 – 9500	2600	6300 ± 300	High	100IAs
ATLAS17nse	58371.38	253.0	VLT	FORS2	4100 – 9100	2600	5300 ± 400	High	100IAs
	58425.21	306.8	VLT	FORS2	4100 – 9600	2600	5300 ± 200	High	100IAs
ASASSN-18bt	58399.45	236.2	KeckII	DEIMOS	4600 – 9700	3600	5700 ± 700	High	Dimitriadis et al. (2019a)
	58427.25	264.0	KeckI	LRIS	3800 – 10000	3600	6100 ± 100	High	Dimitriadis et al. (2019a)
	58430.60	267.3	KeckI	LRIS	3100 – 10300	4800	5700 ± 300	Med	Tucker et al. (2018)
ASASSN-18da	58399.20	220.4	VLT	FORS2	4000 – 9300	2600	7100 ± 600	High	100IAs
DLT18h	58521.21	335.9	VLT	FORS2	4100 – 9500	2600	7600 ± 200	Med	100IAs
DLT18i	58432.31	237.2	VLT	FORS2	4100 – 9600	2600	5300 ± 700	High	100IAs
ASASSN-18hb	58460.30	237.4	VLT	FORS2	4100 – 9100	2600	6200 ± 500	High	100IAs

^a Relative to t_{\max} ^b See §2 for definitions and references.

Table B5. Flux limits for each line in Table 2 and the corresponding H/He mass limit.

SN	H-rich Model				He-rich Model			
	Phase ^a (days)	Line ^b	Flux Limit (erg/s/cm ²)	Mass Limit (M_{\odot})	Phase ^a (days)	Line ^b	Flux Limit (erg/s/cm ²)	Mass Limit (M_{\odot})
SN1972E	418.1	H α	2.52×10^{-16}	4.95×10^{-5}	349.1	HeI-a	3.07×10^{-17}	9.84×10^{-5}
SN1981B	267.3	H α	5.54×10^{-16}	1.49×10^{-3}	267.3	HeI-a	5.86×10^{-16}	2.25×10^{-3}
SN1986G	324.5	H α	1.68×10^{-15}	2.84×10^{-4}	256.5	HeI-b	6.57×10^{-16}	5.29×10^{-4}
SN1990N	280.0	H α	9.52×10^{-17}	5.68×10^{-4}	280.0	HeI-a	2.35×10^{-16}	1.53×10^{-3}
SN1991T	258.0	H α	1.99×10^{-14}	4.78×10^{-2}	349.3	HeI-a	4.84×10^{-14}	> 2.0
SN1991bg	202.4	H α	1.81×10^{-16}	1.26×10^{-3}	202.4	HeI-b	1.35×10^{-16}	2.39×10^{-3}
SN1992A	291.7	H γ	1.87×10^{-15}	2.91×10^{-1}
SN1993Z	212.9	H α	8.16×10^{-16}	2.68×10^{-2}	212.9	HeI-b	5.07×10^{-16}	1.20×10^{-1}
SN1994ae	368.7	H α	5.58×10^{-17}	2.84×10^{-4}	368.7	HeI-a	6.44×10^{-17}	4.20×10^{-4}
SN1995D	285.6	H β	1.50×10^{-16}	2.30×10^{-3}	285.6	HeI-a	2.57×10^{-16}	3.69×10^{-3}
SN1996X	247.2	H α	5.55×10^{-17}	8.24×10^{-4}	247.2	HeI-a	6.36×10^{-17}	1.28×10^{-3}
SN1998aq	240.2	H α	7.75×10^{-16}	4.84×10^{-3}	230.2	HeI-a	8.05×10^{-16}	1.40×10^{-2}
SN1998bu	329.6	H α	2.18×10^{-16}	2.86×10^{-4}	281.0	HeI-b	1.41×10^{-16}	6.45×10^{-4}
SN1999aa	258.5	H α	5.41×10^{-17}	2.82×10^{-3}	258.5	HeI-a	4.89×10^{-17}	3.85×10^{-3}
SN1999by	185.2	H α	3.05×10^{-16}	1.74×10^{-3}	185.2	HeI-b	2.04×10^{-16}	3.11×10^{-3}
SN2000cx	451.2	H α	7.44×10^{-16}	8.94×10^{-4}	451.2	HeI-a	6.91×10^{-16}	> 2.0
SN2001el	318.1	H α	6.84×10^{-17}	3.00×10^{-4}	310.1	HeI-b	2.25×10^{-17}	4.82×10^{-4}
SN2002bo	311.2	H α	3.35×10^{-17}	3.03×10^{-4}	227.2	HeI-a	3.41×10^{-17}	6.66×10^{-4}
SN2002cx	284.0	H β	1.47×10^{-17}	2.55×10^{-3}	232.1	HeI-a	2.30×10^{-17}	2.19×10^{-2}
SN2002dj	272.7	H α	9.53×10^{-17}	1.91×10^{-3}	272.7	HeI-a	8.24×10^{-17}	2.47×10^{-3}
SN2002er	213.7	H α	7.59×10^{-15}	> 2.0	213.7	HeI-a	7.23×10^{-15}	> 2.0
SN2003cg	384.8	H α	2.35×10^{-14}	3.52×10^{-2}	384.8	HeI-a	2.12×10^{-14}	> 2.0
SN2003du	296.4	Pa β	2.28×10^{-15}	1.00×10^{-2}	219.4	HeI-b	9.18×10^{-16}	1.16×10^{-1}
SN2003gs	207.1	H α	5.65×10^{-17}	1.05×10^{-3}	207.1	HeI-b	3.77×10^{-17}	1.80×10^{-3}
SN2003hv	319.5	H α	2.58×10^{-17}	1.82×10^{-4}	319.5	HeI-a	6.89×10^{-17}	4.54×10^{-4}
SN2003kf	400.7	H β	2.29×10^{-17}	2.54×10^{-4}	400.7	HeI-a	1.47×10^{-17}	1.96×10^{-4}
SN2004AS	315.3	H α	9.10×10^{-17}	1.43×10^{-3}	315.3	HeI-a	1.26×10^{-16}	2.69×10^{-3}
SN2004eo	227.3	H α	2.24×10^{-15}	7.38×10^{-1}	227.3	HeI-a	2.78×10^{-15}	> 2.0
SN2005W	213.4	Pa β	5.28×10^{-16}	6.59×10^{-3}
SN2005am	383.0	H α	2.17×10^{-17}	2.00×10^{-4}	300.0	HeI-a	3.50×10^{-17}	1.05×10^{-3}
SN2005cf	352.7	H α	2.27×10^{-17}	2.76×10^{-4}	265.7	HeI-a	4.62×10^{-17}	8.51×10^{-4}
SN2005hk	407.9	H α	1.48×10^{-17}	2.69×10^{-4}	407.9	HeI-a	1.44×10^{-17}	3.56×10^{-4}
SN2006X	359.7	H α	4.13×10^{-18}	3.43×10^{-5}	359.7	HeI-a	3.51×10^{-18}	4.01×10^{-5}
SN2006dd	194.7	H α	1.64×10^{-14}	9.86×10^{-1}	187.7	HeI-a	2.63×10^{-14}	> 2.0
SN2006gz	339.0	H α	3.22×10^{-17}	1.89×10^{-3}	339.0	HeI-a	8.49×10^{-18}	9.77×10^{-4}
SN2007af	302.0	H α	2.49×10^{-16}	1.11×10^{-3}	302.0	HeI-a	1.24×10^{-16}	9.36×10^{-4}
SN2007gi	223.1	H α	5.25×10^{-17}	8.94×10^{-4}	223.1	HeI-b	5.32×10^{-17}	2.10×10^{-3}
SN2007if	420.9	H β	1.95×10^{-18}	7.88×10^{-4}	420.9	HeI-a	3.48×10^{-18}	1.23×10^{-3}
SN2007le	306.5	H β	4.99×10^{-16}	4.34×10^{-3}	306.5	HeI-a	3.72×10^{-16}	3.42×10^{-3}
SN2007on	380.7	H α	2.79×10^{-18}	3.33×10^{-5}	285.6	HeI-a	3.33×10^{-18}	3.64×10^{-4}
SN2008A	288.3	H α	2.96×10^{-17}	1.40×10^{-3}	288.3	HeI-a	3.32×10^{-17}	2.20×10^{-3}
SN2008Q	200.4	H α	1.13×10^{-16}	2.82×10^{-3}	200.4	HeI-b	1.18×10^{-16}	8.04×10^{-3}
SNF-012	319.4	H α	8.08×10^{-18}	4.72×10^{-3}	265.4	HeI-a	9.07×10^{-18}	1.58×10^{-2}
SN2009dc	379.8	Pa β	8.00×10^{-18}	2.72×10^{-4}	287.2	HeI-a	1.32×10^{-17}	2.91×10^{-3}
SN2009ig	405.1	H α	1.18×10^{-17}	1.10×10^{-4}	405.1	HeI-a	1.82×10^{-17}	1.87×10^{-4}
SN2009le	316.5	H α	6.89×10^{-17}	2.45×10^{-3}	316.5	HeI-a	1.29×10^{-16}	6.42×10^{-3}
SN2010ev	270.2	H β	6.34×10^{-17}	2.39×10^{-3}	270.2	HeI-b	1.70×10^{-17}	1.44×10^{-3}
SN2010gp	276.2	H α	6.51×10^{-18}	6.47×10^{-4}	276.2	HeI-a	1.14×10^{-17}	1.36×10^{-3}
SN2010hg	203.2	H α	3.55×10^{-16}	8.95×10^{-3}	203.2	HeI-b	7.22×10^{-17}	5.61×10^{-3}
SN2010lp	264.0	H β	2.00×10^{-16}	4.88×10^{-3}	264.0	HeI-a	1.87×10^{-16}	4.70×10^{-3}
SN2011K	344.2	H β	6.35×10^{-17}	1.73×10^{-3}	344.2	HeI-a	1.11×10^{-16}	2.77×10^{-3}
SNhunt37	306.2	H β	1.01×10^{-16}	9.84×10^{-4}	306.2	HeI-a	1.05×10^{-16}	1.03×10^{-3}
SN2011at	359.1	H β	1.54×10^{-16}	1.17×10^{-3}	359.1	HeI-a	2.87×10^{-16}	1.93×10^{-3}
SN2011by	207.1	H α	2.60×10^{-16}	2.33×10^{-3}	207.1	HeI-b	1.75×10^{-16}	4.28×10^{-3}
SN2011ek	422.4	H α	4.24×10^{-17}	2.06×10^{-4}	422.4	HeI-a	8.19×10^{-17}	4.19×10^{-4}
PTF11kly	228.9	H α	3.70×10^{-15}	2.63×10^{-3}	228.9	HeI-a	8.68×10^{-15}	8.74×10^{-3}
SN2011iy	204.9	H α	8.11×10^{-16}	5.19×10^{-3}	204.9	HeI-b	7.12×10^{-16}	1.38×10^{-2}
SN2011im	313.3	H β	5.13×10^{-17}	3.79×10^{-3}	313.3	HeI-a	8.73×10^{-17}	6.30×10^{-3}

Table B5 – continued Flux limits for each line in Table 2 and the corresponding H/He mass limit if computed. Flux limits are given in [erg/s/cm²] and stripped mass limits are given in [M_{\odot}].

SN	H-rich Model				He-rich Model			
	Phase ^a (days)	Line ^b	Flux Limit (erg/s/cm ²)	Mass Limit (M_{\odot})	Phase ^a (days)	Line ^b	Flux Limit (erg/s/cm ²)	Mass Limit (M_{\odot})
SN2011iv	304.4	H α	1.16×10^{-16}	5.36×10^{-4}	304.4	HeI-a	1.25×10^{-16}	7.79×10^{-4}
SN2012Z	254.3	H β	6.99×10^{-16}	1.25×10^{-2}	247.3	HeI-a	5.71×10^{-16}	1.19×10^{-2}
SN2012cg	338.1	Pa α	1.33×10^{-16}	2.08×10^{-4}	286.3	HeI-a	2.30×10^{-16}	1.13×10^{-3}
SNhunt136	319.1	H α	3.21×10^{-16}	7.37×10^{-4}	319.1	HeI-a	3.48×10^{-16}	1.09×10^{-3}
SN2012ei	254.4	H α	1.71×10^{-17}	2.99×10^{-4}	254.4	HeI-a	2.43×10^{-17}	5.08×10^{-4}
SN2012fr	356.3	Pa α	3.08×10^{-16}	3.64×10^{-4}	289.5	HeI-a	7.73×10^{-17}	5.47×10^{-4}
SN2012hr	458.5	H β	3.42×10^{-17}	4.81×10^{-4}	284.5	HeI-a	5.01×10^{-17}	1.45×10^{-3}
SN2012ht	422.2	Pa α	1.27×10^{-16}	1.84×10^{-4}	422.2	HeI-a	1.73×10^{-16}	4.88×10^{-4}
SN2013aa	426.0	Pa α	6.72×10^{-17}	6.29×10^{-5}	345.9	HeI-b	4.06×10^{-17}	9.53×10^{-4}
SN2013ct	228.9	Pa α	2.23×10^{-16}	4.10×10^{-4}	228.9	HeI-c	3.17×10^{-16}	6.49×10^{-4}
SNhunt196	303.8	Pa α	8.05×10^{-17}	5.48×10^{-4}	262.8	HeI-a	8.54×10^{-17}	2.17×10^{-3}
SN2013dy	419.0	H α	4.30×10^{-17}	1.25×10^{-4}	333.6	HeI-a	3.53×10^{-17}	4.85×10^{-4}
SN2013gy	424.1	H α	8.27×10^{-18}	1.50×10^{-4}	271.1	HeI-a	5.91×10^{-18}	2.72×10^{-3}
SN2014J	267.7	H β	2.60×10^{-15}	7.47×10^{-4}	267.7	HeI-a	5.19×10^{-15}	1.26×10^{-3}
SN2014bv	293.9	H α	1.18×10^{-16}	6.42×10^{-4}	293.9	HeI-a	1.93×10^{-16}	1.28×10^{-3}
ASASSN-14hr	467.6	H α	2.05×10^{-16}	3.70×10^{-3}	467.6	HeI-a	1.29×10^{-16}	> 2.0
ASASSN-14jg	325.5	H α	8.65×10^{-17}	1.91×10^{-3}	222.5	HeI-a	7.37×10^{-17}	7.05×10^{-3}
ASASSN-14jc	390.0	H α	2.19×10^{-16}	1.48×10^{-3}	390.0	HeI-a	1.11×10^{-16}	1.26×10^{-3}
ASASSN-14jz	203.5	H α	2.79×10^{-16}	1.31×10^{-2}	203.5	HeI-b	8.51×10^{-17}	1.21×10^{-2}
ASASSN-14kq	412.9	H α	5.26×10^{-16}	1.74×10^{-2}	412.9	HeI-a	1.73×10^{-16}	> 2.0
ASASSN-14lv	398.0	H α	2.38×10^{-16}	2.18×10^{-2}	398.0	HeI-a	1.10×10^{-16}	> 2.0
ASASSN-14lu	476.6	H α	5.57×10^{-16}	2.99×10^{-3}	476.6	HeI-a	4.44×10^{-16}	> 2.0
ASASSN-14lt	388.9	H α	8.22×10^{-17}	3.86×10^{-3}	388.9	HeI-a	1.03×10^{-16}	> 2.0
ASASSN-14me	362.0	H α	1.22×10^{-16}	2.47×10^{-3}	304.1	HeI-a	1.36×10^{-16}	1.32×10^{-2}
ASASSN-15be	264.8	H β	2.90×10^{-17}	4.20×10^{-3}	264.8	HeI-a	9.48×10^{-17}	1.38×10^{-2}
SN2015F	295.5	H α	1.63×10^{-17}	1.64×10^{-4}	295.5	HeI-a	1.10×10^{-17}	1.70×10^{-4}
ASASSN-15hx	444.8	H α	1.08×10^{-17}	8.98×10^{-5}	250.1	HeI-a	3.25×10^{-17}	2.51×10^{-3}
SN2015I	268.6	H α	2.53×10^{-16}	4.21×10^{-3}	268.6	HeI-a	1.91×10^{-16}	4.97×10^{-3}
PSN J1149	204.7	Pa α	9.61×10^{-17}	9.65×10^{-4}	204.7	HeI-c	1.74×10^{-16}	1.94×10^{-3}
SN2016brx	184.0	H α	3.83×10^{-17}	1.77×10^{-3}	184.0	HeI-b	3.59×10^{-17}	4.24×10^{-3}
SN2016bry	205.7	H β	1.33×10^{-16}	8.25×10^{-3}
ASASSN-16eq	202.1	H β	3.03×10^{-16}	1.03×10^{-2}
Gaia16avm	229.2	H α	2.49×10^{-17}	2.23×10^{-2}	229.2	HeI-a	2.16×10^{-17}	3.34×10^{-2}
ATLAS16cpu	182.3	H α	1.44×10^{-16}	2.42×10^{-2}	182.3	HeI-b	1.35×10^{-16}	1.10×10^{-1}
SN2016gxp	218.3	H α	1.56×10^{-16}	1.02×10^{-2}	218.3	HeI-a	1.42×10^{-16}	1.51×10^{-2}
ASASSN-17cs	219.8	H α	1.25×10^{-16}	9.13×10^{-3}	219.8	HeI-a	5.11×10^{-17}	6.02×10^{-3}
DLT17u	316.0	H α	1.03×10^{-16}	2.43×10^{-4}	316.0	HeI-a	1.51×10^{-16}	4.17×10^{-4}
ATLAS17dfo	288.0	H α	2.14×10^{-17}	8.99×10^{-4}	288.0	HeI-a	3.21×10^{-17}	1.73×10^{-3}
DLT17ar	227.6	H α	4.06×10^{-17}	1.70×10^{-3}	227.6	HeI-a	2.82×10^{-17}	1.84×10^{-3}
DLT17bk	284.3	H α	1.63×10^{-16}	5.13×10^{-3}	284.3	HeI-a	2.60×10^{-16}	1.30×10^{-2}
ASASSN-18hz	228.5	H α	1.77×10^{-16}	1.49×10^{-2}	228.5	HeI-a	7.81×10^{-17}	1.02×10^{-2}
SN2017ezd	255.1	H α	1.55×10^{-17}	1.70×10^{-3}	255.1	HeI-a	3.64×10^{-17}	5.18×10^{-3}
DLT17bx	379.3	H α	1.14×10^{-17}	1.27×10^{-4}	379.3	HeI-a	1.69×10^{-17}	2.11×10^{-4}
ATLAS17jiv	294.9	H α	7.74×10^{-17}	1.14×10^{-3}	294.9	HeI-a	1.74×10^{-16}	3.14×10^{-3}
DLT17cd	228.5	H α	1.90×10^{-16}	3.00×10^{-3}	228.5	HeI-b	1.82×10^{-16}	7.95×10^{-3}
SN2017glq	331.3	H α	2.04×10^{-17}	4.02×10^{-4}	331.3	HeI-a	1.64×10^{-17}	4.73×10^{-4}
ATLAS17nmh	194.8	H α	5.42×10^{-17}	2.31×10^{-3}	194.8	HeI-b	5.35×10^{-17}	6.05×10^{-3}
ATLAS17nse	306.8	H α	2.31×10^{-17}	5.95×10^{-4}	253.0	HeI-a	2.01×10^{-17}	1.69×10^{-3}
ASASSN-18bt	236.2	H α	4.48×10^{-17}	1.94×10^{-3}	267.3	HeI-a	5.52×10^{-17}	5.54×10^{-3}
ASASSN-18da	220.4	H α	8.98×10^{-17}	9.96×10^{-3}	220.4	HeI-a	6.54×10^{-17}	1.16×10^{-2}
DLT18h	335.9	H α	1.55×10^{-17}	3.38×10^{-4}	335.9	HeI-a	1.69×10^{-17}	4.87×10^{-4}
DLT18i	237.2	H α	2.26×10^{-17}	6.84×10^{-4}	237.2	HeI-a	1.18×10^{-17}	6.00×10^{-4}
ASASSN-18hb	237.4	H α	3.28×10^{-17}	2.68×10^{-3}	237.4	HeI-a	5.08×10^{-17}	5.96×10^{-3}

^a Relative to t_{\max} .

^b Corresponds to the lines listed in Table 2.

Table B6. New photometry presented in this study. Some data stem from archival images processed by this study for flux calibration purposes.

SN	MJD	Filter	AB Mag
ASASSN-14jg	57183.78	V	20.49 ± 0.08
ASASSN-15hx	57396.33	V	21.33 ± 0.04
SN2001el	52492.37	I	19.82 ± 0.07
SN2001el	52549.24	I	20.24 ± 0.07
SN2001el	52552.37	I	20.23 ± 0.08
SN2001el	52618.04	I	22.08 ± 0.15
SN2001el	52492.36	R	20.68 ± 0.10
SN2001el	52549.23	R	21.47 ± 0.08
SN2001el	52552.35	R	21.34 ± 0.08
SN2001el	52612.04	R	22.31 ± 0.10
SN2001el	52617.10	R	22.16 ± 0.10
SN2001el	52492.35	V	19.93 ± 0.09
SN2001el	52549.22	V	20.76 ± 0.09
SN2001el	52552.34	V	20.55 ± 0.08
SN2001el	52612.10	V	21.02 ± 0.15
SN2007on	54800.23	r	24.70 ± 0.35
SN2007on	54772.70	r	24.15 ± 0.14
SN2009ig	55484.29	I	22.39 ± 0.07
SN2009ig	55484.28	R	22.53 ± 0.08
SN2009ig	55484.28	V	22.09 ± 0.06
SN2009le	55484.30	V	21.88 ± 0.18
SN2009le	55484.31	I	21.79 ± 0.45
SN2009le	55484.31	R	21.47 ± 0.35
SN2010ev	55655.00	V	20.41 ± 0.07
SN2010ev	55655.00	R	20.58 ± 0.08
SN2010ev	55655.00	I	20.65 ± 0.07
SN2010ev	55655.00	B	20.22 ± 0.05
SN2010gp	55682.27	V	23.19 ± 0.06
SN2010gp	55682.27	R	23.09 ± 0.11
SN2010gp	55682.28	I	22.76 ± 0.11
SN2010gp	55682.26	B	22.16 ± 0.22
SN2010hg	55654.15	B	19.15 ± 0.11
SN2010hg	55654.15	V	19.35 ± 0.07
SN2010hg	55654.15	R	20.05 ± 0.06
SN2010hg	55654.15	I	20.06 ± 0.08
SN2010lp	55834.24	V	20.66 ± 0.16
SN2010lp	55834.26	I	19.50 ± 0.09
SN2010lp	55834.25	R	20.09 ± 0.07
SN2011K	55831.38	I	21.69 ± 0.06
SN2011K	55831.37	R	21.59 ± 0.05
SN2011K	55831.36	V	22.41 ± 0.09
SNhun37	55932.34	V	20.98 ± 0.11
SNhun37	55932.34	R	20.25 ± 0.15
SNhun37	55932.34	I	19.89 ± 0.12
SN2011at	55943.18	I	20.13 ± 0.06
SN2011at	55943.18	R	20.17 ± 0.05
SN2011at	55943.18	V	21.02 ± 0.06
SN2011ek	56210.20	V	23.07 ± 0.17
SN2011ek	56210.20	R	21.95 ± 0.12
SN2011ek	56210.21	I	21.62 ± 0.12
SN2011im	56213.03	I	21.05 ± 0.07
SN2011im	56213.02	R	21.37 ± 0.08
SN2011im	56206.08	R	20.77 ± 0.08
SN2011im	56213.01	V	22.84 ± 0.11
SN2011im	56206.08	V	22.11 ± 0.09
SN2011iv	56207.29	I	17.55 ± 0.13
SN2011iv	56207.29	R	18.08 ± 0.11
SN2011iv	56207.29	V	17.49 ± 0.11
SN2012cg	56444.99	I	19.49 ± 0.11
SN2012cg	56444.99	R	18.40 ± 0.09
SN2012cg	56444.99	V	20.76 ± 0.10
SNhun136	56423.19	I	21.50 ± 0.13
SNhun136	56423.19	R	21.67 ± 0.12
SNhun136	56423.18	V	22.06 ± 0.12
SN2012ei	56414.88	r	20.54 ± 0.11
SN2013gy	56883.41	R	23.50 ± 0.27
SN2014bv	57134.16	g	20.91 ± 0.06

Table B6 – continued New photometry presented in this study. Some data stem from archival images processed by this study for flux calibration purposes.

SN2015F	57273.30	V	18.90 ± 0.02
SN2015F	57306.35	V	19.31 ± 0.02
SN2015F	57334.29	V	19.66 ± 0.02
SN2015F	57403.20	V	20.87 ± 0.07
SN2015F	57424.11	V	20.99 ± 0.03
SN2015F	57443.15	V	21.33 ± 0.07
SN2015F	57494.06	V	22.28 ± 0.08
SN2015F	57273.30	g	18.74 ± 0.02
SN2015F	57306.35	g	19.10 ± 0.02
SN2015F	57334.30	g	19.65 ± 0.02
SN2015F	57403.24	g	20.48 ± 0.05
SN2015F	57424.12	g	20.82 ± 0.03
SN2015F	57443.16	g	20.89 ± 0.05
SN2015F	57494.04	g	22.07 ± 0.05
SN2015F	57273.30	r	19.08 ± 0.03
SN2015F	57306.35	r	19.64 ± 0.03
SN2015F	57334.31	r	20.17 ± 0.06
SN2015F	57403.26	r	21.03 ± 0.08
SN2015F	57424.13	r	21.18 ± 0.04
SN2015F	57443.17	r	21.28 ± 0.07
SN2015F	57494.09	r	21.72 ± 0.08
SN2015F	57273.30	i	19.07 ± 0.04
SN2015F	57306.36	i	19.44 ± 0.04
SN2015F	57334.32	i	19.81 ± 0.05
SN2015F	57403.28	i	20.31 ± 0.05
SN2015F	57424.14	i	20.74 ± 0.04
SN2015F	57443.17	i	19.99 ± 0.04
SN2015F	57494.11	i	21.12 ± 0.05
SN2015F	57395.26	B	20.37 ± 0.07
SN2015F	57395.26	V	20.33 ± 0.09
SN2015I	57426.17	r	20.29 ± 0.04
SN2015I	57396.93	V	20.29 ± 0.02
SN2015I	57396.93	I	19.95 ± 0.04
SN2016bry	57712.14	r	20.71 ± 0.09
ASASSN-16eq	57709.19	r	21.00 ± 0.06
Gaia16avm	57814.42	r	22.55 ± 0.05
ATLAS16cpu	57814.30	r	22.29 ± 0.08
SN2016gxp	57900.43	r	20.82 ± 0.14
ASASSN-17cs	58037.23	V	19.08 ± 0.11
DLT17u	58158.27	r	20.05 ± 0.04
ATLAS17dfo	58138.29	V	20.18 ± 0.08
DLT17ar	58098.28	V	20.81 ± 0.03
DLT17bk	58195.34	V	23.34 ± 0.08
ASASSN-18hz	58164.27	V	20.09 ± 0.07
SN2017ezd	58196.35	V	23.24 ± 0.22
DLT17bx	58339.26	V	21.04 ± 0.08
DLT17cd	58218.03	V	20.08 ± 0.04
ATLAS17jiv	58280.26	V	20.71 ± 0.11
SN2017glq	58347.25	V	22.87 ± 0.06
ATLAS17nmh	58253.17	V	19.47 ± 0.08
ATLAS17nse	58371.38	V	21.24 ± 0.08
ATLAS17nse	58381.36	V	21.47 ± 0.08
ATLAS17nse	58425.20	V	22.21 ± 0.09
ASASSN-18hb	58460.28	V	21.65 ± 0.08
ASASSN-18da	58399.20	V	20.20 ± 0.15
DLT18h	58521.21	V	22.57 ± 0.06
DLT18i	58432.31	V	21.45 ± 0.11

Table B7. Photometry data for each SN Ia studied in this work. N_{tot} refers to the total number of photometric points for a given SN. Phases are given relative to maximum light. Objects denoted with a * are used in deriving the NPPR (Appendix A).

SN	N_{tot}	Phases	Filters	Refs.
ASASSN-14jg*	113	5 – 268	B, V, g, r, i	ASAS-SN; Graham et al. (2017); This work
ASASSN-15hx	202	-16 – 325	V, g, i, SwiftU, SwiftB, SwiftV	ASAS-SN; This work
PSN J1149	16	-12 – 141	B, V, I	ASAS-SN
SN1972E*	468	-23 – 359	U, B, V, R, I	Przybylski (1972); Cousins (1972); Barbon et al. (1972); Ardeberg & de Groot (1973); van Genderen (1975); Osmer et al. (1972); Lee et al. (1972); Frye et al. (1972); Przybylski (1972)
SN1980N*	238	-11 – 368	U, B, V, R, I, H	Hamuy et al. (1991); Blanco et al. (1980); Blanco et al. (1980); Olszewski (1982); Elias & Frogel (1983)
SN1981B	281	-9 – 136	U, B, V, R, J, H, K	Busko et al. (1981); Tsvetkov (1982); Buta & Turner (1983); Tsvetkov (1982); Barbon et al. (1982); Vettolani et al. (1981); Elias & Frogel (1983)
SN1981D*	30	-14 – 274	B, V, J, H	Cragg et al. (1981); Hamuy et al. (1991); Elias & Frogel (1983)
SN1983W*	57	-7 – 161	U, B, V	
SN1986G	93	-7 – 403	U, B, V, R, I	Munch et al. (1986); Phillips et al. (1987); Bues et al. (1986); Blanco et al. (1986); Turatto et al. (1990); Schaefer (1987)
SN1989B*	350	-5 – 263	U, B, V, R, I, J, H, K	Barbon et al. (1990); Suntzeff et al. (1989); Lavery (1989); Tsvetkov et al. (1990); Wells et al. (1994); Pollas et al. (1989);

Table B7 – continued Continuation of Table B7.

SN	N_{tot}	Phases	Filters	Refs.
SN1990O*	41	2 – 309	B, V, R, I	Hamuy et al. (1996)
SN1991T*	669	-13 – 454	U, B, V, R, I, J, H, K	Tsvetkov (1986); Altavilla et al. (2004); Waagen et al. (1991); Lira et al. (1998); Menzies et al. (1991); Krisciunas et al. (2004); Holberg et al. (1991); Ford et al. (1993); Gilmore (1991); Schmidt et al. (1994)
SN1991bg*	171	-10 – 528	B, V, R, I, J, H, K	Leibendgut et al. (1993); Turatto et al. (1996); Krisciunas et al. (2004)
SN1992A*	62	-7 – 536	B, V, R, I	Liller & Buta (1992); Altavilla et al. (2004); Suntzeff et al. (1992)
SN1992bc*	145	-11 – 326	B, V, R, I	Hamuy et al. (1996)
SN1993Z	78	6 – 239	B, V, R, I	Ho et al. (2001)
SN1994D*	371	-14 – 432	U, B, V, R, I, J, H, K	Treffers et al. (1994); Richmond et al. (1995); Cumming et al. (1994); Walker et al. (1994); Heraudeau et al. (1994); Argyle et al. (1994); Mikuz (1994); Altavilla et al. (2004)
SN1994ae*	301	-15 – 530	U, B, V, R, I	Vanmunster et al. (1994); Riess et al. (2005); Riess et al. (1999); Vanmunster et al. (1994); Ho et al. (2001); Tsvetkov & Pavlyuk (1997); Altavilla et al. (2004)
SN1995D*	225	-8 – 424	B, V, R, I	Mikuz (1995); Riess et al. (1999); Altavilla et al. (2004); Ho et al. (2001)
SN1995ac*	100	-5 – 250	B, V, R, I	Riess et al. (1999); Altavilla et al. (2004)
SN1995al*	115	-13 – 182	U, B	Riess et al. (1999)

Table B7 – continued Continuation of Table B7.

SN	N_{tot}	Phases	Filters	Refs.
SN1997br*	223	-9 – 402	U, B, V, R, I	Li et al. (1999); CfA; Altavilla et al. (2004)
SN1997cw*	75	13 – 181	U, B, V, R, I	CfA
SN1998V*	60	2 – 187	U, B, V, R, I	CfA
SN1998aq*	257	-10 – 344	U, B, V, R, I	Riess et al. (2005)
SN1998bu	914	-7 – 56	U, B, V, R, I, J, H, K	Jha et al. (1999); Hernandez et al. (2000); Suntzeff et al. (1999)
SN1998ec*	59	5 – 186	U, B, V, R, I	BSNIP; CfA
SN1999aa	289	-11 – 79	U, B, V, R, I, J, K	Kowalski et al. (2008); BSNIP; CfA; Krisciunas et al. (2000); Altavilla et al. (2004)
SN1999ac*	356	-13 – 183	U, B, V, R, I, H, Ks	Phillips et al. (2006); BSNIP; CfA
SN1999by*	377	-12 – 212	U, B, V, R, I, J, H, K	Garnavich et al. (2004); BSNIP; Toth & Szabó (2000)
SN1999dq*	247	-11 – 154	U, B, V, R, I	BSNIP; CfA
SN1999gd*	35	-3 – 150	U, B, V, R, I	CfA
SN2000E*	287	-16 – 484	U, B, V, R, I, J, H, K	Valentini et al. (2003); Lair et al. (2006)
SN2000cx*	1067	-9 – 500	U, B, V, R, I	BSNIP; Li et al. (2006); Gennari (2006)

Table B7 – continued Continuation of Table B7.

SN	N_{tot}	Phases	Filters	Refs.
SN2001bg*	91	-2 – 358	B, V, R, I	BSNIP; Lair et al. (2006)
SN2001el*	566	-13 – 435	U, B, V, R, I, J, H, K	Krisciunas et al. (2003); This work
SN2002bo	656	-14 – 100	U, B, V, R, I, J, H, K	BSNIP; Benetti et al. (2004); Hicken et al. (2009); Szabó et al. (2003); Krisciunas et al. (2004)
SN2002cx	110	-8 – 50	B, V, R, I	BSNIP
SN2002dj	166	-14 – 65	U, B, V, R, I, J, H, K	Pignata et al. (2008); BSNIP; Hicken et al. (2009)
SN2002dp*	190	-6 – 183	U, B, V, R, I	BSNIP; Hicken et al. (2009)
SN2002er*	339	-16 – 323	U, B, V, R, I	Pignata et al. (2004); BSNIP; Christensen et al. (2003)
SN2002ha*	162	-12 – 237	U, B, V, R, I	BSNIP; Hicken et al. (2009)
SN2003K*	38	1 – 169	U, B, V, R, I	Hicken et al. (2009)
SN2003cg	439	-18 – 413	U, B, V, R, I, J, H, K	Elias-Rosa et al. (2006); Ganeshalingam et al. (2010); Hicken et al. (2009)
SN2003du	628	-12 – 465	U, B, V, R, I, J, H, K	Anupama et al. (2005); Stanishev et al. (2007); Hicken et al. (2009); BSNIP
SN2003gs*	188	8 – 378	B, V, R, I, J, H, K	Krisciunas et al. MNRAS 2000, RSNP (2019)

Table B7 – continued Continuation of Table B7.

SN	N_{tot}	Phases	Filters	Refs.
SN2004eo	768	-12 – 345	U, B, V, R, I, J, H, K, u, g, r, i	CSP; Pastorello et al. (2007); BSNIP
SN2005W	115	-8 – 16	B, V, u, g, r, i	CSP
SN2005am	388	-2 – 76	U, B, V, R, I, J, H, K, u, g, r, i	CSP; Hicken et al. (2009); BSNIP
SN2005cf	1107	-13 – 89	U, B, V, R, I, J, H, K, Ks	Hicken et al. (2009); BSNIP; Pastorello et al. (2007); Friedman et al. (2015); Brown et al. (2014)
SN2005hk	402	-20 – 381	U, B, V, R, I, J, H, Ks, u, g, r, i, z	Sako et al. (2014); Holtzman et al. (2008); Hicken et al. (2009); Friedman et al. (2015); Brown et al. (2014); Sahu et al. (2008)
SN2005ki*	344	-12 – 155	U, B, V, J, H, u, g, r, i	Hicken et al. (2009); CSP
SN2006X*	638	-11 – 151	U, B, V, R, I, J, H, K, Ks, u, g, r, i	Brown et al. (2014); BSNIP; CSP; Hicken et al. (2009); Friedman et al. (2015)
SN2006dd*	284	-11 – 228	B, V, R, I, J, H, K, u, g, r, i	Stritzinger et al. (2010)

Table B7 – continued Continuation of Table B7.

SN	N_{tot}	Phases	Filters	Refs.
SN2007gi	109	-12 – 190	U, B, V, R, I	Brown et al. (2014); Zhang et al. (2010)
SN2007if	224	14 – 358	B, V, R, I, J, H, Ks, u, g, r, i	CSP; Hicken et al. (2012); Friedman et al. (2015); Taubenberger et al. (2013a)
SN2007is*	24	2 – 163	B, V, r, i	Hicken et al. (2012)
SN2007le	484	-11 – 84	B, V, R, I, J, H, Ks, u, g, r, i	CSP; Friedman et al. (2015); BSNIP; Hicken et al. (2012)
SN2007on	665	-9 – 405	U, B, V, Y, J, H, K, u, g, r, i	CSP; Brown et al. (2014); This work; Gall et al. (2018)
SN2007sr*	347	5 – 196	U, B, V, R, I, J, H, Ks	Hicken et al. (2009); BSNIP; Brown et al. (2014); Friedman et al. (2015)
SN2007sw*	101	-2 – 154	B, V, r, i	Hicken et al. (2012)
SN2008A	201	-7 – 208	U, B, V, R, I, J, H, Ks, r, i	Hicken et al. (2012); Brown et al. (2014); Friedman et al. (2015); BSNIP
SN2008Q	84	-9 – 208	U, B, V, R, I, r, i	Brown et al. (2014); Hicken et al. (2012); BSNIP
SN2009dc	672	-20 – 286	U, B, V, R, I, J, H, Ks, u, g, r, i	Silverman et al. (2011); Friedman et al. (2015); Hicken et al. (2012); CSP; Brown et al. (2014)

Table B7 – continued Continuation of Table B7.

SN	N_{tot}	Phases	Filters	Refs.
SN2009nr*	147	-13 - 175	U, B, V, R, I	Khan et al. (2011)
SN2010ag*	102	-3 - 179	B, V, J, H, Ks, u, r, i	Friedman et al. (2015); Hicken et al. (2012)
SN2010dd*	96	-23 - 523	R	Maguire et al. (2014)
SN2010ev*	67	-7 - 270	U, B, V, R, I, u, g, r, i, z	Gutiérrez et al. (2016); Brown et al. (2014); This work
SN2010gp	59	-4 - 276	U, B, V, R, I	Brown et al. (2014); This work
SN2011K	40	-1 - 253	V, R, I, J, H, Ks	Friedman et al. (2015); This work
SNhunt37	90	1 - 312	V, R, I, J, H, Ks	Friedman et al. (2015); This work
SN2011at	57	7 - 463	U, B, V, R, I, J, H, Ks	Brown et al. (2014); Friedman et al. (2015); This work
SN2011by	158	-11 - 44	U, B, V, J, H, Ks	Brown et al. (2014); Friedman et al. (2015)
SN2011ek	68	-6 - 421	U, B, V, R, I	Maguire et al. (2014); Brown et al. (2014); This work
PTF11kly*	1956	-19 - 571	U, B, V, R, I, J, H, K, g, r	Firth et al. (2015); Nugent et al. (2011a); Brown et al. (2014); Guillochon et al. (2017); Tsvetkov et al. (2013); Munari et al. (2013); Richmond & Smith (2012); Weyant et al. (2018)

Table B7 – continued Continuation of Table B7.

SN	N_{tot}	Phases	Filters	Refs.
SN2011iy	127	10 - 150	B, V, Y, J, H, u, g, r, i	Weyant et al. (2018); CSP
SN2012Z	306	-8 - 265	U, B, V, J, H, u, g, r, i	Stritzinger et al. (2015); Brown et al. (2014); Foley et al. (2013)
SN2012cg	176	-16 - 598	U, B, V, R, I	Brown et al. (2014); Munari et al. (2013); This work
SN2012fr	733	-15 - 415	U, B, V, R, I, g, r, i	Brown et al. (2014); Graham et al. (2017); Zhang et al. (2014)
SN2012hr	284	-4 - 457	U, B, V, R, I, g, r, i	Brown et al. (2014); Graham et al. (2017); Smartt et al. (2015a)
SN2012ht	99	-13 - 102	U, B, V, R, I	Brown et al. (2014); Smartt et al. (2015a)
SN2013aa	493	-5 - 399	U, B, V, g, r, i	Brown et al. (2014); Graham et al. (2017)
SNhunt196	233	-20 - 261	U, B, V, R, I, J, H, u, g, r, i	Graham et al. (2017); Walker et al. (2015); Brown et al. (2014); Weyant et al. (2018)
SN2013ct	7	80 - 228	g, r, z	Inserra et al. (2013)
SN2013dy	1210	-16 - 337	U, B, V, R, I, J, H, g, r, i	Graham et al. (2017); Pan et al. (2015); Brown et al. (2014); Zhai et al. (2016)
SN2013gy	155	-17 - 234	U, B, V, R, g, r, i	Zheng et al. (2013); Graham et al. (2014); MNRAS 2010, 1-23 (2019); et al. (2014); This work

Table B7 – continued Continuation of Table B7.

SN	N_{tot}	Phases	Filters	Refs.
SN2015I	70	-10 - 322	U, B, V, I, g, r, i, z,	ASAS-SN; Foley et al. (2018) ; Brown et al. (2014) ; Karamehmetoglu et al. (2015) ; This SwiftB, work SwiftV
SN2016brx	11	10 - 185	V, R, g, r	ASAS-SN
SN2016bry	61	5 - 205	B, V, R, I, g, r	ASAS-SN; This work
ASASSN-16eq	55	-14 - 202	B, V, R, I, g, r	ASAS-SN; This work
iPTF16auf*	198	-15 - 185	B, V, R, I, g, r, i	ASAS-SN; Foley et al. (2018) ; Petrushevska et al. (2016) SwiftU, SwiftB, SwiftV
ASASSN-16fn*	98	-32 - 189	B, V, R, I, g, r, i	ASAS-SN
Gaia16avm	5	-11 - 325	V, r	ASAS-SN; This work
PS16em*	82	-78 - 195	B, V, r, i, SwiftU, SwiftB, SwiftV	ASAS-SN
ATLAS16cpu	81	-6 - 182	V, g, r, i, z, SwiftU, SwiftB, SwiftV	ASAS-SN; Foley et al. (2018) ; This work
Gaia16hj*	65	-11 - 154	B, V, r, i	ASAS-SN; Inserra et al. (2013)
SN2016gxp*	331	-9 - 267	B, V, r, i, SwiftU, SwiftB, SwiftV	ASAS-SN; This work
ASASSN-16lx*	169	-7 - 174	B, V, r, i, SwiftU, SwiftB, SwiftV	ASAS-SN; Brown et al. (2016)
MNRAS 000 , 1–23 (2019)				
Gaia16bql*	90	-13 - 178	B, V, r, i, SwiftU, SwiftB, SwiftV	ASAS-SN

Table B7 – continued Continuation of Table B7.

SN	N_{tot}	Phases	Filters	Refs.
ASASSN-17cs	180	-11 - 219	B, V, r, i, SwiftU, SwiftB, SwiftV	ASAS-SN; This work
DLT17u*	622	-33 - 315	U, B, V, r, i, SwiftU, SwiftB, SwiftV	ASAS-SN; Brown et al. (2014) ; This work
ATLAS17dfo	166	-17 - 288	B, V, r, i, SwiftU, SwiftB, SwiftV	ASAS-SN; This work
DLT17ar*	184	-14 - 227	B, V, r, i, SwiftU, SwiftB, SwiftV	ASAS-SN; This work
DLT17bk*	212	-8 - 284	B, V, r, i, SwiftU, SwiftB, SwiftV	ASAS-SN; This work
ASASSN-18hz*	88	-10 - 228	B, V, r, i, SwiftU, SwiftB, SwiftV	ASAS-SN; This work
SN2017ezd	139	-7 - 255	B, V, g, r, i, SwiftU, SwiftV	ASAS-SN; This work
DLT17bx	781	-13 - 379	B, V, g, r, i, SwiftU, SwiftV	ASAS-SN; This work
DLT17cd	427	-13 - 228	B, V, g, r, i, SwiftU, SwiftB, SwiftV	ASAS-SN; This work
ATLAS17jiv	269	-7 - 294	B, V, r, i, SwiftU, SwiftB, SwiftV	ASAS-SN; This work
SN2017glq	828	-17 - 331	B, V, r, i, SwiftU, SwiftB, SwiftV	ASAS-SN; This work

Table B7 – continued Continuation of Table B7.

SN	N_{tot}	Phases	Filters	Refs.
ATLAS17nmh*	301	35 – 194	B, V, g, r, i	ASAS-SN; work This
ATLAS17nse*	10	-4 – 306	V, i	Inserra et al. (2013); This work
ASASSN-17u*	129	-14 – 196	B, V, r, i, SwiftB, SwiftV	ASAS-SN
ASASSN-18hb	108	-7 – 237	B, V, g, r, i	ASAS-SN; work This
ASASSN-18bt	576	-9 – 265	B, V, g, r, i, SwiftU, SwiftB, SwiftV	ASAS-SN; Tucker et al. (2018); Dimitriadis et al. (2019a)
ASASSN-18da	31	-10 – 220	B, V, r, i, SwiftU, SwiftB, SwiftV	ASAS-SN; work This
DLT18h*	200	-24 – 335	B, V, g, r, i, SwiftU, SwiftB, SwiftV	ASAS-SN; work This
DLT18i	340	-18 – 237	B, V, g, r, i, SwiftU, SwiftB, SwiftV	ASAS-SN; work This
SNF-012	4	55 – 272	B, V, R, I	Taubenberger et al. (2013a)